2017

ILLUMINATE THE PATHWAY OF MEMBRANE PROTEIN ASSOCIATION AND DEGRADATION

Zhaoshuai Wang
University of Kentucky, wangzhaoshuai599@gmail.com
Digital Object Identifier: https://doi.org/10.13023/ETD.2017.419

STUDENT AGREEMENT:

I represent that my thesis or dissertation and abstract are my original work. Proper attribution has been given to all outside sources. I understand that I am solely responsible for obtaining any needed copyright permissions. I have obtained needed written permission statement(s) from the owner(s) of each third-party copyrighted matter to be included in my work, allowing electronic distribution (if such use is not permitted by the fair use doctrine) which will be submitted to UKnowledge as Additional File.

I hereby grant to The University of Kentucky and its agents the irrevocable, non-exclusive, and royalty-free license to archive and make accessible my work in whole or in part in all forms of media, now or hereafter known. I agree that the document mentioned above may be made available immediately for worldwide access unless an embargo applies.

I retain all other ownership rights to the copyright of my work. I also retain the right to use in future works (such as articles or books) all or part of my work. I understand that I am free to register the copyright to my work.

REVIEW, APPROVAL AND ACCEPTANCE

The document mentioned above has been reviewed and accepted by the student's advisor, on behalf of the advisory committee, and by the Director of Graduate Studies (DGS), on behalf of the program; we verify that this is the final, approved version of the student's thesis including all changes required by the advisory committee. The undersigned agree to abide by the statements above.

Zhaoshuai Wang, Student

Dr. Yinan Wei, Major Professor

Dr. Mark A. Lovell, Director of Graduate Studies

ILLUMINATE THE PATHWAY OF MEMBRANE PROTEIN ASSOCIATION AND DEGRADATION

DISSERTATION

A dissertation submitted in partial fulfillment of the requirements for the degree of Doctor of Philosophy in the College of Arts and Sciences at the University of Kentucky

By

Zhaoshuai Wang

Lexington, Kentucky

Director: Dr. Yinan Wei, Professor of Chemistry

Lexington, Kentucky

2017

ABSTRACT OF DISSERTATION

ILLUMINATE THE PATHWAY OF MEMBRANE PROTEIN ASSOCIATION AND DEGRADATION

Escherichia coli transporter protein AcrB and its homologues are the inner membrane components of the Resistance-Nodulation-Division (RND) family efflux pumps in Gram-negative bacteria. It is well accepted that soluble proteins are only marginally stable, but such insight is missing for membrane proteins. The lack of stability data, including thermodynamic stability and oligomer association affinity is a result of intrinsic difficulties in working with membrane proteins. In addition, the degradation of soluble proteins in *E. coli* has been extensively studied whereas the degradation process of membrane proteins remains unclear. A focus of my thesis is the validation and development of methods used to measure the thermo- and oligomeric- stability of membrane proteins. I investigated the mechanism of a popular thermal-stability assay developed specifically for the study of membrane proteins uses a thiol-specific probe, 7-diethylamino-3-(4-maleimidophenyl)-4-methylcoumarin (CPM). I found that, contrary to current understanding, the presence of a sulfhydryl group was not a prerequisite for the CPM thermal stability assay. The observed fluorescence increase is likely caused by binding of the fluorophore to hydrophobic patches exposed upon protein unfolding. I then applied these methods in the study of three projects. In the first project, I investigated how suppressor mutations restore the function of $AcrB_{P223G}$, in which the Pro223 to Gly mutation compromised the function of AcrB via disrupting AcrB trimerization. The results suggested that the function loss resulted from compromised AcrB trimerization could be restored through various mechanisms involving the compensation of trimer stability and substrate binding. In the second project, I created two AcrB fusion proteins, with C-terminal yellow fluorescence protein (YFP) and cyan fluorescence protein (CFP), respectively. YFP and CFP form a fluorescence resonance energy transfer (FRET) pair. Using this pair of fusion proteins, I studied AcrB assembly both in detergent micelles and in lipid bilayers. A positive cooperativity was observed in kinetic studies of association of AcrB trimer. Reconstitution experiment revealed that the association showed a higher FRET efficiency and faster association rate in liposome than in DDM. In the last project, I developed a fluorescence method to study the degradation of AcrB-ssrA by the ClpXP system. Comparing to the degradation of GFP-ssrA, degradation of AcrB-CFP-ssrA showed a lower maximum velocity and tighter binding to the enzymes with a positive

cooperativity.

Key words: multidrug efflux pump, AcrB, FRET, oligomerization, degradation, ssrA.

Zhaoshuai Wang

Sep 19th, 2017

ILLUMINATE THE PATHWAY OF MEMBRANE PROTEIN ASSOCIATION AND DEGRADATION

By

Zhaoshuai Wang

Dr. Yinan Wei

Director of Dissertation

Dr. Mark A. Lovell

Director of Graduate Studies

Sep 19th, 2017

Dedicated to my wife Caihong and my precious daughter Adelyn

ACKNOWLEDGEMENTS

My dissertation could not be finished without the help from many people. The first person I want to thank is Dr. Yinan Wei, my advisor. Dr. Wei set a great example for me to shadow as a researcher. She is willing to share her ideas to the students and always welcomes my questions. She is very detail-oriented and very passionate about her research. She taught me how to find the new research topic out of the old projects. Mostly importantly, she taught me how to think independently, which is a precious treasure to me. She has a noble character. She cares a lot about her advisees and students in the Chemistry department. She creates a great and warm working environment. I sincerely appreciate her dedication to my training, without which, I could not become the current me.

Secondly, I would like to express my sincere thanks to my committee members, Dr. Stephen Testa, Dr. Arthur Cammers from Chemistry Department, Dr. Haining Zhu from Department of Molecular & Cellular Biochemistry, and my outside examiner Dr. Jianhang Jia also from Department of Molecular & Cellular Biochemistry. They have graciously sacrificed their time and attention to attend my committee meetings, shared their knowledge, proof-read my dissertation, and provided great advices both on my research and my career.

I sincerely enjoyed the accompany of all my group members. Our postdoc Dr. Wei Lu taught me fundamental biochemistry techniques and given me valuable advices about my projects. Discussions with previous graduate students Dr. Linliang Yu, Dr. Meng Zhong, Dr. Cui Ye, and Dr. Qian Chai always inspired deeper thinking. Our present group members

Xinyi Zhang, Thilini Abeywansha, Prasangi Rajapaksha, Aaron Thompson, and Isoiza Ojo have provided me a lot of help and brought me tons of fun in everyday lab work. All these people have made our lab a great learning and researching community.

I want to thank Dr. Rebecca Dutch and Dr. Stacy Webb from Department of Molecular & Cellular Biochemistry for offering me help in pulse-chase experiment, Dr. Robert Sauer from Massachusetts Institute of Technology for providing me strains and plasmids.

I also want to thank ladies and gentlemen from main office and IBU office, who have offered me numerous help. Their kindness has created such a warm and friendly climate in Chemistry department.

I need to thank National Science Foundation (NSF), National Institutes of Health (NIH) and UK Research Challenge Trust Fund (RCTF) for the funding support which makes my research possible.

Last but not least, I would like to extend my deepest gratitude to my parents, my elder brother, my wife's parents, my wife Caihong and my daughter Adelyn. Without their unconditional love, trust, support and encouragement, I will not have the chance to come to Lexington and finish my graduate study at UK. My family is the most precious treasure in my life.

TABLE OF CONTENTS

LIST OF TABLES

LIST OF FIGURES

LIST OF ABBREVIATIONS

AAA+: ATPases associated with diverse cellular activities

ABC: ATP-binding cassette

ADP: Adenosine diphosphate

ATP: adenodine triphosphate

BN-PAGE: blue native-polyacrylamide gel electrophoresis

CD: circular dichroism

CFP: cyan fluorescent protein

CL-AcrB: cysteine free (cysless) AcrB

CMC: critical micelle concentration

CPM: 7-diethylamino-3-(4-maleimidophenyl)-4-methylcoumarin

Cryo-EM: cryo-electron microscopy

Cys: cysteine

DDM: n-dodecyl β-D-Maltopyranoside

DMSO: Dimethyl sulfoxide

DNA: Deoxyribonucleic acid

DSP: dithiobis succinimidyl propionate

DTT: Dithiothreitol

ERAD: endoplasmic reticulum associated degradation

EGFP: enhanced GFP

FLIM: Fluorescence lifetime imaging microscopy

FRET: Förster Resonane Energy Transfer

GFP: green fluorescent protein

IF: initiation factor

IPTG: isopropyl β-D-1-thiogalactopyranoside

LB: Luria Broth

LPL: large periplasmic loops

MATE: multidrug and toxic compound extrusion

MDR: multidrug resistance

MDR-TB: multi-drug-resistant tuberculosis

MFP: membrane fusion protein

MFS: major facilitator superfamily

MIC: minimum inhibitory concentration

MRE: mean residue ellipticity

NaCl: sodium chloride

Ni-NTA: nickel-nitriloacetic acid

NMR: Nuclear magnetic resonance

OD: optical density

OFP: orange fluorescent protein

OMP: the outer membrane protein

PaβN: phenylalanylarginine-β-naphthylamide

PB: phosphate buffer

PCR: phlymerase chain reaction

PDB: Protein Data Bank

PMF: proton motive force

PMFS: phenylmethysulfonyl fluoride

RF: release factor

RFP: red fluorescent protein

RND: resistance-nodulation-division

SDS: sodium dodecyl sulfate

SDS-PAGE: sodium dodecyl sulfate-polyacrylamide gel electrophoresis

SMR: small multidrug resistance

SspB: stringent starvation protein B

TMH: transmembrane helix

T_m: melting temperature

tmRNA: aminoacylated-ssrA RNA

UV: Ultraviolet

χ: molar ratio of SDS to DDM

WT-GFP: wild type green fluorescent protein

WT-AcrA: wild type AcrA

WT-AcrB: wild type AcrB

XDR-TB: extensively drug resistant tuberculosis

YFP: yellow fluorescent protein

ΔacrB: acrB knocked out strain

Chapter I. Introduction

1.1 A brief introduction of multidrug resistance

Penicillin, a wonder discovered by Alexander Fleming in 1928, saved thousands of lives in World War Ⅱ. However, the good situation didn't last for long. Twelve years later, even before the massive production of penicillin as a therapeutic, researchers discovered bacterial penicillinases (also called β-lactamase) which provides resistance to β-Lactam antibiotics.[1] Later on, researchers found some bacteria are resistant to more than one kind of antibiotics and named them multiple antibiotic resistance or multidrug resistance (MDR) bacteria. With more and more cases of MDR infection reported, soon MDR became a severe public health threat all over the world.[2] In Europe, close to 25,000 people died from MDR every year. In the United States, the effect of MDR is more severe, with over 63,000 people died from MDR every year.[3] In contrast to the fast growth of drug resistant infections, the development of new antibiotics is lagging behind. Thus, more efforts are needed to thoroughly understand the mechanism of MDR in order to find effective ways to treat infections caused by drug resistant pathogen.

There are five main mechanisms that lead to bacterial drug resistance (Figure 1.1): (1) inactivation or detoxification of antibiotics by enzyme[4] (for instance, penicillinases catalyze the hydrolysis of penicillin to reduce the effective concentration of the drug in bacteria), [5] (2) reduced uptake into cells or active efflux from cells (e.g. Drug efflux pumps such as the AcrAB-TolC complex expel a broad range of antibiotics to reduce the cellular concentration to a sub-toxic level), [6] (3) modification of targets to reduce binding with the

antibiotics (e.g. The affinity with antibiotics is reduced by mutations of the genomic copy of the target enzyme or acquisition of a new plasmid-borne enzyme to compensate for the loss of function),[7] (4) reduced uptake of the drug caused by the change of the expression level or structure of cell wall proteins,[8] and (5) metabolic bypass of antibiotics (e.g. the resistance to glycopeptide antibiotic vancomycin).[9]

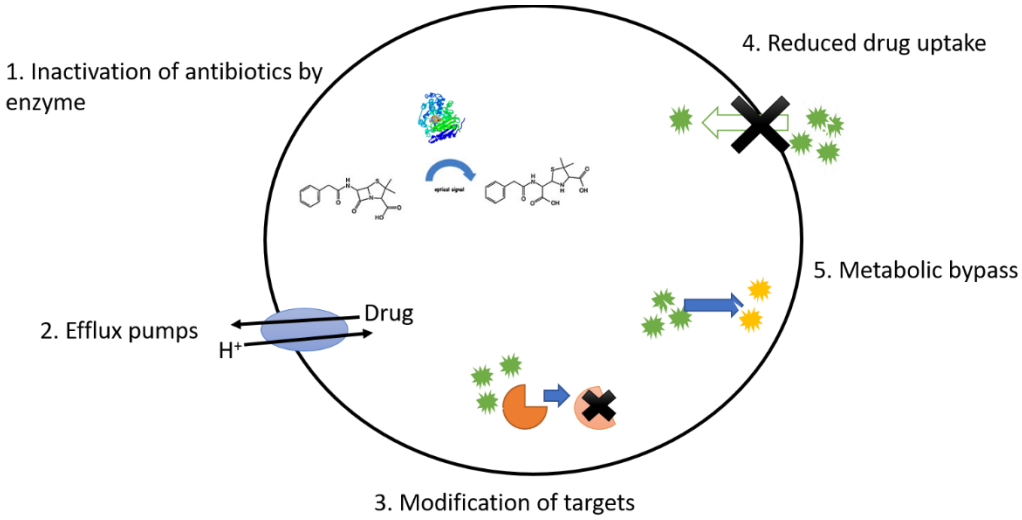

Figure 1.1 Some examples about the mechanism of drug efflux pumps.

Based on amino acid sequence, energy sources, and substrates, bacterial efflux pumps could be classified into five families: the major facilitator superfamily (MFS), the resistance-nodulation-division (RND) family, the ATP-binding cassette (ABC) superfamily, the small multidrug resistance (SMR) family, and the multidrug and toxic compound extrusion (MATE) family (Figure 1.2).[10]

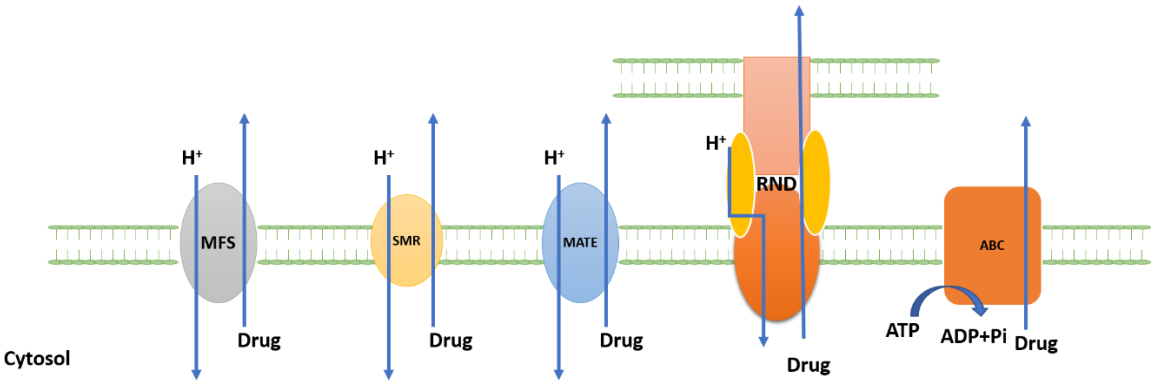

Figure 1.2 Families of MDR efflux pumps.

MFS family exists in almost all kingdoms of life importing or exporting substrates which include simple sugars, inositols, drugs, amino acids, oligosaccharides, nucleosides, esters and a large variety of organic and inorganic ions coupled with the transport of proton as energy source.[11; 12] All of the MFS transporters share a common characteristic structure known as the MFS fold, which contains 12 transmembrane helices and two domains (N-domain and C-domain).[13] Efflux pumps of RND family, widely found in Gram-negative bacteria, play key roles in providing multidrug resistance. Using proton motive force as the energy source, RND efflux pumps export a lot of substrates directly to external medium. There are three components in the efflux pumps: inner membrane transporter, adaptor protein, and outer membrane channel.[14] ABC transporters are ubiquitously present in all prokaryotes, fungi, plant, and animals. It's worth noting that the ABC superfamily transport substrates using ATP hydrolysis as the energy source, which is different from the other four superfamilies. In the human genome, there are 49 ABC genes whose mutation cause severe hereditary diseases. The transporters are also involved in translocation of drugs and metabolites, which is related to cancer therapy.[15] Composed of four transmembrane α-helices of 100-140 amino acids in length, the bacterial SMR proteins need to oligomerize

for substrate extrusion. The SMR pumps export peptides, complex carbohydrates, sugars, drugs, and metals in various ionic states driven by the proton motive force (PMF) mechanism.[16; 17] The MATE family, the most recently identified transporter family, exists in all three kingdoms: Eukarya, Archaea, and Eubacteria. Prokaryotic MATE proteins utilize H^+ or Na^+ electrochemical gradient as energy source while eukaryotic MATE proteins utilize only H^+ gradient.[18; 19]

MDR related diseases, including multidrug resistant tuberculosis (MDR-TB) and infections caused by multidrug resistant *Acinetobacter baumannii,* have threatened thousands of people. MDR-TB is caused by *Mycobacterium tuberculosis* which is resistant to two most potent first-line anti-tuberculosis drugs — isoniazid and rifampicin.[20] In 2015, around 480,000 cases of MDR-TB were reported globally, among which about 9.5% cases were estimated to be extensively drug resistant tuberculosis (XDR-TB) with additional resistance to fluoroquinolones and second-line injectable drugs. MDR-TB has a mortality rate of up to 80%. A best estimate from some reports in 2012 showed that there were 150,000 deaths out of 450,000 patients globally.[21] To treat MDR-TB, a recommended regimen is the combination of at least four antituberlosis drugs to *Mycobacterium tuberculosis*. Multidrug resistant *Acinetobacter baumannii*, resistant to a lot of antibiotics including aminopenicillins, ureidopenicillins, cephalosporins, cephamycins, aminoglycosides, chloramphenicol, and tetracyclines, has been found in many hospitals since 1980.[22] As a rapidly emerging pathogen in healthcare settings, *A. baumannii* causes infections including pneumonia, bacteremia, meningitis, urinary tract and wound infections.[23] An estimated mortality rate of 30% – 75% was reported for nosocomial

pneumonia caused by *A. baumannii*.[24] Up to now, two methods have been used to treat infections caused by multidrug resistant *A. baumannii*: 1) monotherapy with using carbapenem or ampicillin or sulbactam, and 2) combined therapy with two or more drugs.[25]

1.2 The resistance nodulation cell division (RND) family

Unlike the other four families of multidrug resistance efflux pumps, RND efflux pumps are only present in Gram-negative bacteria. In the early 1990s, RND pumps were first identified in *E. coli* and *Pseudomonas aeruginosa* by two different research groups respectively.[26] Functioning as a tripartite complex, these pumps are composed of the transporter protein (RND: the inner membrane component), membrane fusion protein (MFP: the periplasmic component), and the outer membrane protein channel (OMP: the outer membrane protein). All these three proteins are essential for drug translocation; any defect in any one component can cause the entire complex totally non-functional.[14] These three proteins form a continuous channel across the bacterial envelope which ensures substrate molecules (likely captured from the outer leaflet of the inner membrane bilayer) to be exported directly across the periplasm and the outer membrane. Yet, it is still not clear whether the periplasm or inner membrane is the predominant location of substrate capture, and how and to what extent the substrates may be captured from the cytosol.[27]

To date, over 30 types of RND pumps have been identified. Among them, MexAB-OprM, MexCD-OprJ, MexEF-OprN, and MexXY-OprM from *P. aeruginosa*, and AcrAB-TolC, AcrAD-TolC, and AcrEF-TolC from *E. coli* have been intensively studied.[28-31] *P. aeruginosa*, an opportunistic pathogen, is notable for high level resistance to antimicrobial

agents due to the existence of Mex efflux pumps MexAB-OprM and MexXY-OprM.[32] In addition to antibiotics, Mex efflux pumps also export organic solvents, biocides, dyes, and cell signaling molecules. Single crystal structures of MexA, MexB and OprM have been obtained through high-resolution X-ray crystallography (Figure 1.3). OprM, the trimeric protein channel, consists of a 4-nm-long transmembrane domain with 12 strands that form a β-barrel and a 10-nm-long periplasmic domain with 12 α-helices and a mixed α/β equatorial domain. Trimeric transporter MexB contains a 12 transmembrane α-helices domain in each protomer and a large periplasmic part including a porter domain and a funnel domain. MexA consists of four consecutive domains: membrane proximal, β-barrel, lipoyl and α-helical hairpin domains. MexA is anchored to the inner membrane via palmitoylation of an N-terminal cysteine residue.[32]

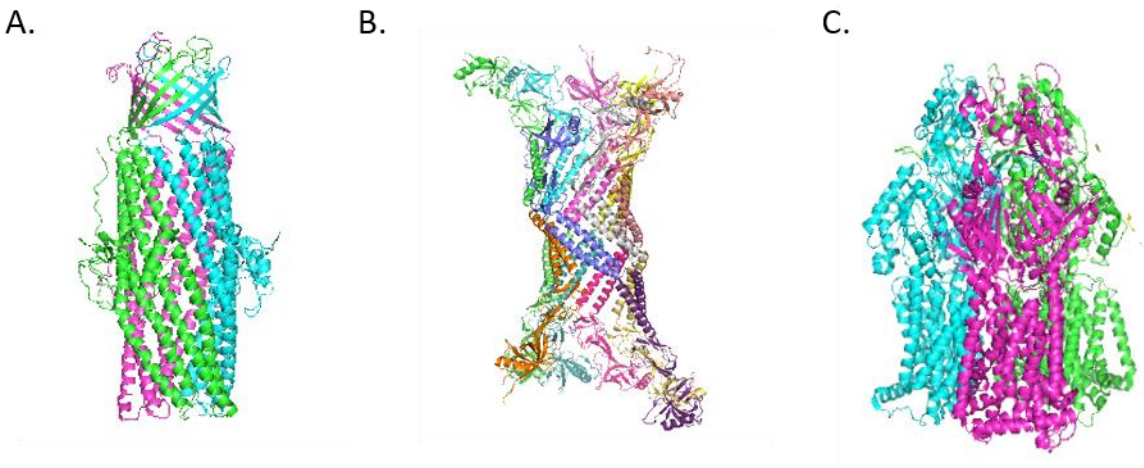

Figure 1.3 Crystal structures of OprM (***A***), MexA (***B***), and MexB (***C***). Protein Data Bank (PDB) ID are 4Y1K for OprM, 1VF7 for MexA, 3W9I for MexB, respectively.

Although the crystal structures of MexA, MexB and OprM have been individually obtained, the assembly mechanism of the tripartite system is particularly challenging because the

complex span across two different membranes and periplasm. With the development of advanced electro tomography technique such as cryo-EM, complicated protein structures, particularly for complex like MexAB-OprM (Figure 1.4, *A*) and AcrAB-TolC (Figure 1.4, *C*), have been resolved. For MexAB-OprM, a sandwich-shape with an intermembrane distance of 21 nm was observed in lipid nanodisc system where MexA did not directly contact to OprM.[31] For AcrAB-TolC, the intense debate about whether AcrB directly contacts TolC came to an end after the whole structure of AcrAB-TolC was obtained from cryo-EM in 2014. There was no interaction between AcrB and TolC observed from their result.[33; 34]

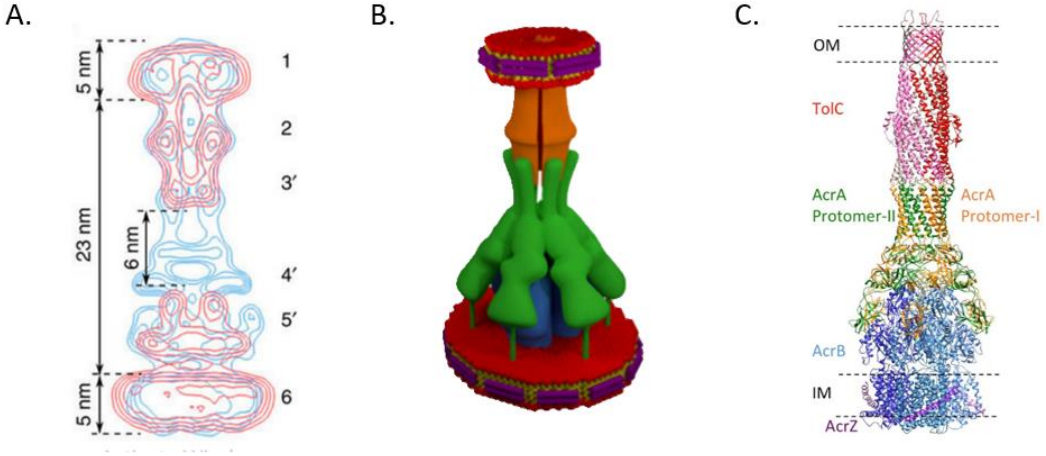

Figure 1.4 Structure models showing complex MexAB-OprM and AcrAB-TolC. *A.* Isocontours of MexB-ND and OprM-ND (red) overlaid on isocontours of tripartite complex. *B.* Assembly model of MexAB-OprM in nanodisc.[31] *C.* 5.9 Å resolution cryo-EM asymmetric structure of the AcrABZ-TolC pump in presence of puromycin.[35] Reprinted with permission from Rightslink® Service and Elife Sites.

1.3 Efflux pump complex AcrAB-TolC

The multidrug efflux pump AcrAB-TolC (**Figure 1.4, *C***), a member of the RND family and one of the most extensively studied systems, is a tripartite efflux transporter.[36] 'Acr' is the acronym of "acriflavin resistance", one of the first compounds that the AcrAB-TolC system is found to transport, and TolC refers to "tolerance to colicin". Like other members in the RND family, AcrAB-TolC complex comprises three components: the proton-driven transporter protein AcrB, the membrane fusion protein AcrA, and the outer membrane channel TolC.[37]

In 2006, Mikolosko and coworkers determined the crystal structure of AcrA.[38] According to the crystal structure they obtained, AcrA is a dyad symmetric dimer of dimers which are divided into α helical hairpin domains, β-barrel domains, and lipoyl domains (Figure 1.5). As a membrane fusion protein, the main function of AcrA is stabilizing the connection between AcrB and TolC through the interaction of apices of their periplasmic domain.[39] Previous studies suggest that the α helical hairpin domain is likely to interact with the channel protein TolC while the β-barrel domain contacts with the transporter protein AcrB, so that the drug efflux pump works to pump out the antibiotics.[40-42] Unlike AcrB and TolC functioning as trimers, AcrA acts as a hexamer in the AcrAB-TolC complex according to a study by Xu.[43]

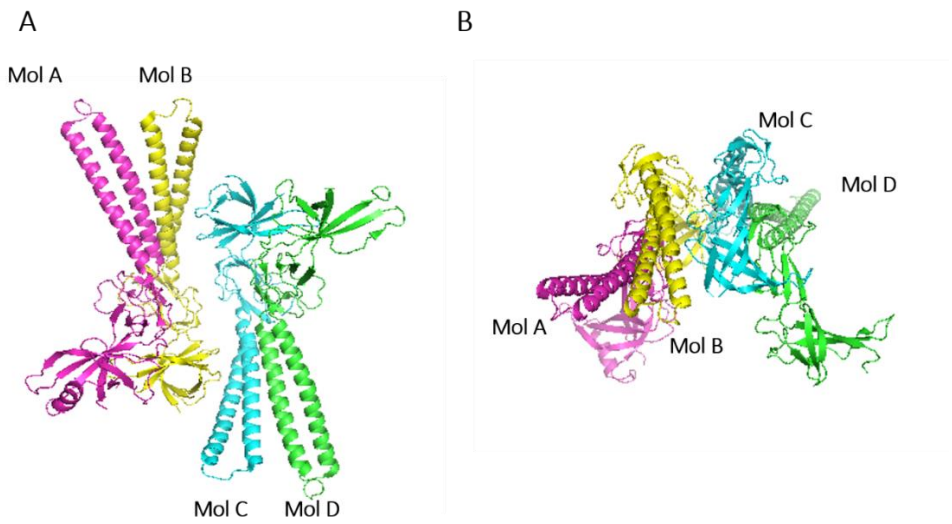

Figure 1.5 Structure of AcrA. *A*: side view. Ribbon representation of two apparent dimers in one subunit. *B*: top view. The structures were generated using Pymol (PDB ID: 2F1M).[38]

The crystal structure of TolC was determined by Koronakis *et al.* in 2000 (Figure 1.6).[44] According to the crystal structure obtained, the trimeric channel TolC comprises three parts: a β-barrel domain, an α helical domain (periplasmic domain), and a mixed α/ β domain (equatorial domain) in each protomer.[44] The overall length of TolC is about 140 Å with 40 Å in the β-barrel domain mainly composed of β strands, and 100 Å in the periplasmic domain mainly composed of α helices. The β-barrel domain in the outer membrane and the periplasmic domain in periplasm form a continuous channel with an internal diameter of 35 Å, which is one of the largest known protein structure .[44] *E. coli* strains deficient in TolC are more sensitive to a wide variety of chemicals in the environment (e.g. detergents, drugs, bile salts, and organic solvents) than wild type strains. Besides exporting small molecules of chemical compounds, TolC is also involved in the transport of large molecules such as proteins.[45]

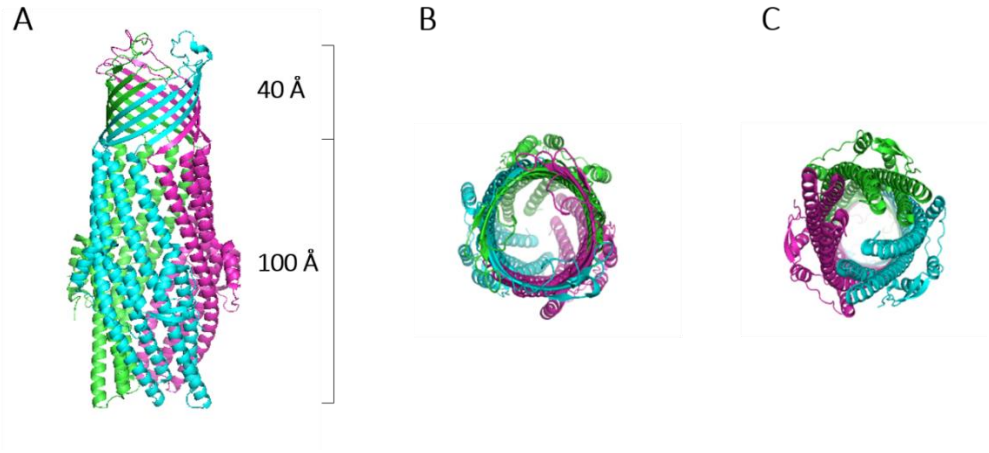

Figure 1.6 The overall architecture of TolC. *A*: side view. *B*: top view. C: bottom view. The ribbon structure was created using Pymol.[50] (PDB code: 1EK9)

The RND transporter protein AcrB, responsible for the drug recognition and energy transduction, resides in the inner membrane of bacteria cells. The crystal structure of AcrB was first described by Murakami *et al.* in 2002.[46] AcrB, in a jellyfish shape, is a trimeric protein containing 1049 amino acids in each protomer. It is composed of three domains: transmembrane domain, pore domain, and TolC docking domain (**Figure 1.7, *A***). Driven by the proton motive force, a broad range of substrates are recognized and pumped out by AcrB. These substrates include acriflavin, rhodamine 6G, berberine, tetraphenyl-phosphonium, ethidium, ciprofloxacin, erythromycin, acridine, etc.[47] Exchange of AcrB and AcrD periplasmic loops altered the substrate preference of the proteins, suggesting that residues dictating substrate specificity reside in the porter domain. A deep binding pocket was later defined through additional mutational and crystallographic studies. While initially the three protomers in a trimer were considered to adopt the same conformation, two papers published by Pos group[48] and Yamaguchi group[49] in 2006 showed that in an AcrB trimer, each monomer adopts a different conformation. They speculated that each

conformation represents a different state during the transport cycle, loose (L), open (O) and tight (T), which leads to a completely new model about the mechanism of drug translocation. Using Bodipy-FL-maleimide labeling, Nikaido and coworkers elucidated the entire substrate translocation pathway *in vivo*. Their observations showed that the substrates are captured in the lower cleft region of AcrB, then translocated to binding pocket and transported to the AcrB funnel through the gate, and finally exported by TolC.[50] Later, the substrates were divided into two groups depending on where they interact: groove binder and cave binder. Groove binders are defined as the substrates found within the narrow groove in the part of the binding pocket far away from the membrane surface, whereas cave binders are defined as other substrates bound with a larger cave area close to the membrane surface.[51; 52]

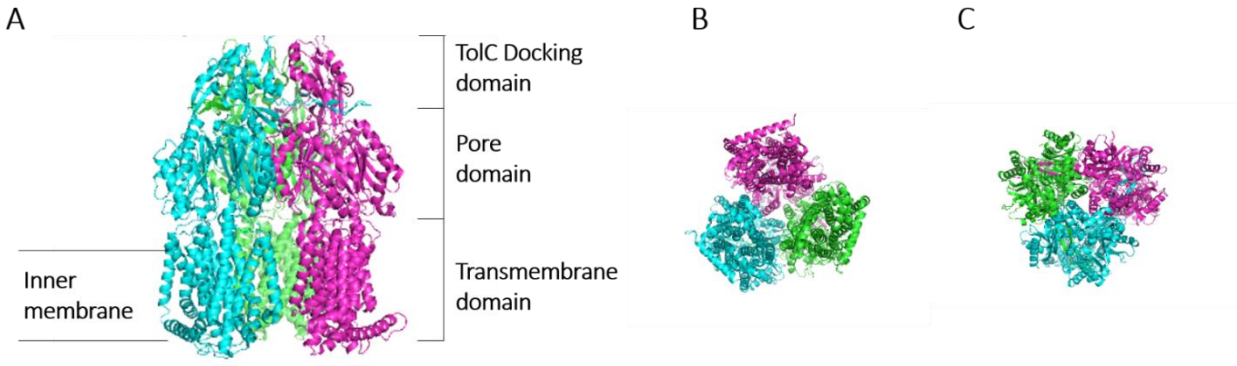

Figure 1.7 Crystal structure of AcrB. *A*. Side view of ribbon representation, three protomers are colored cyan, pink and green, respectively. From top to bottom, the three domains, TolC docking domain (about 30 Å), pore domain (about 40 Å) and transmembrane domain (about 50 Å) are shown. *B*. Top view. *C*. Bottom view. The structures are generated using Pymol (PDB ID: 2GIF).[46]

Individual crystal structures of AcrA, AcrB and TolC have been resolved for more than ten

years, which shed light on the substrate recognition and binding. However, how the components are assembled into a functional pump and the stoichiometry was not clear until 2014 when the first AcrABZ-TolC structure was obtained through cryo-EM (Figure 1.8).[34] With the help of linkers between each component, AcrA-AcrZ and AcrA-AcrB fusions with endogenous TolC were co-expressed and purified. The complex remained intact after purification, making observation of the assembled structure possible. Three important findings rose from the final model which agreed well with the density envelope. Firstly, there is no direct interaction between TolC and AcrB in the pump, which is inconsistent with the model hypothesized by Martyn F. Symmons *et al*.[53] Secondly, the stoichiometry for AcrB: AcrA: TolC is 3:6:3. Thirdly, a resting state of TolC was observed.

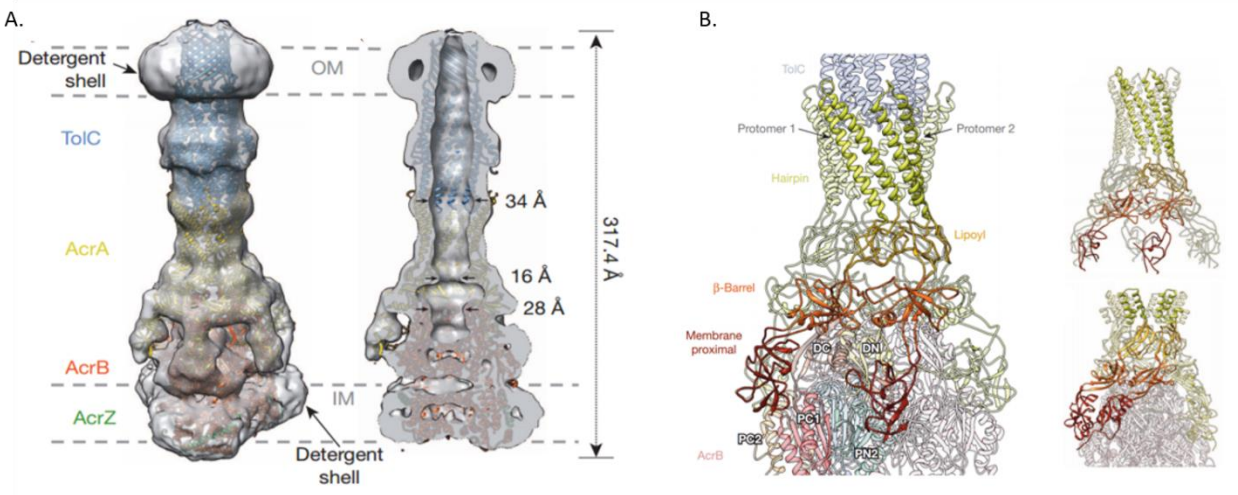

Figure 1.8 *A.* A pseudo-atomic model of the drug efflux pump AcrAB-TolC. *B.* Modeled interactions of the efflux pump components.[34] Reprinted with permission from Rightslink® Service.

Another series of cryo-EM structures of AcrAB-TolC in resting and drug transporting states were then reported (Figure 1.9).[35] In resting state, TolC is in a closed conformational state

as shown in Figure 1.9 *A*. When the substrates bind to AcrB, AcrB monomers circulate the three conformational states — loose (L), tight (T), and open (O),[54] then TolC channel opens to pump out the substrates transported from AcrB. In this process, AcrB monomers rotate using proton motive force as energy source. The pump inhibitor MBX3132 binds to AcrB tightly which locks the pump in a more homogeneous conformation in which all AcrB subunits are shown in the same (TTT) conformation.[35]

Figure 1.9 2D average structures showing the pump states of resting (*A*), in presence of puromycin (*B*) and pump inhibitor MBX3132 (*C*).[35]

To control the spread of antibiotic resistance, discovering and screening efflux pump inhibitors becomes urgent. To date, several efflux pump inhibitors have been reported, including D13-9001, MC207110 (phenylalanylarginine-β-naphthylamide, PAβN), and MBX2319 (Figure 1.10).[55] All inhibitors reported act under similar mechanism. MBX2319 binds tightly to the lower part of the distal pocket in the AcrB protomer, interacting with phenylalanines lining the hydrophobic trap, where D13-9001 also binds. However, PAβN appears to bind to a different area of the distal pocket in the protomer. Besides investigating how inhibitors work on the transporter AcrB, researchers also focus on developing efflux

pump inhibitors of other components. Narges Abdali *et al.*[55] screened efflux pump inhibitor candidates and found that NSC60339 showing positive inhibition effect bound to different sites of AcrA which could be used as a potential therapeutic target.

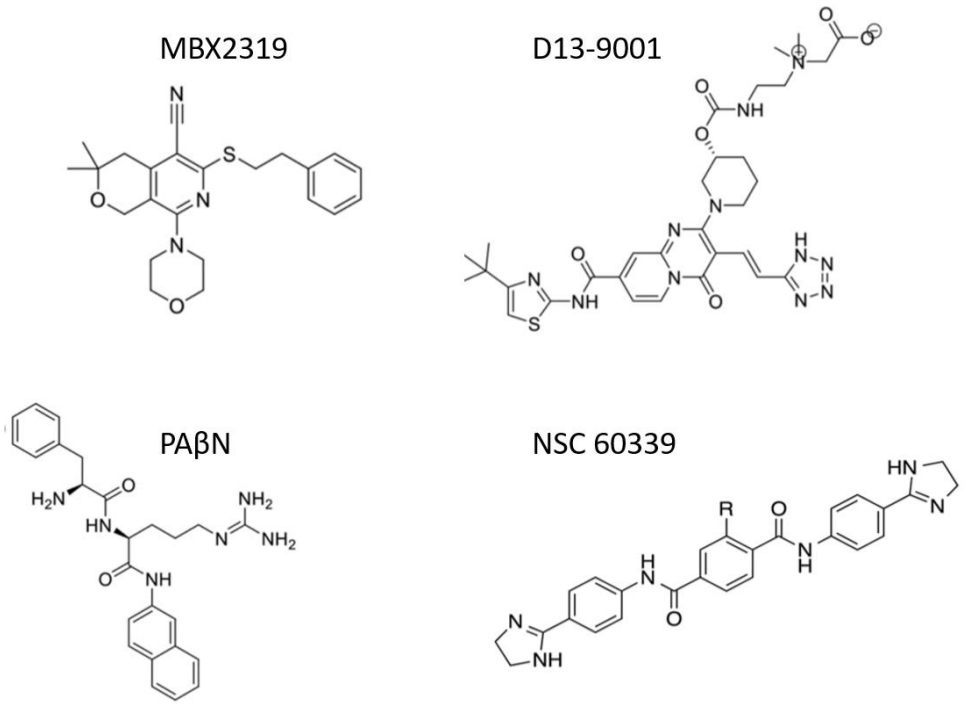

Figure 1.10 RND efflux pump inhibitors developed, MBX2319, D13-9001 and PaβN for AcrB, and NSC 60339 for AcrA.[56; 55]

1.4 Fluorescent protein and FRET.

Fluorescence is defined as a phenomenon that a substance absorbs light or other radiation source and emits light with a different wavelength. The main principle of fluorescence is that electrons of fluorophore excited by light or other radiation source go to higher singlet states and then relax to ground state by emitting photons. Fluorescence was firstly reported by a Spanish physician and botanist, Nicholάs Monardes in 1565.[57] He reported the observation of fluorescence from a wood called *lignum nephriticum* which was used as

medicine by Aztecs (Figure 1.11). In 1819, Edward D. Clark found some crystals of fluorite reflected light and displayed a deep sapphire blue color from Weardale, Durham, England. The word "fluorescence" was firstly used by George Gabriel Stokes, physicist and professor of mathematics at Cambridge in his famous paper entitled "On the Refrangibility of Light" in 1952. The *Stokes' shift* which describes the difference between maxima of excitation and emission peaks in fluorescence spectrum was also named after him.

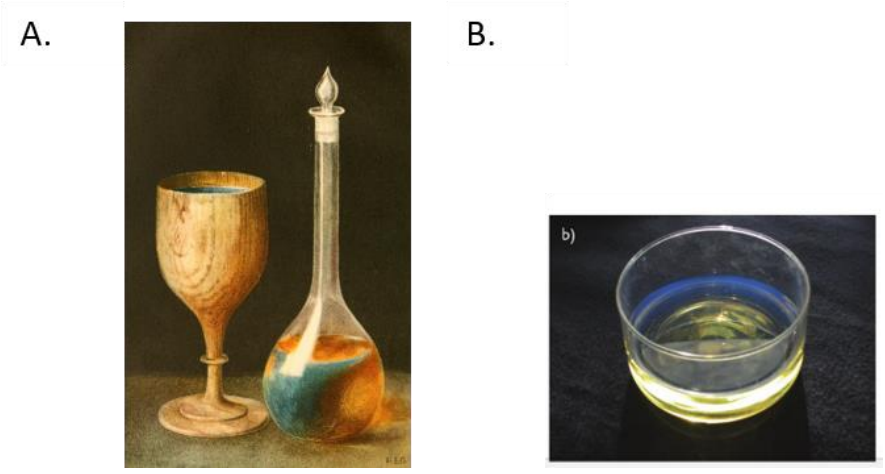

Figure 1.11 *A.* Absorption and fluorescence colors of an infusion of *Lignum nephriticum* under day light. *B.* The solution obtained from infusion of the wood. Taken from Safford, W. E. (1915).[58]

Although the phenomenon of Förster resonance energy transfer or Fluorescence resonance energy transfer (FRET) had been observed before the 20th century, the first quantum mechanical theories of FRET was developed by Heisenberg, Schrödinger and Dirac in 1925.[59] As shown in Figure 1.12, FRET takes place between two fluorophores that are close to each other, resulting in the energy transference from a "donor" fluorophore to an "acceptor" fluorophore through non-radiative dipole-dipole coupling.[60] In this process, electrons of donor excited by absorbing photons with high energy go from electronic

ground state S_0 to electronic singlet state S_1, and then the electrons from different vibrational levels of S_1 state relax to lowest vibrational level, followed by transition to S_0 state. Finally, the acceptor which absorbs the energy from the donor is excited to S_1 state, and emits light at a different wavelength from the donor fluorophore when it relaxes from S_1 to S_0.[61] Because FRET occurs only when two fluorophores are close enough, measurement of FRET can be used to determine the relative distance between the two molecules. Based on this principle, the applications of FRET have been extended in many disciplines including biology and chemistry with the development of techniques and fluorescent proteins. FRET has many advantages, for instance, it is highly sensitive due to the use of fluorescence spectrometer; it can be used in *in vivo* studies, especially suitable for live cell imaging; and sometimes it can be developed into assays for high-throughput screening.[62] FRET is especially useful for studies involving membrane proteins, since it is compatible with the lipid bilayer environment. There are mainly two FRET strategies that can be used in membrane protein studies — donor quenching and acceptor sensitization: donor quenching relies on the monitor of quenching of the donor fluorescence in the presence of acceptor, whereas acceptor sensitization monitors the fluorescence signal increase of acceptor when the donor is excited.[63]

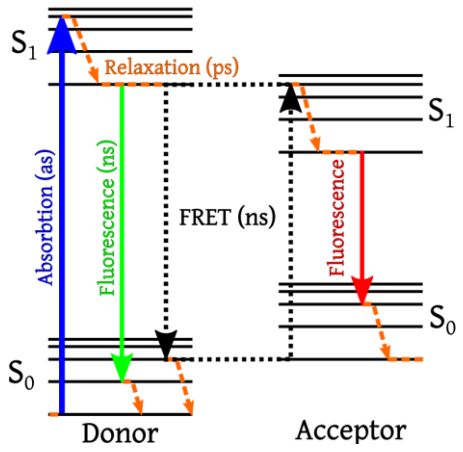

Figure 1.12 Jablonski diagram of FRET with typical timescales indicated.

Green fluorescent protein (GFP) was discovered from *Aequorea* jellyfish (Figure 1.13, *A*) by Shimomura *et al.* (1962) as a companion protein to aequorin.[64] Soon the same group published the emission spectrum of GFP with an emission peak at 508nm.[65] Later, researchers crystalized GFP and analyzed its structure, discovered that the chromophore was formed from residue 65-67 (Ser-Tyr-Gly) in the native protein.[66] High resolution crystal structure was resolved in 1996 by Ormö *et al. (*PDB ID 1EMA) (Figure 1.13, *B*).[67] The crystal structure showed the dimeric wild type GFP (WT-GFP) is cylinder-shaped with an 11-stranded β-barrel threaded by an α-helix inside. The chromophore attached to the α-helix is perfectly buried in the center of the cylinder called β-can.[68] WT-GFP folds efficiently when expressed at or below room temperature. However, such folding efficiency declines drastically when the temperature is higher than the room temperature. WT-GFP has some undesirable properties including a lag in the development of fluorescence, poor expression in other host cells, and low fluorescent intensity when excited by blue light. Compared with other reporters such as β-galactosidase used in mammalian cells, the sensitivity of WT-GFP is lower. So an enhanced GFP version "EGFP" (where GFP has two

mutations—Phe64 to Leu and Ser65 to Thr) was developed by Zhang *et al.* in 1996.[69] A 1.5 Å crystal structure of EGFP was obtained in 2012, showing that the side chain in the central chromophore is smaller due to the mutation F64Land β-strand 2 is packed tighter with the core. S65T disrupts the hydrogen bonding with Glu222, removing the electrostatic clash with an anionic form of ground state of chromophore. These changes give EGFP better excitation characteristics and higher folding efficiency at 37 ºC.[70]

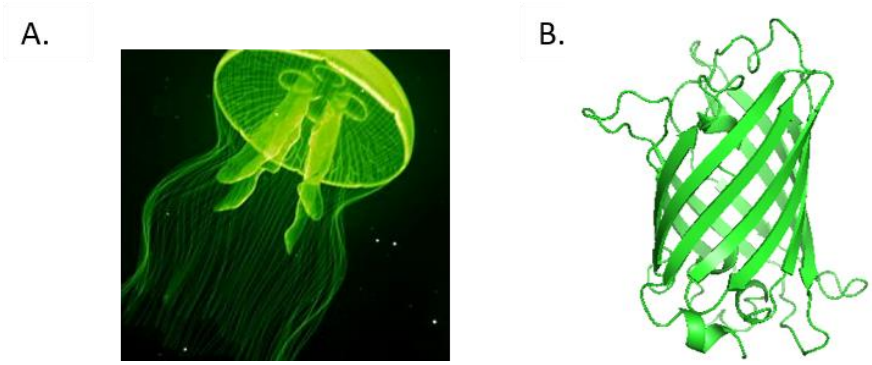

Figure 1.13 *Aequorea* jellyfish (***A***). Green fluorescent protein (GFP, ***B***), PDB ID: 1EMA.

With the application of FRET techniques and wide use of fluorescent proteins in studies of biochemical processes, more and more GFP derivatives such as CFP, YFP, OFP, RFP, and their enhanced versions have been developed (Table 1.1). The purpose of the mutations is a) to make the protein fold faster, b) to improve the brightness and c) increase the quantum yield by creating or removing some interactions in chromophore, or d) to shift the excitation and emission wavelengths so that the fluorescent proteins can suit the studies better.[71; 72] With fluorescent proteins having different colors, five primary FRET approaches have been used in research:[73] 1) sensitized emission, or two color ratio imaging with controls (e.g. spatiotemporal dynamics of CaMKII activation in individual dendritic spines during long-term potentiation was monitored using FRET between mEGFP and

REACh, a green fluorescent protein as donor and a yellow fluorescent protein as acceptor),[74] 2) acceptor photo-bleaching where the FRET efficiency can be calculated by subtracting the donor intensity in presence or absence of the acceptor, 3) fluorescence lifetime imaging microscopy (FLIM), a method takes advantage of the fact that the rate of fluorescence exponential decay is sensitive to environmental change that quenches the fluorescence and thus the amount of quenching of donor fluorescence could be indicated via the shortening of the fluorescence decay time, 4) spectral imaging, where the fluorescence spectra for both donor and acceptor are collected to determine the level of FRET, and 5) polarization anisotropy imaging, a method well-suited for high-content screening with a high signal-to-noise ratio based on the measurement of fluorescence polarization.

Table 1.1 Representatives of GFP variants and the mutations relative to WT-GFP.[71; 72]

GFP variant	Mutations relative to WT-GFP
EGFP	F64L, S65T
Emerald	F64L, S65T, S72A, N149K, M153T, I167T
EYFP	S65G, V68L, S72A, T203Y
mYFP	S65G, V68L, Q69K, S72A, T203Y, A206K
Citrine	S65G, V68L, Q69M, S72A, T203Y
mCitrine	S65G, V68L, Q69M, S72A, T203Y, A206K

Table 1.1 Representatives of GFP variants and the mutations relative to WT-GFP (continued).[71; 72]

Venus	F46L, F64L, S65G, V68L, S72A, M153T, V163A, S175G, T203Y
YPet	F46L, I47L, F64L, S65G, S72A, M153T, V163A, S175G, T203Y, S208F, V224L, H231E, D234N
ECFP	F64L, S65T, Y66W, N149I, M153T, V163A
mCFP	F64L, S65T, Y66W, N149I, M153T, V163A, A206K
Cerulean	F64L, S65T, Y66W, S72A, Y145A, H148D, N149I, M153T, V163A
CyPet	T9G, V11I, D19E, F64L, S65T, Y66W, A87V, N149I, M153T, V163A, I167A, E172T, L194I
Clover	S30R, Y39N, S65G, Q69A, N105T, Y145F, M153T, V163A, I171V and T203H
EBFP	F64L, S65T, Y66H, Y145F
T-Sapphire	Q69M, C70V, S72A, Y145F, V163A, S175G, T203I

1.5 AAA+ proteases

AAA+ proteases, with at least one protein component which belongs to ATPase Associated with diverse cellular Activities, are generally comprised of ClpXP, ClpAP, ClpCP, Lon, FtsH, HslUV, PAN/20S, the 26S proteasome, and their homologues.[75] The protease degrading the misfolded protein substrate is a complicated biological process: it usually starts with the AAA+ rings binding the exposed peptide segment in the axial pore, followed by the conformation changes of the rings driven by ATP hydrolysis, and ends with the protein unfolding and translocation into the degradation machine where unfolded peptides are degraded. Different families of the proteases have different architectures. Lon and FtsH families only contain one component, that is, hexamers of six identical subunits with a protease domain and an ATP binding domain.[76] Other families such as ClpXP, ClpAP, and HslUV include two components with different structures and assemblies: ClpX, ClpA, and HslU protein form a hexameric AAA+ rings with six identical subunits, whereas ClpP and HslV protease form a double-ring structure that consists of 12 and 14 subunits, respectively.[77] More complicated structures were observed in the PAN/20S protease and 26S proteasome which include an AAA+ ring and α7β7β7α7 compartmental protease as their basic architectural features.[78; 79]

ClpXP is a well-studied degradation system among all the AAA+ proteases. To recognize and degrade the protein substrates, a recognition/degradation tag (also known as degron) is necessary. In *E.coli*, ssrA tag with an 11-amino acid sequence "AANDENYALAA" serves as the degradation tag. The aminoacylated-ssrA RNA (tmRNA) is recruited to ribosomal A site when the ribosome stalls on an incomplete or untranslatable message. The

nascent chain encoding original gene is replaced by tmRNA with gene encoding ssrA tag translated by ribosome.[80] Substrates bearing new synthesized ssrA tag is recognized by the SspB adaptor and ClpX. The SspB adaptor binds to the first seven amino acid "AANDENY" of the tag, tethering the substrate to ClpXP protease, while ClpX recognizes the last three amino acid "LAA" and unfolds the protein substrate. Finally, denatured polypeptides are translocated and degraded into smaller pieces by ClpP.[81]

ClpX is a hexameric AAA+ machine which uses ATP as the energy source to unfold and translocate denatured polypeptides to ClpP. The hexamer of ClpX is asymmetric in both nucleotide-free and nucleotide-bound structures (Figure 1.14, *A*). Each monomer has two domains, a large domain (residues 61-314) and a small domain (residues 320-416) with a linker between the two domains (residues 315-319). The asymmetry of ClpX is generated by changes in the interfaces between each subunit or between the two domains when the nucleotide-free and nucleotide-bound structures switch.[77] $ClpX_6$ has six ATP/ADP binding sites that locate at the interface between the large and small domains from adjacent subunits.[78] Interestingly, only four out of the six binding sites could actually be used to bind with ATP/ADP. This phenomenon could be explained by the crystal structure of $ClpX_6$ obtained by Dr. Sauer's lab. That is, there are two types of subunit conformations (named type 1 and type 2) in the closed ClpX hexamer, which has a 1-1-2-1-1-2 pattern (Figure 1.14, *B*). Two ATP/ADP binding sites are occupied by the small domain in type 2 subunit, so only four out of six binding sites can bind with ATP/ADP.

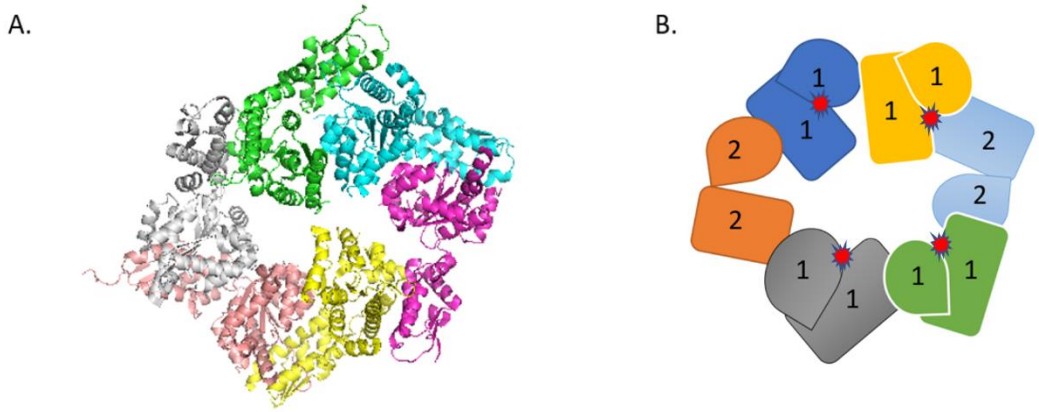

Figure 1.14 *A.* Crystal structures of ClpX (PDB ID: 3HTE). *B.* Model shown type 1 and type 2 subunits and ATP/ADP binding sites (red stars).

ClpP, a tetradecamer with two rings (each contains seven subunits), is a serine-peptidase cleaving peptides after hydrophobic residues.[82] Ser 97, His 122, and Asp 171 are identified as three components of the catalytic triad of ClpP.[83] ClpP alone only cleaves peptides of fewer than six residues while it degrades longer peptides with the help of ATPase such as ClpX and ClpA. Producing degradation fragments of 7 to 10 residues, the degradation does not show any clear sequence specificity.[84; 85] The crystal structure of ClpP which has a cylindrical shape of 90 Å both in height and diameter shows that the active sites are in a central chamber (Figure 1.15, *A*). Theoretically, the central chamber could accommodate several hundred unfolded polypeptide residues. The cleavage of polypeptides is efficient due to two factors: the high local concentration of active sites (about 350 mM) and the long distance between two adjacent active sites in ClpP chamber (around 25 Å, which could span across 8 residues). Therefore, a polypeptide could simultaneously bind to multiple active sites, increasing the efficiency of degradation. With such a mechanism, the cleavage

rate of ClpP reported is about 10,000 min^{-1}.[86; 87] When the unfolded polypeptides are translocated into $ClpP_{14}$, a conformational switch between a compressed state (i.e. closed active sites/open equatorial pores; Figure 1.15, *B*) and an extended state (i.e. open active sites/closed equatorial pores) give researchers insight into how ClpP cleaves the protein substrates and how degradation products are exited.[88]

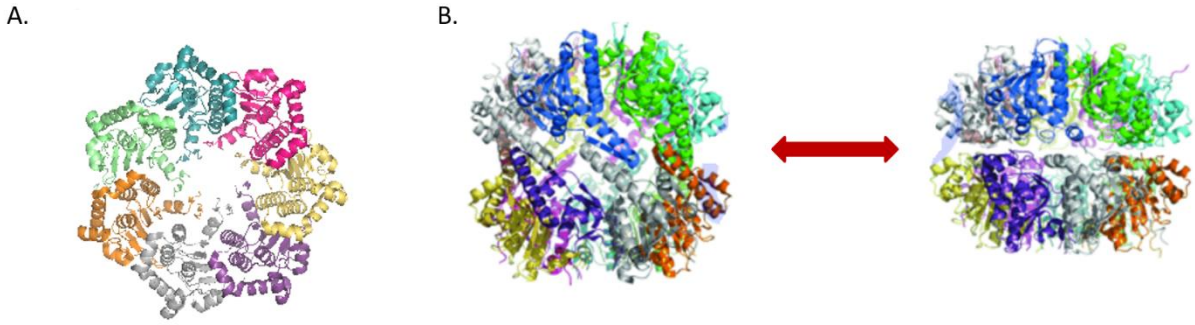

Figure 1.15 *A.* Crystal structure of ClpP, one subunit (PDB ID: 3QWD). *B.* Structure switch between closed state and extended state.

SspB (stringent starvation protein B) is a dimeric delivery/adaptor protein which binds specifically to the first seven residues of ssrA tag "Ala^1 Ala^2 Asn^3 Asp^4 Glu^5 Asn^6 Tyr^7", enhancing the degradation of ssrA-tagged protein by ClpXP and inhibiting the degradation by ClpAP.[89; 90] Consisting of a single α-helix and a β-sandwich formed by stacking of a-β sheet (β2- β1- β6- β7) onto another β-sheet (β5- β4- β3), the overall dimension of SspB is around 63×33×22 Å (Figure 1.16, *A*). An important role of SspB is tight binding of the ssrA tag in the hydrophobic pocket, mainly the side chain of Ala^1 and Ala^2. ClpA also recognizes Ala^1 and Ala^2 and thus cannot degrade SspB bound substrate. Another critical residue in the ssrA tag is Tyr^7, the aromatic ring of which is sandwiched between several SspB side chains.[89] From the model of SspB delivery system, two ssrA tagged protein substrates could be bounded simultaneously to one SspB dimer and delivered to the central

pore of ClpX due to the flexible binding domain (**Figure 1.16, *B***).[90]

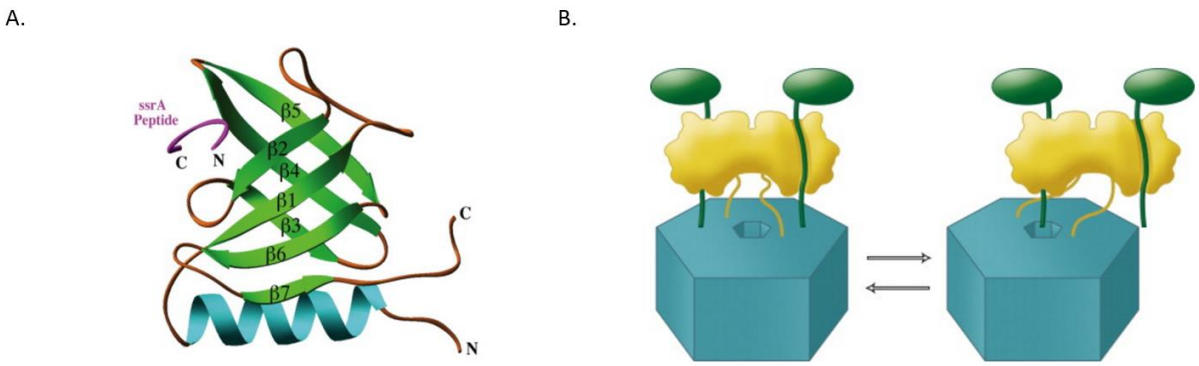

Figure 1.16 *A.* Crystal structures of SspB monomer. (PDB ID: 1OX8) *B.* Model for the SspB-Mediated of an ssrA-tagged protein to ClpX. The pictures belong to Cell Press.[90]

Chapter II. Probing Membrane Protein Stability Using CPM Fluorescence - a Mechanistic Study

Part of this chapter are taken from "CYSTEINE RESIDUE IS NOT ESSENTIAL FOR CPM PROTEIN THERMAL-STABILITY ASSAY", 2015, *Analytical and bioanalytical chemistry*. 407, 3683-3691.[134]

2.1 Introduction

Stability measurement of membrane proteins is a challenging task because of the scarcity of high-resolution protein structures and the lack of proper techniques.[91; 92] Methods developed to reversibly unfold and refold soluble proteins are not always useful for membrane proteins.[93] A variety of techniques have been developed or adapted to probe membrane protein unfolding, including analytical ultracentrifugation, FRET, disulfide cross-linking, and chemical and thermal denaturation.[92]

For soluble proteins, CD spectroscopy has been the method of choice to monitor protein thermal denaturation.[94] The ellipticity at a specific wavelength, usually a signature of a specific secondary structure type, is recorded upon heating. The unfolding of the protein leads to a reduction of the secondary structure content, and thus a reduction of ellipticity. But for α-helical membrane proteins, it is well-established that the transmembrane helices are highly stable and do not completely unfold even at temperature close to the boiling point.[95] Therefore, in many cases a clear transition point cannot be observed. In addition, the properness of using CD to monitor α-helical membrane protein unfolding is questionable, because the unfolded state of the protein could be a bundle of loosely associated helices. Therefore, the protein could have already unfolded with little change of the helical content being observed.

In a popular method used to investigate the thermal stability of membrane proteins, unfolding was monitored via the exposure of Cys residues and the subsequent reaction with (N-[4-(7-diethylamino-4-methyl-3-coumarinyl) phenyl] maleimide (CPM). CPM is a thiol-specific probe whose fluorescence emission intensity increased drastically upon the reaction with a sulfhydryl group in a protein.[96] The formation of a thioether and the concurrent attachment to the protein is revealed by a surge of fluorescence emission at 463 nm (excited at 387 nm). The presence of reactive free sulfhydryl groups in the protein structure is considered a prerequisite. Since free Cys residues are usually found in the hydrophobic core of a folded protein structure, the unfolding of the protein and subsequent exposure of the Cys is expected to greatly accelerate the thiol-specific reaction. The sensitivity and versatility of this method has made it a very convenient technique, which has been used to probe the stability of many membrane proteins.[97; 98]

Table 2.1 Melting temperature of membrane proteins determined using the CPM-thermal denaturation method.

Full name	Buffer condition	T_m (°C)	Reference
Fatty acid amide hydrolase (FAAH)	400 mM NaCl, 10% glycerol, 20 mM HEPES (pH 7.5), 0.1% (w/v) DDM	46	[96]
FAAH with inhibitor MAFP	400 mM NaCl, 10% glycerol, 20 mM HEPES (pH 7.5), 0.1% (w/v) DDM	58	[96]
Human apelin receptor (APJ receptor)	400 mM NaCl, 10% glycerol, 20 mM HEPES (pH 7.5), 0.1% (w/v) DDM	44.7-44.9	[96]
Rce1	20 mM MES, pH 6.5, 200 mM NaCl, 0.029% (w/v) UDM and 0.86% (w/v) OG	48.2	[99]
Connexin 26/ ATP binding cassette transporter MsbA	20 mM Tris (pH 8.0) and 1 M NaCl. 1% (w/v) detergent (DDM, FA-3, FA-4, or FA-5)	52	[100]

Table 2.1 Melting temperature of membrane proteins determined using the CPM-thermal denaturation method (continued).

5-hydroxytryptamine Receptor (5-HT_3R)	50 mM Tris/HCl, 125 mM NaCl, 0.010% (w/v) C12E9, pH 7.4	61	[101]
Human adenosine A2A receptor	0.1% (w/v) DDM, 0.1% (w/v) CHAPS, and 0.02% (w/v) cholesteryl hemisuccinate (CHS) in 50 mM sodium phosphate buffer (pH 7.0)	42	[97]
Nociceptin/orphanin FQ peptide receptor (ORL1)	50 mM HEPES (pH 7.5), 500 mM NaCl, 20 mM KCl, 10% glycerol (v/v), 5 μM C-24, and 5 × CMC of each detergent being tested.	41.4-61.4	[102]
Chemo-attractant receptor homologous	10 mM HEPES (pH 7.0), 5 mM NaCl, 0.0053% (w/v) Fos16	47-55	[103]
nociceptin/orphanin FQ peptide receptor ORL-1	50 mM HEPES (pH 7.5), 500 mM NaCl, 20 mM KCl, 10% glycerol (v/v), 5 μM C-24, 1 mM DDM supplemented with various sterols	56.6	[104]
Opsin	10 mM HEPES (pH 7.5), 100 mM NaCl, 0.1 mM $MgCl_2$, and 0.03% (w/v) DDM	60.4/56.3	[105]

Using the CPM thermal denaturation method, many research groups profiled membrane proteins and got their melting temperatures (Values of T_m from literature are shown in Table 2.1). However, it is an interesting phenomenon that most of the values cluster into a narrow range of temperature around 45 ºC to 55 ºC. A thorough understanding of the mechanism behind the observed signal changes is critical for the interpretation of the protein-unfolding data. Here we investigated the thermal-denaturation process of two α-helical membrane proteins, AcrB and AqpZ, under different experimental conditions using the CD and CPM assay (Figure 2.1). AqpZ and AcrB are inner-membrane proteins from *E.coli*. The structures of both proteins have been determined. AqpZ is a tetrameric water-specific aquaporin. It contains two free Cys residues, at positions 9 and 20.[106] AcrB is a trimeric

transporter and a component of the AcrAB-TolC multidrug efflux pump. It also contains two free Cys residues, C493 and C887, both in the transmembrane domain.[107] Our experimental results revealed that the transition temperature determined using the CPM assay was irrespective of the exact location of the Cys residues, which is inconsistent with what would be expected from the currently accepted mechanism. To further investigate the mechanism of the observed signal change, we investigated the thermal denaturation of two soluble proteins, ovalbumin and lysozyme (Figure 2.1).Ovalbumin was chosen because it contains four free Cys.[108] In contrast, lysozyme is a well characterized small soluble protein without free Cys.[109] The comparison of unfolding profiles monitored using the CD and CPM methods, and the comparison of unfolding profiles of wild-type and mutant proteins, provided valuable insight into not only the proteins under study, but also the mechanism of the CPM assay.

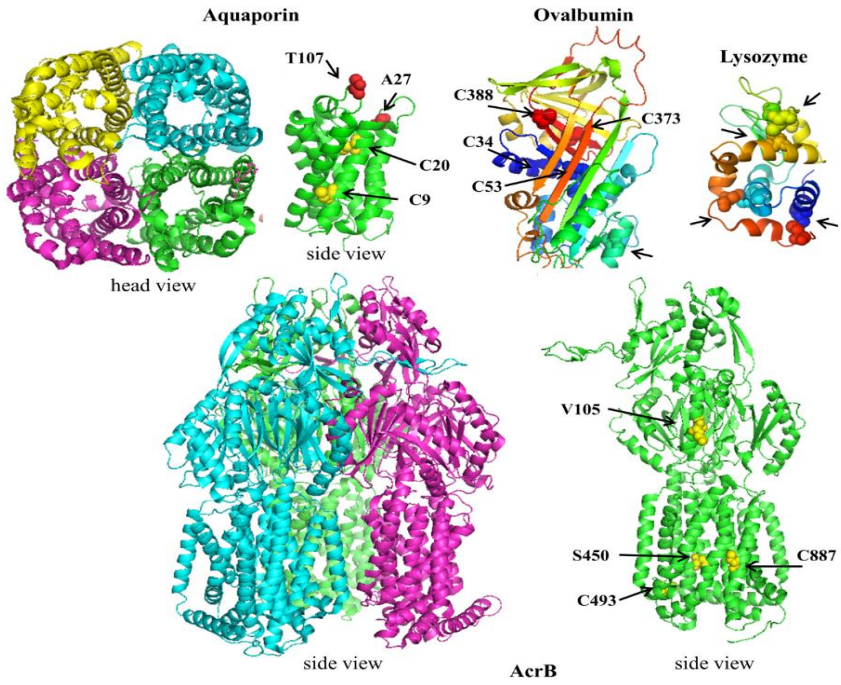

Figure 2.1 Structure of proteins used in this study. Free Cys residues are shown as spheres and their positions labeled. In AqpZ, T107 and A27 are also shown and labeled. Ovalbumin and lysozyme contain one and four pairs of disulfide bonds, respectively. These disulfide bonds are highlighted using spheres and their positions marked with arrows. For AqpZ and AcrB, the side view of an individual subunit was also shown to highlight the locations of Cys.

2.2 Materials and Methods

2.2.1 AcrB and Aquaporin Z (AqpZ) expression and purification

All reagents including ovalbumin and chicken egg white lysozyme were obtained from SIGMA (ST. LOUIS, MO) unless otherwise noted. All point mutations were introduced using the QuikChange Site-Directed Mutagenesis Kit following the instruction (AGILENT TECHNOLOGIES, SANTA CLARA, CA) and confirmed through DNA sequencing. All plasmids containing genes coding AcrB and its variants were transformed into a BW25113*ΔacrB* gene knockout strain for expression to avoid contamination from chromosomal AcrB in cells. A single colony from the transformed plate was picked and inoculated into 5 mL medium containing the appropriate antibiotics. After 8 hours of incubation, the medium was used to inoculate 400 mL LB medium and cultured at 37 ºC with shaking overnight. Target protein was purified immediately from the pellet when cells were harvested by centrifuge the next morning. The cell pellet was resuspended in the lysate buffer (20 mM phosphate buffer, 300 mM sodium chloride, pH 7.9) and then 0.5 mM phenyl-methane-sulfonyl-fluoride (PMSF) was added into the buffer to inhibit the serine protease in the cell lysate. Then the buffer containing cell pellet was sonicated for 20 minutes in ice/water bath with 5 s on/off intervals. The cell lysate was centrifuged at the

speed of 10000 rpm or 15317 ×g under 4 ºC for 20 minutes. 2% Triton X-100 was used to extract the protein AcrB from the membrane when the pellet was resuspended. After 2-hour shaking in ice bath, the solution was centrifuged at 10000 rpm for 20 minutes and the supernatant was transferred into a column containing Ni-NTA and 10 mM imidazole. The mixture was incubated with shaking in the 4 ºC freezer for 40 min to allow protein to bind with the Ni-NTA resin. Next, the column was drained, and washed with the lysis buffer supplemented with 50 mM of imidazole, before AcrB was eluted using the lysis buffer containing 0.5 M imidazole. The elution fractions were analyzed using SDS-PAGE to evaluate the purity and concentration of the samples. Fractions containing AcrB were collected and dialyzed overnight at 4 ºC against a dialysis buffer (20 mM phosphate, 0.3 M NaCl, 0.03% DDM (w/v), pH 7.9).

Gene encoding *aqpZ* was amplified from the genomic DNA of *E.coli* K-12 using PCR and inserted into plasmid pET28a between two restriction enzymatic sites (NdeI and XhoI). A vector-derived six-histidine tag was introduced at the N terminal of protein for the convenience of protein purification. Primers used in the construction of expression plasmids were as follows: 5'-CATATGTTCAGAAAATTAGCAGCTGAATGTTTTGG and 5'-CTCGAGTTAAT CACGCTTTTCCAGCAGGGTC with restriction enzymatic sites underlined. Cells were cultured at 37 °C in LB media containing 50 μg/mL kanamycin to an OD_{600nm} of approximately 0.6. The protein expression was induced by the addition of IPTG to a final concentration of 1 mM. After 5 hours, cells were harvested by centrifugation at 7,000×g for 10 min at 4 °C. Cell pellets were stored at -80 °C before purification. AqpZ was purified following the protocol described above for AcrB with

minor modifications. In the elution step, the elution buffer contained 0.25 M imidazole, 0.03% (w/v) DDM, 20 mM Na-phosphate, 0.3 M NaCl, pH 7.9. Protein samples were dialyzed overnight over the same buffer in the absence of imidazole at 4°C. The same buffer was used throughout this study as the assay buffer unless otherwise noted. Purity of proteins were examined using SDS-PAGE after Coomassie Blue staining. Protein concentration was determined using Pierce BCA Protein Assay Kit (THERMAL SCIENTIFIC INC., ODESSA, TX).[110]

2.2.2 Thermal denaturation analyses of model proteins

Thermal denaturation was measured by monitoring the ellipticity at 222 nm with the increase of temperature at 2.0 deg/min and recorded every 4ºC with 8 s equilibration time on a JASCO-J810 machine. For ovalbumin and lysozyme, the ellipticity readings at each temperature were converted into a folded percent by designating the readings at 4 and 98ºC as zero and 100% folded, respectively. For AcrB and AqpZ, the ellipticity was normalized against the reading at 4ºC to better represent the effect of mutations. Each experiment was performed at least three times and values of T_m were analyzed using the Boltzmann equation as described.[111; 96]

2.2.3 CPM fluorescence assay

N-[4-(7-diethylamino-4-methyl-3-coumarinyl) phenyl] maleimide (CPM) was purchased from Invitrogen (GRAND ISLAND, NY). The CPM reactivity experiment was conducted as described in literature with minor modifications.[96] Briefly, a DMSO solution of CPM was freshly made at a concentration of 4.0 mg/mL. It was diluted in the assay buffer by

40-fold to make a work solution of 100 μg/mL, which was kept on ice during the experiment. 30 μL of the CPM working solution was mixed with 570 μL assay buffer in which the final concentration of protein was 4 μM. The fluorescence signal excited at 387 nm and emitted at 463 nm was monitored upon heating. Fluorescence emission intensity was normalized against the maximum intensity. Each experiment was performed at least three times and values of T_m were analyzed using the Boltzmann equation as described.[111; 96] For studies with soluble proteins, DDM was left out from the assay buffer. To evaluate the effect of covalent interaction, 30 μL of the CPM working solution was mixed with 570 μL assay buffer containing 50 mM glycine (buffered at pH 8.0) and incubated at 80 ºC in the dark for 30 min. The samples were then cooled to 20ºC before lysozyme was added to a final concentration of 4 μM. The fluorescence intensity change upon heating was then monitored as described.

2.3 Results and discussion

2.3.1 Effect of pH on CPM fluorescence assay

To investigate the effect of pH on CPM fluorescence assay, the change of fluorescent intensity of samples containing CPM alone or CPM with ovalbumin were monitored at different pH (Figure 2.2). The result illustrated that CPM itself had a small fluorescence surge (Figure 2.2, *C*), which is much smaller than the intensity measured in the presence of ovalbumin. This surge is due to the hydrolysis of the maleimide group and is sensitive to the change of pH (Figure 2.2, *B*). For the five trials, from higher pH to lower pH, T_m shifted from 22 ºC, 36 ºC, 63 ºC, 70 ºC, to 79 ºC. The rate of hydrolysis depends on the pH of the solution, and at higher pH the hydrolysis showed a lower T_m. However, T_m of

samples containing both CPM and ovalbumin in different pH buffer were very close. These results indicated that the reactivity of CPM with sulfhydryl group in ovalbumin was not affected drastically by pH. In the following studies, a sodium phosphate buffer at pH 7.0 was used.

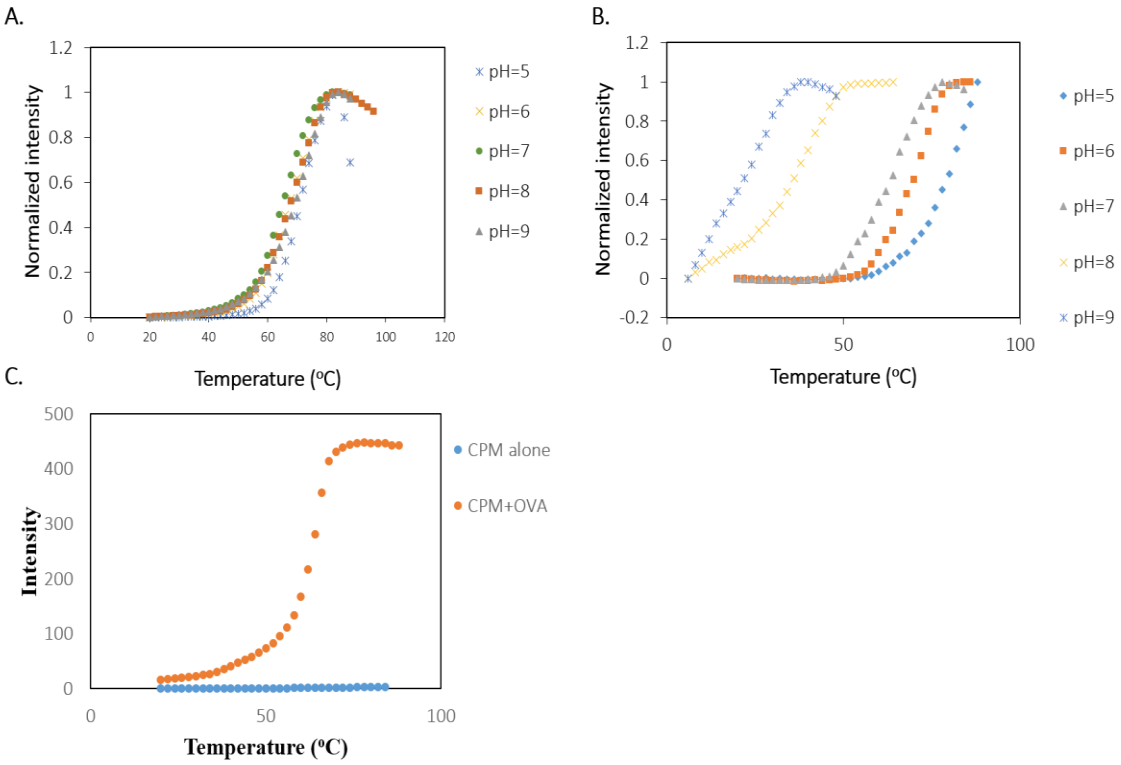

Figure 2.2 The effect of pH on CPM fluorescence assay. *A*. CPM in the presence of ovalbumin (Normalized). *B*. CPM alone (Normalized). *C*. CPM alone and CPM with ovalbumin in pH 7 buffer (original intensity).

2.3.2 Dilution of CPM dye with or without DDM

A stock solution of CPM (4 mg/mL) was routinely prepared in DMSO. It was first diluted into an aqueous solution to make a work solution, which was diluted further into samples for the assay. We found that it was important to have detergent of low concentration in the

work solution during the first dilution step, while it was not necessary to contain detergent in the final assay buffer. As shown in Figure 2.3, if there was no detergent included in the work solution but there was in the final assay buffer, the data were still wired with poor reproducibility.

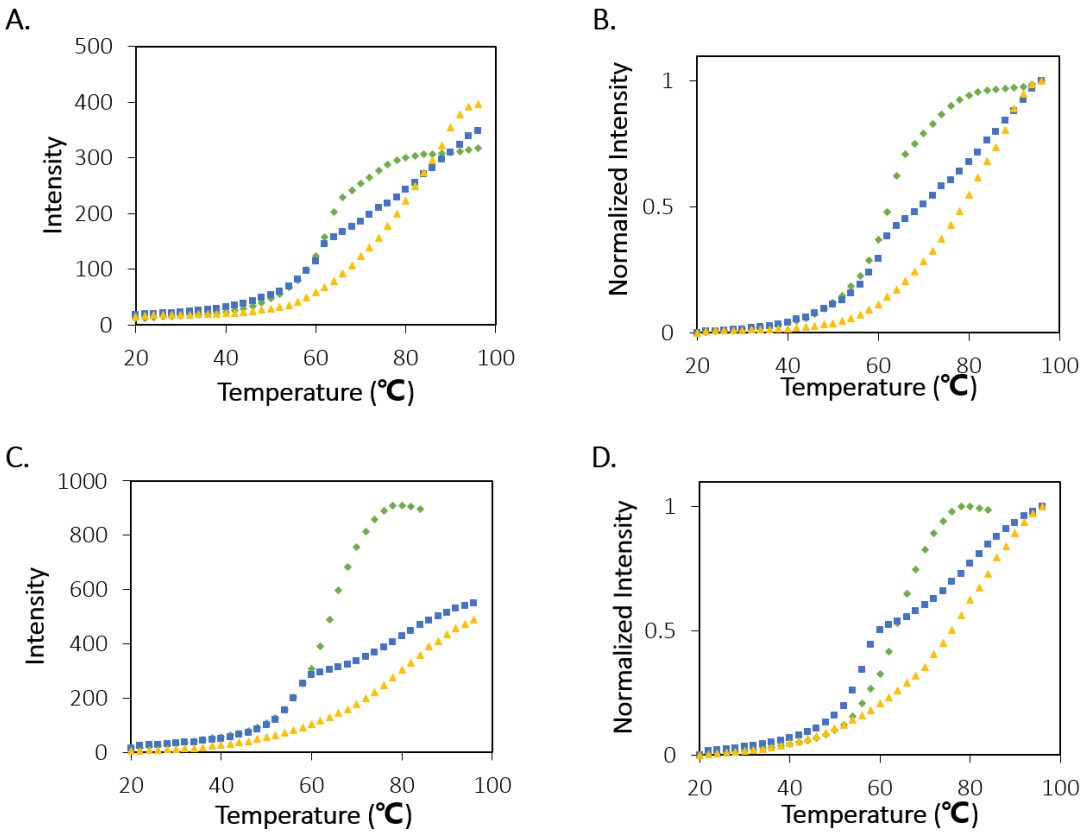

Figure 2.3 CPM assay of ovalbumin. CPM dye was diluted in pH 7 PB buffer in the work solution without any detergent. The three colored lines indicate three trials using the same diluted CPM dye. *A*. CPM assay was conducted in PB buffer, original fluorescence intensity. *B*. Normalized intensity data of Panel A. *C*. CPM assay in PB buffer with 0.03% (w/v) DDM. *D.* Normalized data of Panel C.

When detergent was included in the work solution but not in the final assay buffer, the

experimental result could be very reproducible (Figure 2.4). T_m of ovalbumin in phosphate buffer without DDM was 70.2 ºC ± 0.9 ºC while it was 64.6 ºC ± 0.5 ºC in phosphate buffer with 0.03% (w/v) DDM. We speculate that a small amount of detergent is necessary in the work solution to keep CPM soluble in water, so that it made the assays reproducible.

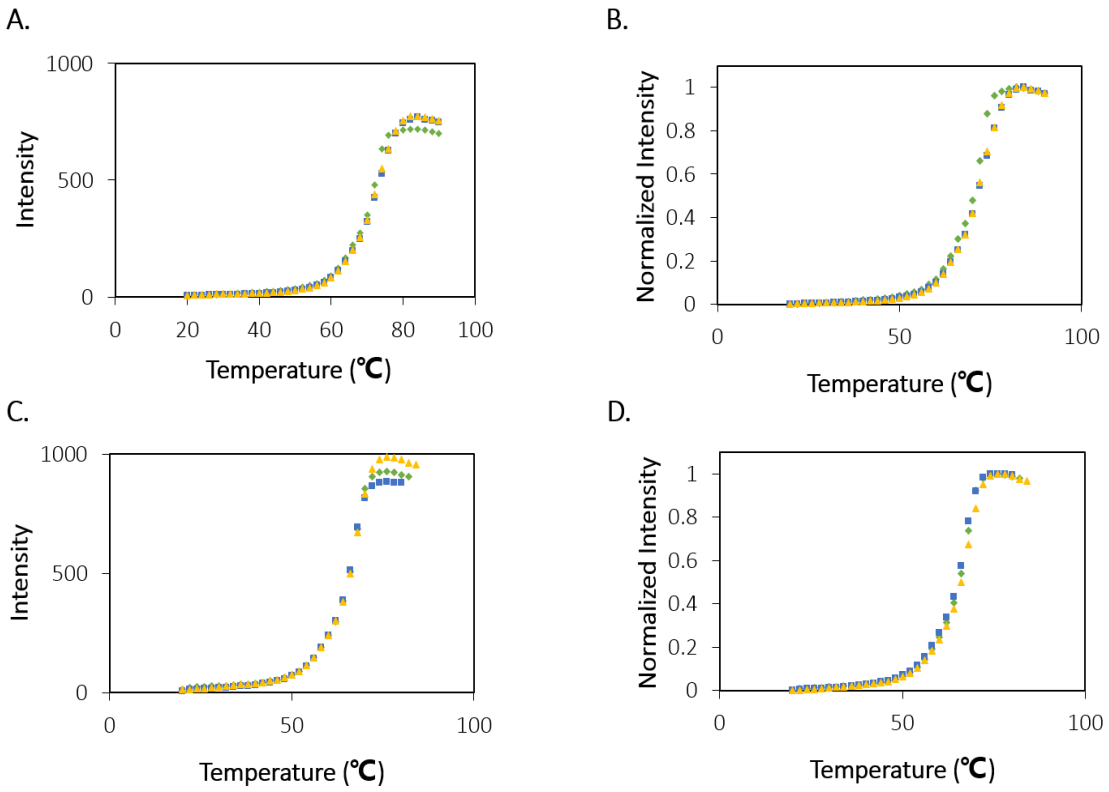

Figure 2.4 CPM assay of ovalbumin with DDM dissolved dye. CPM dye was diluted in PB buffer with 0.03% (w/v) DDM in the work solution. The three colored curves represent three repeat trials. *A*. CPM assay was conducted in pH 7 PB buffer without DDM, original fluorescence intensity is shown. *B*. Normalized data of Panel A. *C*. CPM assay was in pH 7 PB buffer with 0.03% (w/v) DDM. *D*. Normalized results of C.

2.3.3 Effect of other detergents on CPM dilution

To investigate whether other similar detergents had such an effect, SDS and Triton X-100

were tested. As DDM, the same concentration 0.03% (w/v) of the two detergents was used to dilute CPM dye and then CPM fluorescence assay of ovalbumin was conducted (Figure 2.5). T_m was measured to be 66.9 ºC ± 0.5 ºC when SDS was used in the work solution, while it was 66.0 ºC ± 1.3 ºC when Triton X-100 was used in the work solution. No detergent was included in the assay buffer. The final detergent concentration in the sample was 0.0015% (w/v). The requirement of detergents in the work solution was not specific, as all tested detergents worked equally well. Critical micelle concentration (CMC) is an important characterization index for a detergent. CMC of DDM, SDS and triton X-100 are 0.17 mM (0.009% w/v) 8.2 mM (0.2304%) and 0.24 mM (0.0155% w/v), respectively.[112; 113] Therefore, it is not necessary to use a detergent at a concentration higher than its CMC in the work solution. The lack of specificity further confirmed our speculation that a small number of detergent molecules are necessary to keep CPM fully soluble in the work solution.

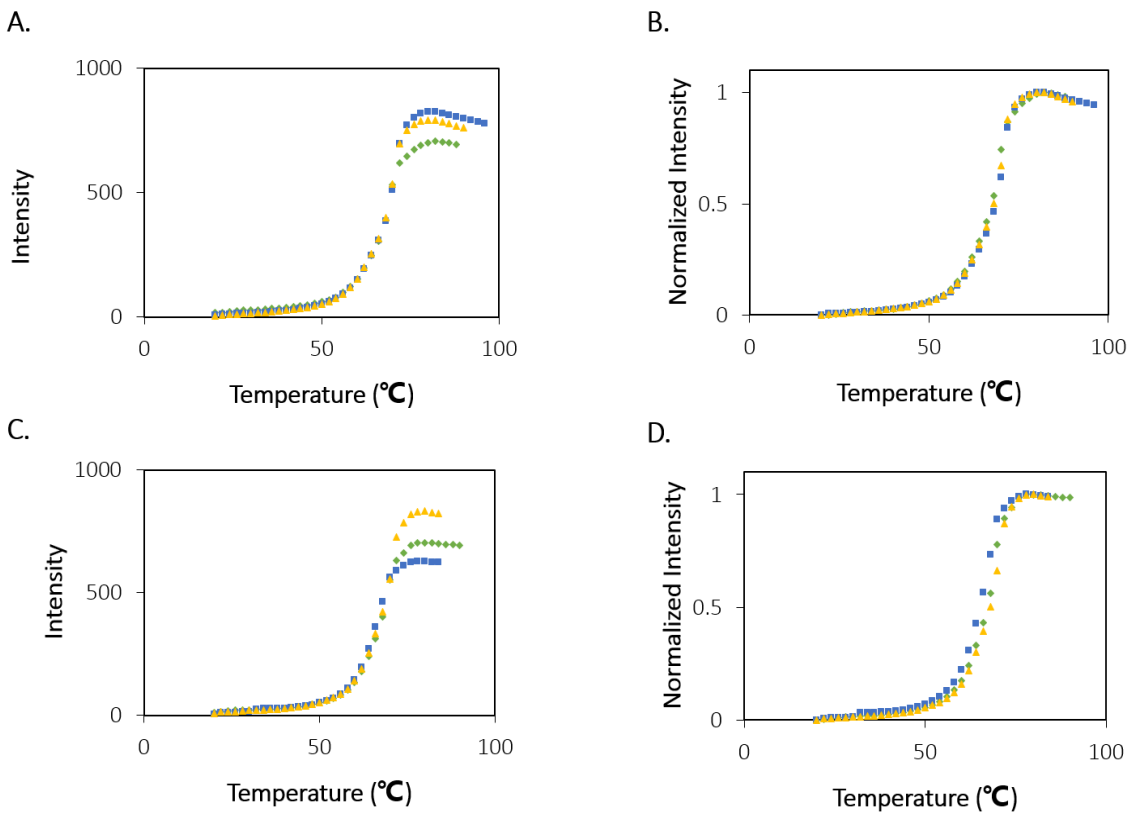

Figure 2.5 CPM assay of ovalbumin in a phosphate buffer. The three colored lines indicate three repeat trials. *A*. CPM dye was diluted in phosphate buffer with 0.03% (w/v) SDS in the work solution. *B*. Normalized results of A. *C*. CPM dye was diluted in phosphate buffer with 0.03% (w/v) Triton X-100 in the work solution. *D*. Normalized results of C.

2.3.4 CPM assay of AqpZ and its mutants

We have constructed two AqpZ mutants, AqpZ$_{A27P}$ and AqpZ$_{T107P}$. The original goal was to improve the stability of AqpZ, since the introduction of a Pro residue into the β-turns had been reported to have a stabilizing effect on proteins.[114] Both mutants could be expressed and purified at levels comparable to the wild-type protein. Wild-type AqpZ migrated as a tetramer in SDS-PAGE, as reported in literature.[115] Under the SDS-PAGE experimental condition, SDS did not abolish the non-covalent interaction between

neighboring subunits in the AqpZ tetramer. While $AqpZ_{T107P}$ also migrated as a tetramer, $AqpZ_{A27P}$ migrated as a monomer. This result suggested that the Ala27 to Pro mutation weakened the quaternary structure association. The thermal denaturation profiles of all three proteins were first measured using CD (Figure 2.6, *A* and *B*). AqpZ is a highly α-helical membrane protein. In the absence of urea, the helical content only decreased by a small portion upon heating. $AqpZ_{T107P}$ behaved similarly as the wild-type protein, while $AqpZ_{A27P}$ had a lower T_m and reached a higher level of unfolding at 98°C. To further investigate the relative stability of the three proteins, we repeated the experiment in the presence of 6 M urea. In the presence of 6 M urea, the T_m of wild-type AqpZ dropped by ~10°C. The three proteins had similar T_m and unfolded to similar levels. The difference between $AqpZ_{A27P}$ and the other two proteins disappeared. In summary, these results suggest that the Ala27 to Pro mutation decreased the oligomer stability, which subsequently caused the secondary structure to unfold at a lower temperature. In the presence of 6 M urea, while the melting temperature of all three proteins decreased, the difference between A27P and the other two proteins disappeared. We speculate the high concentration of urea must have disrupted the tetramer association, and thus eliminated the difference between the proteins.

Table 2.2 T_m of AqpZ and its mutants determined using the CD and CPM fluorescence assays in presence and in absence of 6M urea.

AqpZ construct	In absence of 6M urea		In presence of 6M urea	
	CD (ºC)	CPM assay (ºC)	CD (ºC)	CPM assay (ºC)
WT	>100	52.2 ± 0.3	>90	42.1 ± 0.6
A27P	>90	53.5 ± 0.1	>90	43.6 ± 0.6
T107P	>100	53.1 ± 0.2	>90	44.0 ± 0.6

Next, we repeated the thermal denaturation experiment and monitored protein unfolding using CPM fluorescence assay (Figure 2.6, *C* and *D*). The transition temperatures were much lower than those observed using CD (Table 2.2). While the lack of a plateau at the high temperature prevented the estimation of a melting temperate when monitored using CD, a clear transition followed by a plateau could be observed using the CPM fluorescence method. In addition, all three proteins behaved similarly both in the presence and absence of urea, indicating that the CPM method was not sensitive to the change of quaternary structure resulted from the A27P mutation. The presence of 6 M urea also decreased the T_m by approximately 10 ºC.

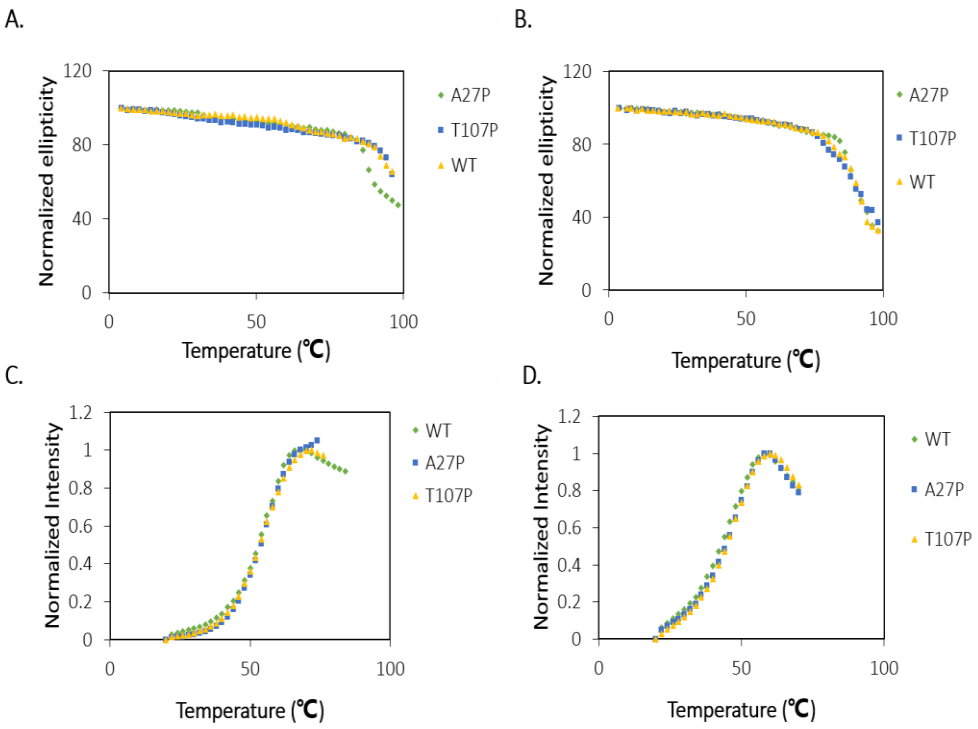

Figure 2.6 Unfolding study of AqpZ and its mutants. *A*. In the absence of urea, monitored using CD. *B*. In the presence of 6 M urea, monitored using CD. *C*. In the absence of urea, monitored using the CPM fluorescence assay. *D*. In the presence of 6 M urea, monitored using the CPM fluorescence assay.

2.3.5 CPM assay of WT-AcrB and its mutants

We have shown in previous studies that when monitored using CD, the thermal denaturation profile of AcrB does not display a clear transition point and a high helical content remains at 98 ºC.[110] Using the CPM assay, a clear transition point could be observed (Figure 2.7). To probe if the CPM assay is sensitive to the location of the reactive Cys, we created three mutants with a unique Cys at a carefully chosen position. We first replaced the two intrinsic Cys residues C493 and C887 from AcrB to create CL-AcrB. On the CL -AcrB background, we constructed two single Cys mutants, CL-AcrB$_{S450C}$ and CL-

$AcrB_{V105C}$. In addition, we constructed a third mutant by replacing C493 with Ala, so $AcrB_{C493A}$ also only contains one free Cys residue (C887). Locations of residues mentioned were shown in Figure 2.7. These sites represent Cys residues exposed at the trimer interface, in the soluble periplasmic domain (V105C) or transmembrane domain (S450C and C887). The other intrinsic Cys, C493, is hidden in the core of the transmembrane helix bungle. We expected the CPM thermal denaturation curve of different AcrB constructs to be different, depending on the exact location of the unique Cys residues. CD spectra of all mutants superimposed well onto the spectrum of WT-AcrB, indicating that the mutations did not lead to a drastic conformational change (data not shown). The CPM thermal denaturation plots of CL- $AcrB_{V105C}$, CL- $AcrB_{S450C}$, and $AcrB_{C493A}$ were similar to that of the wild-type AcrB, with T_m values within the error range to each other (Table 2.3 and Figure 2.7). Considering the difference in locations of the Cys residues, the CPM assay seemed to be insensitive to the location of the reactive Cys. Since it is generally considered that during thermal denaturation, previously hidden Cys becomes more exposed upon protein unfolding and accessible for CPM labeling, the insensitivity of T_m to the location of Cys seemed to be very odd.

Table 2.3 T_m of AcrB and its mutants determined using the CD and CPM fluorescence assays.

AcrB	T_m (^oC)
WT	52.8 ± 0.2
CL-V105C	54.3 ± 0.7
CL-S450C	54.5 ± 0.5
C493A (C887)	54.9 + 0.6
CL	56.6 ± 1.1

To further investigate the specificity of CPM labeling, we tested the thermal denaturation of CL-AcrB (Figure 2.7). Since there is no Cys in this protein, we used it as a control to investigate the necessity of Cys in the process. We found the peak intensity of CPM fluorescence was lower in CL-AcrB. In addition, the shoulder at a lower transition temperature, which was present in all AcrB constructs containing one or two Cys residues, was missing in the curve of CL-AcrB. We speculate that this lower temperature transition might correspond to the reaction of Cys with CPM, which is immediately followed by a second transition. Other than Cys, another possible residue for CPM labeling is Lys. Though at a lower rate, maleimide also reacts with the amino group. Among the 1049 residues in each AcrB subunit, there are 43 Lys. And since Lys is in general exposed on the surface of a protein, it is not surprising that it may also react with CPM during the thermal denaturation process. However, the reaction of surface exposed Lys with CPM should not require protein unfolding. Then what does the transition temperature in the melting curve actually reveal?

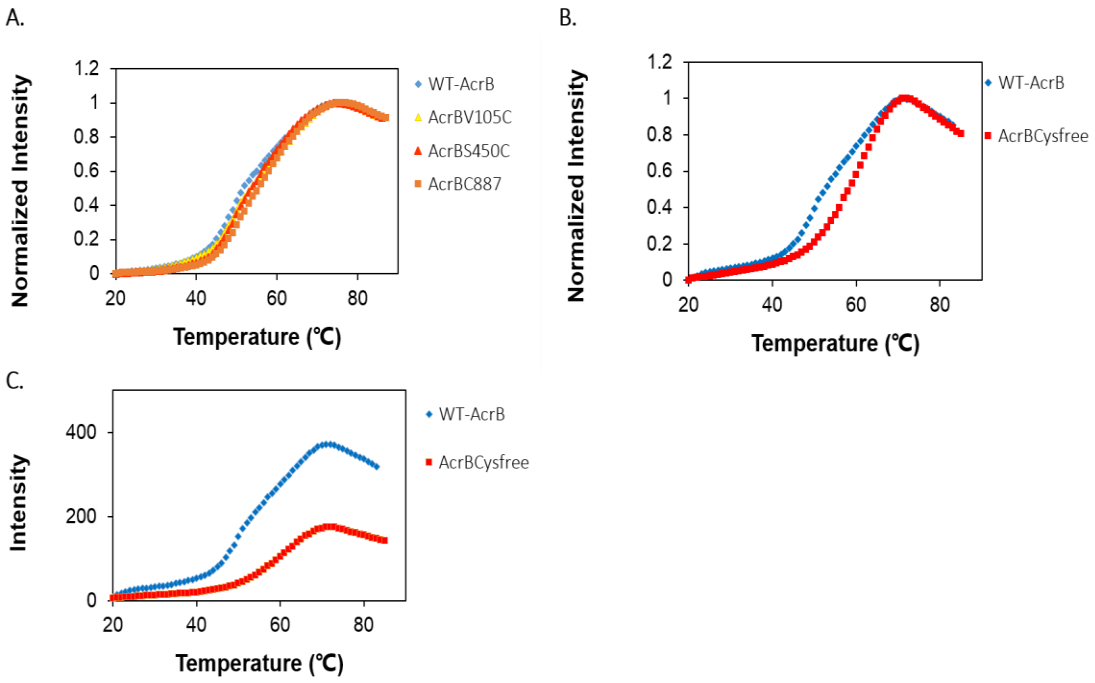

Figure 2.7 Thermal denaturation of AcrB and its mutants. *A*. CPM fluorescence assay of WT-AcrB, $AcrB_{V105C}$, $AcrB_{S450C}$ and $AcrB_{C887}$ (actually $AcrB_{C493A}$). *B*. Normalized data for CPM assay of WT-AcrB and CL-AcrB. *C*. CPM assay of WT-AcrB and CL-AcrB.

Table 2.4 MICs of BW25113ΔacrB containing plasmid encoding the indicated AcrB constructs.

Strain	MIC(μg/mL)	
	Erythromycin	Novobiocin
WT-AcrB	160	160
$AcrB_{V105C}$	40	40
$AcrB_{S450C}$	160	80
$AcrB_{C887}$	160	80
$AcrB_{D795C}$	160	80
ΔacrB	20	40

2.3.6 CPM assay of urea denatured ovalbumin

To understand the nature of the fluorescence surge in the CPM assay, we continued our study using two soluble proteins, ovalbumin and lysozyme. With the increase of temperature, the detergent in the membrane protein studies may lead to artifacts and interfere with the experimental result. By using soluble proteins, we could exclude detergent from the assay buffer and thus eliminate a potential source of artifact. Thermal denaturation of ovalbumin was monitored using both CD and CPM. As shown in the CD wavelength scan in Figure 2.8, ovalbumin retained certain secondary structure component even at the maximum temperature tested (98 ºC). The structure transition occurred at a T_m of 66.3 ± 1.9 ºC. When temperature rose to 80 ºC, protein structure no longer changed. The thermal denaturation curve of ovalbumin approached a plateau at approximately 80 ºC as well when monitored using the CPM method, with a T_m of 65.0 ± 0.2 ºC. Therefore, the melting temperature of ovalbumin measured using these two methods were in good agreement. This result validated the CPM assay as an approach to reveal protein stability.

Table 2.5 T_m of soluble proteins determined using the CD and CPM fluorescence assay.

Urea (M)	CD (ºC)	CPM assay (ºC)
Ovalbumin		
0	66.3 ± 1.9	65.0 ± 0.2
2	61.5 ± 1.3	49.2 ± 0.4
4	57.1 ± 1.3	42.2 ± 0.5
6	51.9 ± 0.4	37.4 ± 0.5
Lysozyme		
0	74.2 ± 0.4	72.4 ± 0.2

To gain more insight into the nature of the CPM detection method, we repeated the thermal denaturation measurement in the presence of urea. Thermal denaturation was performed in the presence of 2, 4, or 6 M of urea, and monitored using CD and CPM fluorescence. The T_m under each condition was determined and listed in Table 2.5. The presence of a high concentration of urea prevented the collection of the CD spectra to wavelengths lower than 210 nm. However, it was clear that less secondary structure presented in the protein at 98 ^oC when urea was present (Figure 2.8). In addition, while the T_m determined from CPM fluorescence and CD methods were consistent in the absence of urea, the melting temperatures determined in the presence of urea were quite different. The presence of urea led to a much larger decrease of the melting temperature when monitored using CPM fluorescence. This result suggests that the presence of urea has a larger effect on the disruption of the hydrophobic core of ovalbumin than on the unfolding of the secondary structure. Even though high concentration urea and high temperature were used in denaturation of ovalbumin, the secondary structure did not completely unfold. Comparing to the secondary structure which was mostly α-helix at 4 ^oC, the secondary structure at 98 ^oC was mostly β-sheet.

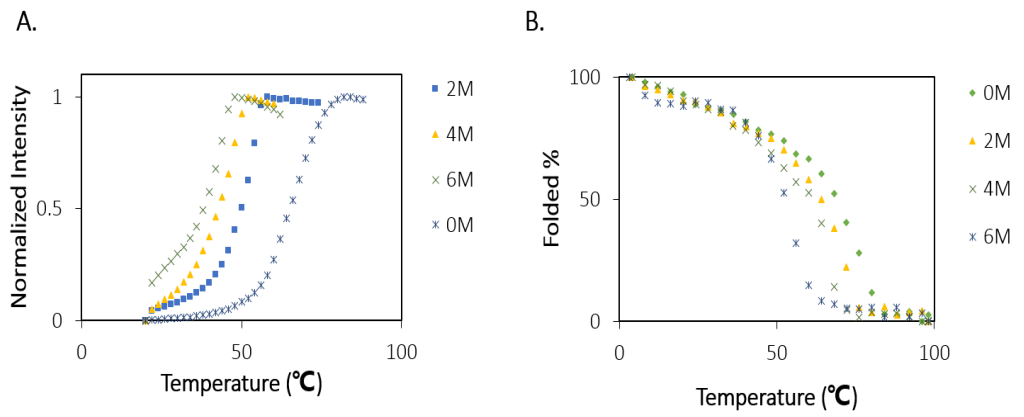

Figure 2.8 Study of ovalbumin unfolding with CPM assay and CD. A. Ovalbumin denaturation monitored using CPM assay in the presence of 0 M, 2 M, 4 M or 6 M urea. B. Urea denaturation of ovalbumin was monitored using CD. The concentration of urea solution was 0 M, 2 M, 4 M and 6 M.

In summary, ovalbumin thermal denaturation monitored using CPM assay and CD were comparable in absence of urea. T_m obtained from these two methods were almost the same and the end points where the state transition finished were similar. In CD melting experiment, the secondary structure shifted from α-helix to β-sheet after high temperature denaturation while the overall unfolding of ovalbumin finished at about 80 ℃. The plateau of CD melting curve matched the end point of CPM assay, indicating that the structure transition completed at the same temperature 80 ºC. However, in presence of urea, ovalbumin denaturation temperature monitored using CPM assay and CD displayed different results. The plateau of CD did not match the end point in CPM assay, indicating the structure transition did not finished at the same temperature. CPM assay monitors the opening up of the tertiary structure, while CD monitors the change of secondary structure. The effect of urea on protein structure seemed to be different at these two levels in

ovalbumin.

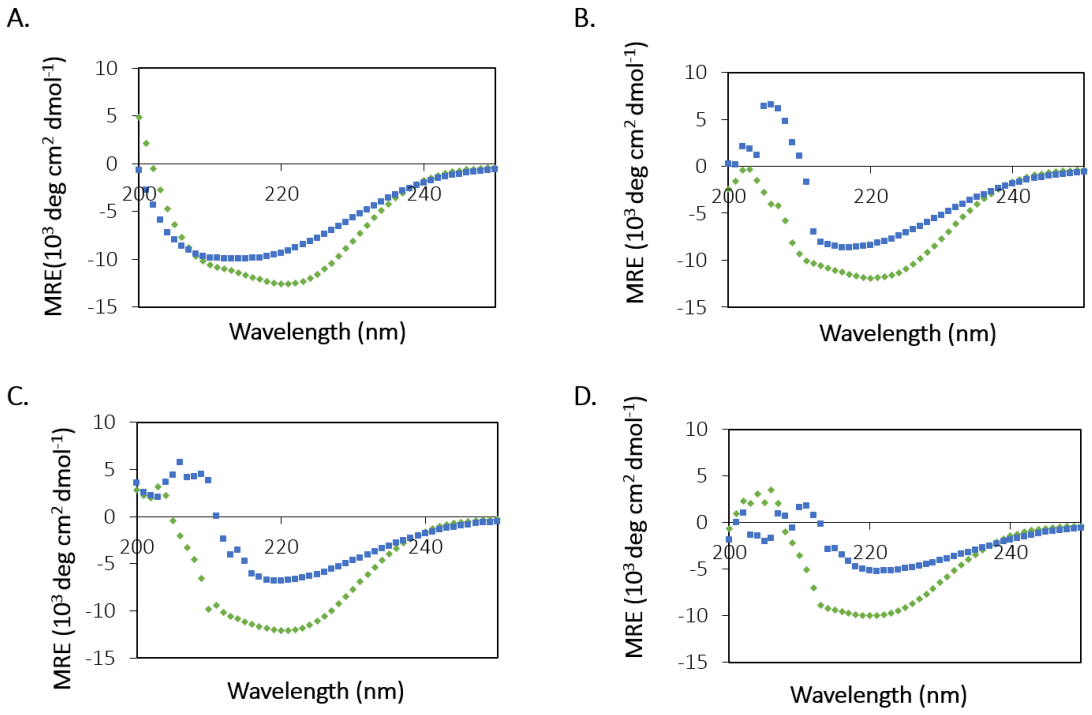

Figure 2.9 Wavelength scan of ovalbumin in the absence or presence of urea at different concentrations at 4 ºC (green) and 98 ºC (blue). *A.* In PB buffer, no urea. *B*. In 2 M urea. *C.* In 4 M urea. *D.* In 6 M urea.

2.3.7 CPM assay of lysozyme

To investigate the specificity of the CPM reaction, we chose another well-characterized soluble protein to measure its melting temperature. Chicken egg white lysozyme is a small soluble protein of 129 residues with four pairs of disulfide bond but no free Cys. It contains 6 Lys residues, all exposed to the surface of this small globular protein. Thermal denaturation of lysozyme was monitored using both the CD and CPM fluorescence method. The melting temperatures were very similar (Table 2.5).

To exam if the reaction and formation of a covalent bond is important for the measurement, we first blocked the maleimide group in CPM using a pretreatment in the presence of a high concentration (50 mM) of glycine, and then monitored the fluorescence intensity of the treated CPM in the presence of lysozyme upon heating (Figure 2.10). The initial fluorescence intensity was much higher than CPM without pre-treatment, due to the chemical reaction between maleimide and glycine. As monitored earlier, reaction of the maleimide group led to an increase of fluorescent signal. With the increase of temperature, the fluorescent intensity first gradually decreased due to a non-specific collision quenching effect. At the transition point of lysozyme unfolding, a sharp increase of the fluorescence could still be observed, indicating that the observed fluorescence increase did not require covalent attachment of the fluorophore to the protein. In the control samples lacking lysozyme, or in the presence of just DTT, a peak could not be observed. These results confirmed that the peak observed was actually due to interaction between CPM and lysozyme.

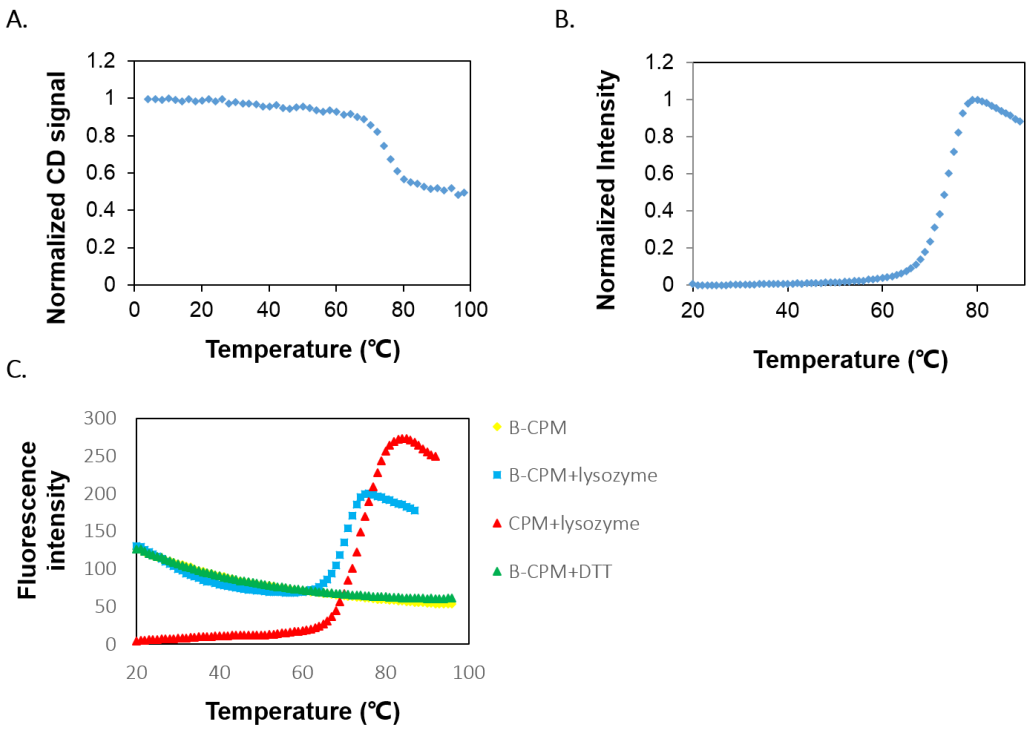

Figure 2.10 Thermal denaturation of lysozyme. *A*. Denaturation monitored using CD at 222 nm. Ellipticity at different temperatures was converted into a folded percentage as described in Materials and Methods. *B*. Normalized fluorescence intensity during denaturation as monitored using the CPM assay. *C*. Interaction of pre-treated CPM with lysozyme (blue squares). Pre-treated CPM in the assay buffer (yellow diamonds) and in the presence of 1 mM DTT (green triangles) were shown as controls. The curve of lysozyme reacted with CPM not subjected to pre-treatment was also shown again as a control (red triangles).

2.3.8 CPM kinetics study of AcrB quaternary structure

To investigate the usefulness of the CPM fluorescence method in detecting protein quaternary structure stability, we monitored the increase of CPM fluorescence over time at a constant temperature (30 °C). We used five AcrB constructs in this study, the wild-type

(WT) protein and four mutants, W13C, W895C, W13C/P223G, and W895C/P223G. All four mutants were created on the CL-AcrB background. W13 and W895 belong to transmembrane helices 1 and 8, respectively. Both are on the inter-subunit interface in the transmembrane domain. We have shown that W13C and W895C mutations do not affect AcrB function, indicating that the mutants still exist as trimers.[116] The P223G mutation has been shown previously to disrupt AcrB trimer stability.[114] Therefore, CL-AcrB$_{W13C}$ and CL-AcrB$_{W895C}$ are trimers, while the corresponding P223G mutants are monomers. The increase of the CPM fluorescence signal in the presence or absence of proteins was monitored at 30 ºC for 2 min with excitation and emission wavelengths of 387 and 463 nm, respectively (Figure 2.11, *A*). The slopes of the traces were determined, which reflected the rate of CPM reaction with the protein (Figure 2.11, *B*). The reaction rates between CPM and CL-AcrB$_{W13C}$ or CL-AcrB$_{W895C}$ were similar to the rate of CPM reaction with wild-type AcrB, which was significantly slower than the reaction rate with the corresponding P223G mutants (Figure 2.11, *B*). This observation is consistent with the expectation from their quaternary structure, indicating that the CPM fluorescence method in the kinetic mode could reveal information about protein quaternary structure stability.

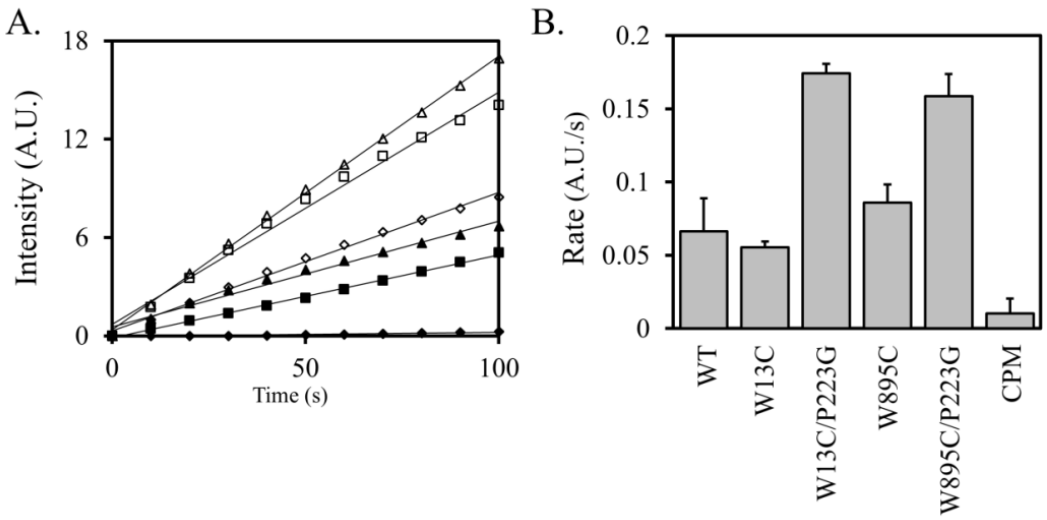

Figure 2.11 Kinetics of CPM-AcrB interaction. *A*. Representative traces of CPM fluorescence intensity increase over time in the absence (black diamonds) or presence of wild-type AcrB (black triangles), CL-AcrB$_{W13C}$ (black squares), CL-AcrB$_{W13C/P223G}$ (open triangles), CL-AcrB$_{W895C}$ (open diamonds), CL-AcrB$_{W895C/P223G}$ (open squares). *B*. Rate as obtained from the slope of the traces. Each experiment was conducted at least three times. The average values and standard deviations are shown.

2.4 Discussion and conclusion

In this study, we investigated the thermal denaturation of four proteins using the CD and CPM fluorescence methods. This study was prompted by the observation that the T_m of membrane proteins determined using the CPM fluorescence method reported in literature are closely clustered, with most of them in the temperature range of 45-55 ^oC (Table 2.1). The melting temperatures of AqpZ and AcrB were found to be in the range as well. If this narrow range of stability is not a measurement artifact, then it may reflect the fact that the cell membrane is a somewhat limited environment, which eliminated the requirement of a large variation of protein thermal stability. Another possibility is, the intrinsic differences

between membrane proteins were not faithfully reflected when probed in detergent micelles. It has been established that the T_m is sensitive to the presence of different lipid molecules. Another interesting observation is the different effect of urea on T_m measured using CD or the CPM method. For example, in the absence of urea, T_m of ovalbumin was similar when measured with the two methods. However, in the presence of 2 M urea, the T_m dropped by 5ºC and 15ºC, respectively, when measured using the CD or the CPM assay. The first step of protein unfolding was the expansion of the hydrophobic core, in both thermal denaturation and urea denaturation.[117] The presence of urea during thermal denaturation clearly lowered the energy barrier for the disruption of the hydrophobic core, allowing easier access for the fluorescence probe.

Based on our study, we found that the T_m measured using the CPM assay does correlate with protein unfolding, although the exact mechanism of fluorescence surge was not as previously proposed. In a sense, this makes the method even more useful, since the presence of free Cys residues is no longer a prerequisite. The chemical reaction and subsequent covalent attachment is not critical for the observed increase of fluorescence signal. This mechanism can also explain the observed lack of sensitivity to neither the exact location of reactive Cys nor protein quaternary structure. The CPM fluorescence surge reflects the expansion of the hydrophobic core and oligomer dissociation is not likely to generate such an effect. Different locations of cysteine showed different CPM reaction rate, indicating that CPM thermal stability assay could be used to evaluate protein quaternary structure.

As discussed above, CPM could be coupled with thermal denaturation to monitor protein

unfolding. Here we also investigated the usage of CPM to study protein quaternary structure through monitoring the kinetics of labeling. According to the location of a cysteine in a protein, the accessibility for CPM is different. Therefore, we expect to observe different reaction rate. Based on this analysis, measurement of fluorescence increase over time will provide insight into the accessibility of a specific Cys residue. When coupled with careful design for the location of the reporter Cys residue, information can be obtained regarding protein quaternary structure.

Chapter III. Repressive Mutations Restore Function-loss Caused by the Disruption of Trimerization in *Escherichia. Coli* Multidrug Transporter AcrB

Part of this chapter are taken from "REPRESSIVE MUTATIONS RESTORE FUNCTION-LOSS CAUSED BY THE DISRUPTION OF TRIMERIZATION IN *ESCHERICHIA COLI* MULTIDRUG TRANSPORTER ACRB", 2015, *Frontiers in Microbiology*. 6, 4.[122]

3.1 Introduction

Escherichia coli transporter protein AcrB as well as its homologues are the inner membrane components of the RND family efflux pumps.[118] AcrB, together with membrane fusion protein AcrA and outer membrane protein TolC, forms a tripartite pump system. The proper function of AcrB requires the accurate assembly of the tripartite complex. While extensive studies have been conducted to understand substrate binding, proton relay, and interaction between AcrB with AcrA/TolC, relatively less effort has been devoted to investigating the trimerization of AcrB and the relationship between trimerization and other functional aspects.

To date, more than 30 crystal structures of AcrB, with or without substrates, have been deposited in the Protein Data Bank. AcrB is an obligate asymmetric homo-trimer.[119] Each protomer consists of 12 transmembrane helices (TMH, transmembrane domain) and two large periplasmic loops (LPL, periplasmatic domain) with more than 300 amino acids (Figure 3.1, *A*).[46] The first LPL (LPL1) locates between TMH1 and TMH2, while the second LPL (LPL2) locates between TMH7 and TMH8. In translocation of protons, important residues such as D407, D408, K940, and T978 could form salt bridge/hydrogen bonding networks among TM4, TM10, and TM11 (Figure 3.1, *B*).[120] Mutations D407A, D408A, K940A, and T978A disable AcrB pump by distorting or disrupting the regular H-

bonding interactions of the backbone H and C=O groups characteristic of α-helix.[120]

The fact that a long-extended loop in one AcrB subunit also inserts into the neighboring subunit is clearly critical to the formation of AcrB trimer. Relatedly, through mutations and truncation of such loop, we have created a well-folded monomeric AcrB mutant. Our group has found that a single Pro223 to Gly mutation is sufficient to disrupt trimerization resulting in a drastic loss of function.[110]

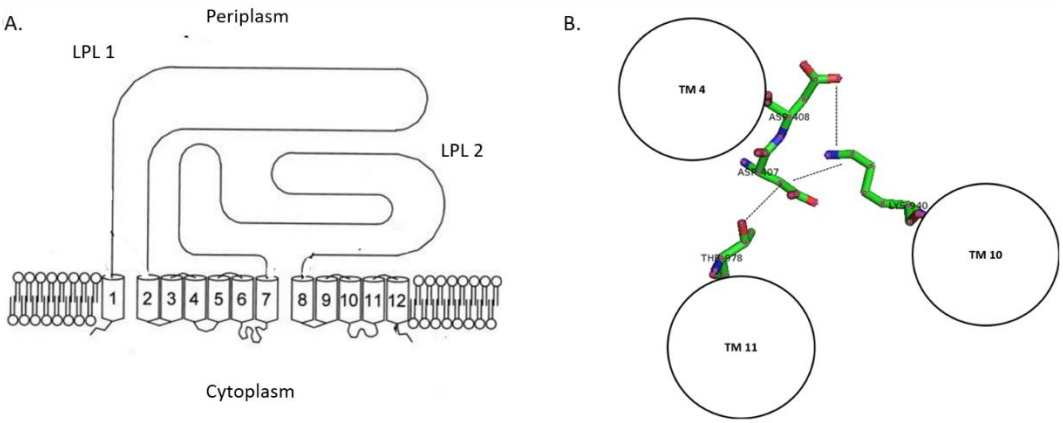

Figure 3.1 *A.* Topological model for AcrB efflux pump, showing two LPLs. Taken from the reference with minor modification.[121] *B.* Model for putative salt bridge/hydrogen-bonding network D407-D408-K940-T978 in AcrB protomer, modified from PDB file 1IWG according to reference. The size and location of TM and residue are not shown in scale.[120]

To advance our understanding about interactions that stabilize AcrB trimer, random mutagenesis was conducted to identify suppressor mutations that restore functions to $AcrB_{P223G}$. Nine single mutations were found to restore the function of $AcrBP_{223G}$ (Table 3.1). We originally expected the suppressor mutant to restore function by strengthening the

trimer association, as we hypothesized that the loss of activity in AcrB$_{P223G}$ was due to reduced trimer affinity. However, purification and blue native-PAGE (BN-PAGE) analyses showed that none of the mutants significantly improved the content of AcrB trimer.

Table 3.1 The results of drug susceptibility assay of AcrB mutants.[122]

Plasmids	MIC (μg/ml)				
	Ery	Nov	Tet	TPP	R6G
pQE70-AcrB (positive control)	128	320	2.56	320-640	>640
pQE70-AcrB$_{P223G}$	8	40-80	0.64-1.28	20-40	40-80
pQE70-AcrB$_{P223G/T199M}$	128	160	2.56	320-640	>640
pQE70-AcrB$_{P223G/A209V}$	64	80	1.28	40-80	>640
pQE70-AcrB$_{P223G/D256N}$	32-64	160-320	2.56	320	>640
pQE70-AcrB$_{P223G/G257V}$	64	160	2.56	80-160	>640
pQE70-AcrB$_{P223G/M662I}$	64-128	80	1.28	160	160
pQE70-AcrB$_{P223G/Q737L}$	64	160	2.56	160-320	>640
pQE70-AcrB$_{P223G/D788K}$	128	160	2.56	160-320	160-320
pQE70-AcrB$_{P223G/P800S}$	64	80	1.28	40-80	>640
pQE70-AcrB$_{P223G/E810K}$	128	160	2.56	160-320	>640

Here we investigated the mechanism of function restoration of the suppressor mutants. The suppressor mutants could be clustered according to their location. Eight out of the nine mutants (Figure 3.2) which restored the activity of AcrB$_{P223G}$ locate in the docking domain. The last mutation M662I is in the porter domain, which is far from the outer membrane channel protein TolC, so we chose this mutation as our research objective.

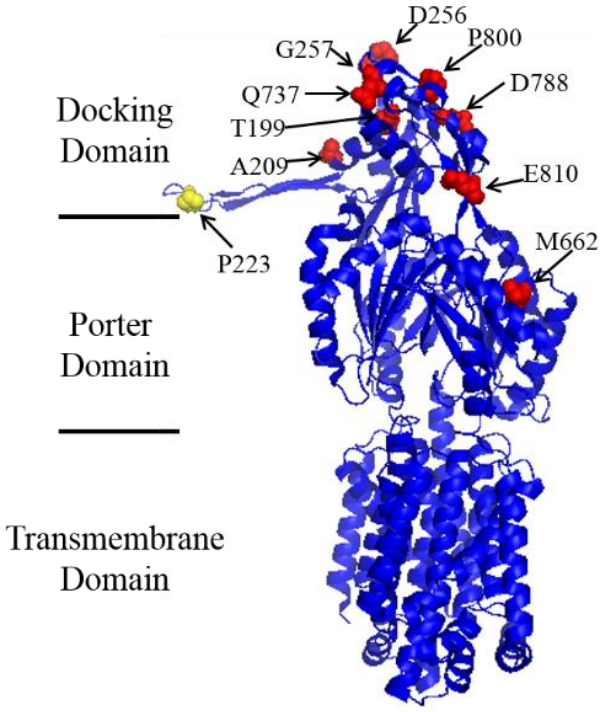

Figure 3.2 Structure of AcrB monomer. P223 is colored in yellow while suppressor mutants are colored in red.

3.2 Materials and Methods

3.2.1 Sited directed mutagenesis, expression and purification

Sited directed mutagenesis, protein expression and purification were conducted as described in section 2.2.1.

3.2.2 Analyses of secondary structure using circular dichroism (CD) spectroscopy

The secondary structure of AcrB variants were characterized with CD spectroscopy conducted on a JASCO J-810 spectrometer. The protein samples were dialyzed into a low salt buffer (10 mM sodium-phosphate, 50 mM NaCl, 10% glycerol, 0.03% DDM, pH 7.5) before the CD measurement. Blank scans were collected using the dialysis buffer. The spectrum wavelength scans were collected from 255nm to 195nm in a 1 mm path-length cuvette. CD thermal denaturation experiments were performed using the same spectrometer with a PELTIER temperature controller as described.[123] Thermal denaturation was measured by monitoring the ellipticity at 222 nm with the increase of temperature at 2.0 ºC/min and recorded every 4 ºC with 8 s equilibration time.

3.2.3 Cross-linking of AcrA-AcrB in intact cells

The plasmid *pET22* containing *wild type acrA (wt-acrA)* was co-transformed into *acrA/acrB* knockout strain with the plasmid *pBAD33* containing *wt-acrB*, or $acrB_{P223G}$, or $acrB_{P223G,M662I}$ for expression. A single colony was picked from a freshly transformed plate and grown with shaking at 37°C in 3 ml LB medium containing 100 μg/ml of ampicillin and 50 μg/ml of kanamycin for 8 hours. 2 ml of this cell culture was used to inoculate 200 ml LB medium containing 100 μg/ml of ampicillin and 50 μg/ml of kanamycin overnight. Cells were harvested by centrifugation at 5000×g for 10 min. The cell pellet was resuspended in 10 ml cross-linking buffer (20 mM sodium phosphate, 300 mM NaCl, pH 7.2) and incubated with 0.4 mM dithiobis succinimidyl propionate (DSP) cross-linker at 37°C for 30 min. After quenched with 20 mM Tris, cells were centrifuged, harvested and resuspended in lysis buffer (20 mM Tris-HCl, 300 mM NaCl, pH 8.0). The proteins were

purified as described in the previous paragraph.

3.2.4 Chemical denaturation

Unfolding of AcrB by chemical denaturants was monitored as described with slight modification.[124] Briefly, protein unfolding was initiated by titrating concentrated urea (8.0 M) or SDS (0.2% or 2%, w/v) into 400 μL of freshly purified AcrB in the dialysis buffer (20 mM phosphate, 0.3 M NaCl, 0.03% (w/v) DDM, pH 7.5). A fluorescence emission spectrum between 300 to 400 nm was recorded at each titration point with a LS-55 fluorescence spectrometer (PerkinElmer, Inc., Waltham, MA) with excitation wavelength of 280 nm. The intensity of the fluorescence peak was collected and converted into fraction of protein folded through normalizing to the reading before the addition of the denaturant, and plotted as a function of urea molar concentration or SDS/DDM molar ratio. A titration plot of L-tryptophan with SDS was used as a control to confirm the lack of a non-specific effect of SDS on fluorescence emission.

3.2.5 CPM thermal stability assay

The CPM reactivity experiment was conducted as described in literature with minor modifications.[96] Briefly, a DMSO solution of CPM was freshly made at a concentration of 4.0 mg/mL. It was diluted in the assay buffer by 40-fold to make a work solution of 100 μg/mL, which was kept on ice during the experiment. 30 μL of the CPM working solution was mixed with 570 μL assay buffer in which the final concentration of protein was 4 μM. The fluorescence signal excited at 387 nm and emitted at 463 nm was monitored upon heating. Fluorescence emission intensity was normalized against the maximum intensity.

Each experiment was performed at least three times and values of T_m were analyzed using the Boltzmann equation as described.[111; 96]

3.3 Results

3.3.1 Analyses of secondary structure with CD

To investigate whether the second mutation M662I had any influence on the secondary structure of $AcrB_{P223G}$, CD was conducted according to the protocol as described in method. CD is a spectroscopic technique measuring the differential absorption of left and right-hand circular polarized light for certain chiral molecules. For proteins, CD provides a lot of information including secondary structure composition, tertiary structure fingerprint, integrity of cofactor binding sites, conformational changes, and protein folding and conclusion about the overall structure. Far-UV CD spectra (240 nm and below) is useful to analyze the secondary structure of proteins, because different spectra are associated with different secondary structure types: α-helix, β-sheet, β-turn, irregular structure, etc.[125; 94] CD analysis was conducted to evaluate the second structures of the three proteins WT-AcrB, $AcrB_{P223G}$ and $AcrB_{P223G/M662I}$ at the same concentration of 0.37 μM (Figure 3.3). The original unit of millidegree "mdeg" was converted into mean residue ellipticity (MRE) according to the following equation:

$$[\theta] = \frac{\theta}{10 \times c \times l}$$

where [θ] with a unit of "degree•cm^2/$dmol^{-1}$" indicates MRE, θ indicates mdeg obtained from the spectrometer, c is the molar concentration of the sample (mol/L), and l is the pathlength in cm.[126] Two negative peaks around 208 nm and 222 nm and one positive peak at around 193 nm which are characteristic peaks for α-helices were present.[127] The

secondary structures of the three proteins were almost identical according to the CD spectra obtained, which suggested that the second mutation M662I did not have an observable effect on the secondary structure.

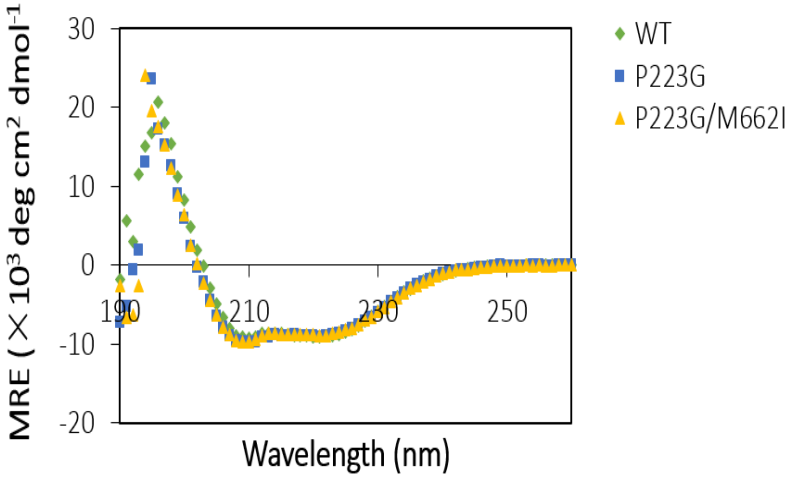

Figure 3.3 CD spectra of WT-AcrB, AcrB$_{P223G}$ and AcrB$_{P223G/M662I}$.

3.3.2 Chemical cross linking of AcrA-AcrB in intact cells

Another factor which may result in the recovery of the efflux function of AcrB$_{P223G}$ is that the mutation M662I may increase the interaction between AcrB and its partner proteins AcrA or TolC. Here we used chemical cross-linking to determine whether M662I improved the interaction. Chemical cross-linking is a useful technique for probing the interaction between proteins in large protein complexes.[128] Several types of cross-linkers have been applied to identify the cross-linked products, such as isotope-labelled cross-linkers or proteins, fluorogenic cross-linkers and cleavable cross-linkers.[129] Among them, DSP, an amine-reactive cross-linker having NHS-ester reactive ends and a cleavable disulfide bond

in its spacer arm,[130] was used as cross-linker to investigate the potential effect of M662I on the interaction between AcrA and AcrB in cells in the study. The experiment was conducted as described in Materials and Methods, and SDS-PAGE and Western blot were used to quantify the amount of AcrA crosslinked with $AcrB_{P223G}$ and $AcrB_{P223G/M662I}$. WT-AcrB was used as the positive control (Figure 3.4). The levels of AcrA cross-linked, and thus pulled down by AcrB, were similar. This result did not support the hypothesis that the repressor mutation restore function via improving interaction with AcrA.

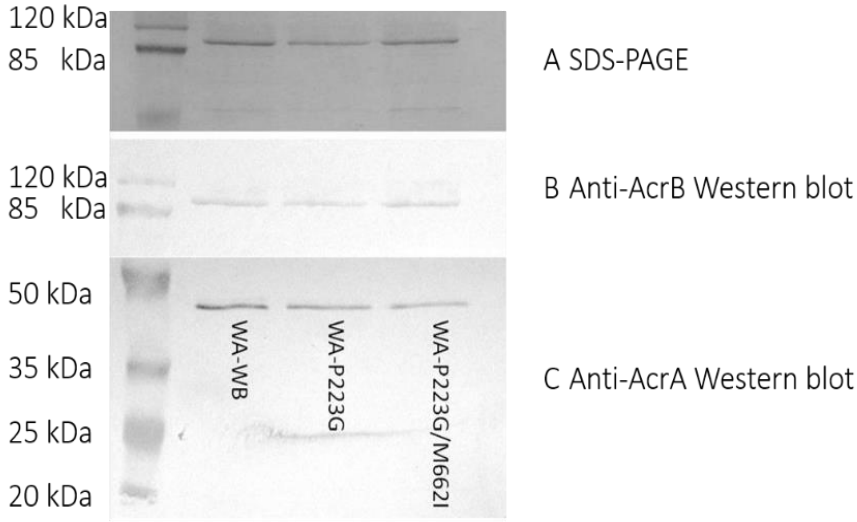

Figure 3.4 Cross-linking experiment was used to determine the level of AcrA interacting with different AcrB constructs. AcrA does not bind to Ni-NTA beads. Only those cross-linked with AcrB would be purified and detected in the anti-AcrA immunoblotting. The P223G mutation did not decrease the level of AcrA crosslinked with AcrB, and the additional repressor mutation M662I did not increase the level either.

3.3.3 Protein stability determination of WT-AcrB, $AcrB_{P223G}$ and $AcrB_{P223G/M662I}$ by thermal denaturation in a CD instrument.

To determine whether M662I restored the function of $AcrB_{P223G}$ by increasing the protein stability, thermal denaturation was conducted and monitored using a CD instrument. CD signal at 222 nm primarily associated with α-helical structure has been extensively used to assess the thermal stability of membrane proteins *in vitro*.[131] In the study, the change of the CD signal at 222 nm was used to evaluate the change of secondary structure when purified protein lost secondary structure during thermal denaturation. All the data obtained from CD were normalized and converted into folded fraction according to the following equation: $\text{Folded fraction} = \frac{Y}{Y_{max}}$, where Y indicated the value of MRE normalized and Y_{max} indicated the maximum value which was defined as 100% folded.

The result showed around 80% α-helices was lost for all three proteins when the temperature increased to 98 ºC (Figure 3.5, *A*). The ellipticity at 222 nm did not recover when temperature lowed back to 4°C, indicating that the unfolding was irreversible (data not shown). The similar melting curves of WT-AcrB, $AcrB_{P223G}$ and $AcrB_{P223G/M662I}$ resembled their structure similarity and the additional mutation M662I did not have an observable influence on protein stability.

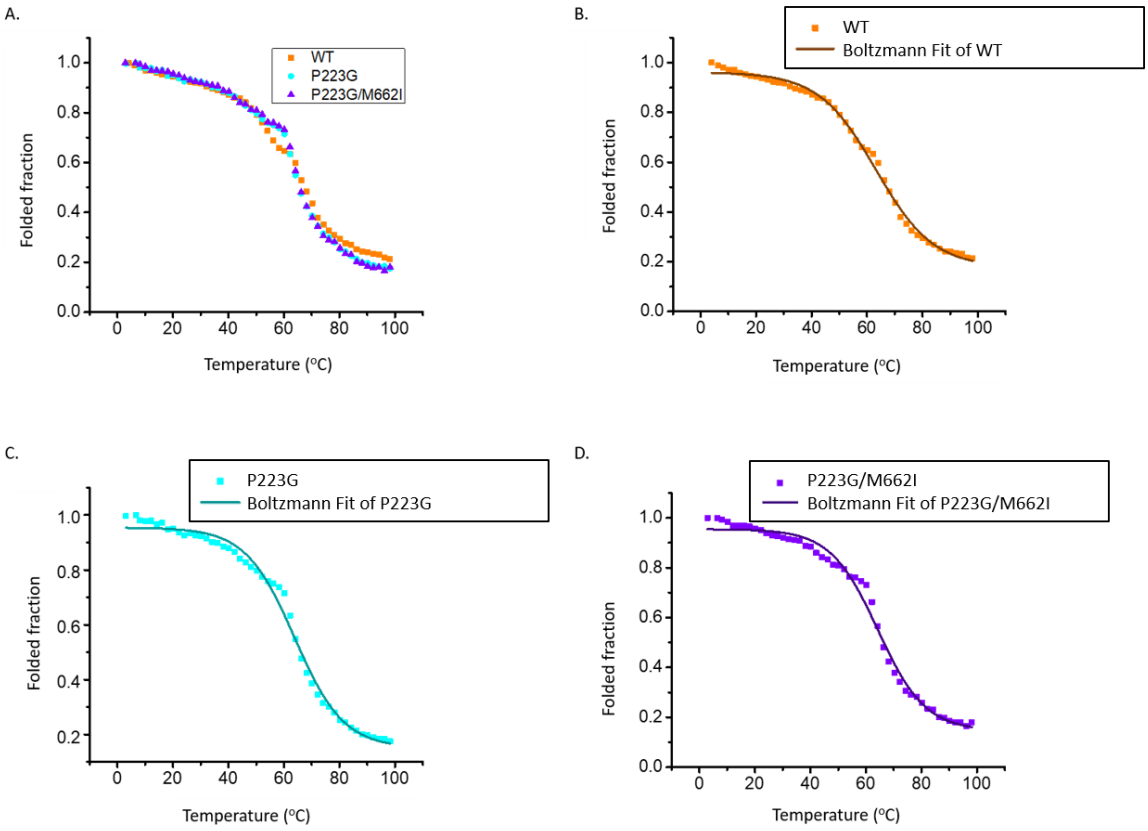

Figure 3.5 Protein stability was assessed by thermal denaturation on CD machine. *A.* Thermal denaturation curves of WT-AcrB, AcrB$_{P223G}$, and AcrB$_{P223G/M662I}$. *B.* Boltzmann fit of WT-AcrB. *C.* Boltzmann fit of AcrB$_{P223G}$. *D.* Boltzmann fit of AcrB$_{P223G/M662I}$.

To compare the curves more accurately, all the data were analyzed through OriginLab 9.0. Boltzmann equation,[132] shown in the following, was applied to fit all the data (Figure 3.5, *B, C,* and *D*).

$$\text{Folded fraction} = \frac{A_1 - A_2}{1 + e^{(T - T_m)/dT}} + A_2$$

where A_1 and A_2 represent the minimum and maximum value of denaturation, T represents the temperature, and T_m represents the melting temperature.

The result showed that R square is greater than 0.99, indicating most of the data were

covered in the equation. T_m obtained from CD are similar without significant difference (Table 3.2), suggesting that all the three proteins had similar secondary structure and confirmed the result obtained from CD wavelength scan.

Table 3.2 Protein melting temperature calculation results.

Strain	Melting temperature (T_m, ºC)
WT-AcrB	63.2 ± 0.5
$AcrB_{P223G}$	63.8 ± 0.6
$AcrB_{P223G/M662I}$	64.3 ± 0.6

3.3.4 Chemical denaturation of WT-AcrB, $AcrB_{P223G}$ and $AcrB_{P223G/M662I}$ induced by SDS

Chemical denaturation, a method of rendering proteins unfolding via addition of denaturants, is commonly used to characterize the conformational stability of globular proteins. Some spectroscopic methods such as fluorescence or CD are used to monitor the process in the denaturation assay. In this study, SDS denaturation was conducted through titrating aliquots of concentrated SDS solution into a solution of AcrB, and intrinsic fluorescence excited at 280 nm was recorded. The peak emission intensities at each SDS concentration were converted into folded percentage. As described in Figure 3.6, WT-AcrB showed the highest resistance to SDS while $AcrB_{P223G/M662I}$ had lowest resistance. Comparing to the curve of WT-AcrB, $AcrB_{P223G/M662I}$ did not recover the folding according to the denaturation curves.

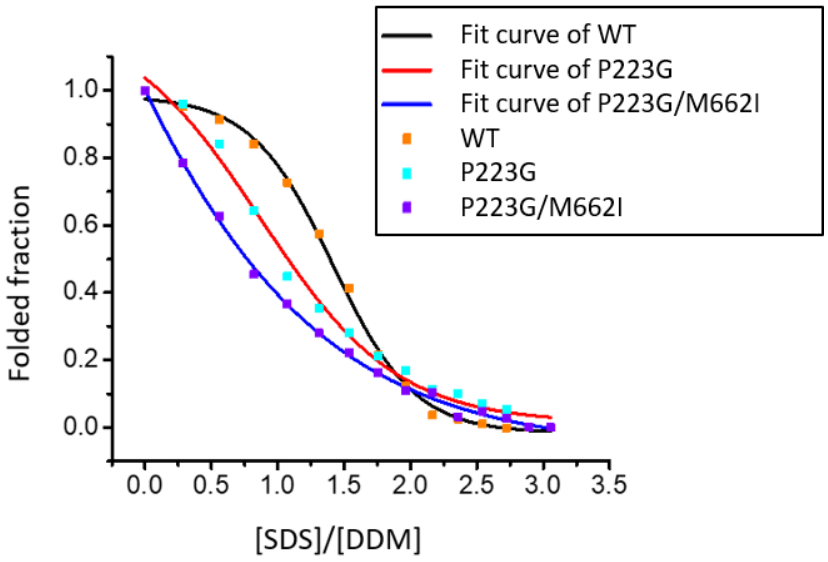

Figure 3.6 SDS denaturation of WT-AcrB, $AcrB_{P223G}$ and $AcrB_{P223G/M662I}$ and Boltzmann fit of the three curves.

3.3.5 CPM thermal denaturation analysis of WT-AcrB, $AcrB_{P223G}$ and $AcrB_{P223G/M662I}$ monitored on a fluorescence spectrometer.

CPM thermal stability assay was widely used to evaluate the stability of protein. A fluorescence dye CPM is supposed to interact with the hydrophobic core when the proteins unfold due to thermal denaturation. [132; 134] In CPM thermal stability assay, all the three proteins showed similar curves (Figure 3.7) and T_m (all the P values are greater than 0.05, which indicated that there was no significant difference), suggesting that the overall structure or the stability for all three AcrB variants are almost identical.[134] The values obtained from data analysis (Table 3.3) also showed there was not significant difference, although the values obtained seemed different. Both results suggested that the second mutation M662I did not increase the stability of AcrB.

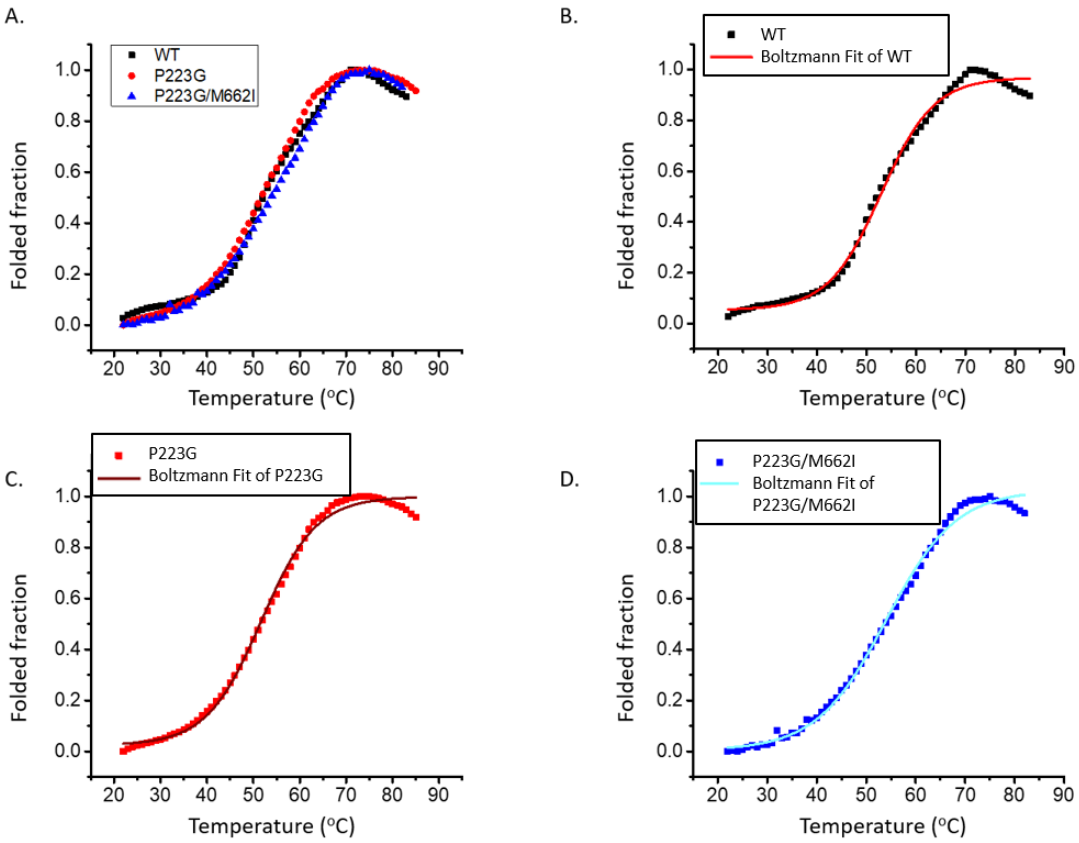

Figure 3.7 CPM thermal denaturation of WT-AcrB, AcrB$_{P223G}$ and AcrB$_{P223G/M662I}$ monitored using fluorescence spectrometer. *A.* CPM thermal denaturation curves of all the three proteins. *B.* Boltzmann fit of WT-AcrB. *C.* Boltzmann fit of AcrB$_{P223G}$. *D.* Boltzmann fit of AcrB$_{P223G/M662I}$.

Table 3.3 Protein melting temperature (T_m) fitting results.

Strain	T_m (°C)
WT-AcrB	52.9 ± 0.2
AcrB$_{P223G}$	51.7 ± 0.2
AcrB$_{P223G/M662I}$	54.0 ± 0.3

3.4 Discussion and conclusion

Several factors are critical for the proper function for AcrB: drug binding, interaction with AcrA and TolC, proton relay through the transmembrane domain, and AcrB trimerization. In this study, firstly we identified nine single suppressor mutations that could restore function to $AcrB_{P223G}$. Trimer affinity of purified mutants was examined using BN-PAGE. Although three mutants had higher trimer stability than $AcrB_{P223G}$, while remained drastically lower than that of the WT-AcrB including the mutation M662I. Stability assay was conducted using three different methods, thermal denaturation monitored using CD, chemical denaturation and CPM thermal stability assay monitored by fluorescence spectrometer. All the results showed that M662I did not improve the stability of $AcrB_{P223G}$. The next factor we tested was the interaction with partner proteins. We chose to investigate the interaction between AcrA and AcrB, since they make direct contact according to both wrapping model and bridging model. However, western blot results showed that M662I did not increase the interaction between them. At last, we determined whether M662I increased the substrate binding. Using a fluorescent labelling experiment, we found that M662 is involved in drug translocation pathway. Substrate binding in AcrB involves mainly hydrophobic interactions, and Ile is slightly hydrophobic than Met according to hydrophobicity scales generated by different studies.[135] It is interesting to notice that such a small change of hydrophobicity could significantly increase the MIC for all substrates tested.[122] We further measured the level of labeling of residue in the deep binding pocket, D276C (Figure 3.8). We found that the M662I mutation doubled the relative level of labeling at this site on the P223G background. Finally, we confirmed that the additional

M662I mutation did not induce an observable change on $AcrB_{P223G}$ structure and stability. While ligand-induced oligomerization has been observed in many receptor and signaling proteins, the ligand binding sites in these cases usually locate at the inter-subunit interface.[136] In AcrB, the substrate translocation pathway, including M662, is distant from the inter-subunit interface. Therefore, the potential effect on AcrB trimer stability, if any, has to be allosteric. Interaction between neighboring subunits in an AcrB trimer is clearly critical for function. During drug efflux, each subunit adopts a different conformation and cycles through the three conformations in turn. Recently researchers determined the structure of AcrB at high enough resolution to resolve unambiguously the side chains of critical residues involved in proton translocation in the transmembrane domain and rationalized how the cross-talk among protomers across the trimerization interface might lead to a more kinetically efficient efflux system.[137] Therefore, each subunit has to be able to "sense" the state of it's the state of its neighbors and undergoes conformational change in a concerted manner. A key element differentiates the various conformational states is the mode of interaction with the substrate. Therefore, it is possible that improved interaction with substrate could enhance efflux activity either directly through more efficient uptake or indirectly via increasing trimer affinity. Interestingly, some ligands are found to enhance the transport of other ligands by AcrB, suggesting that ligand binding could potentially play a more active role in efflux.[138]

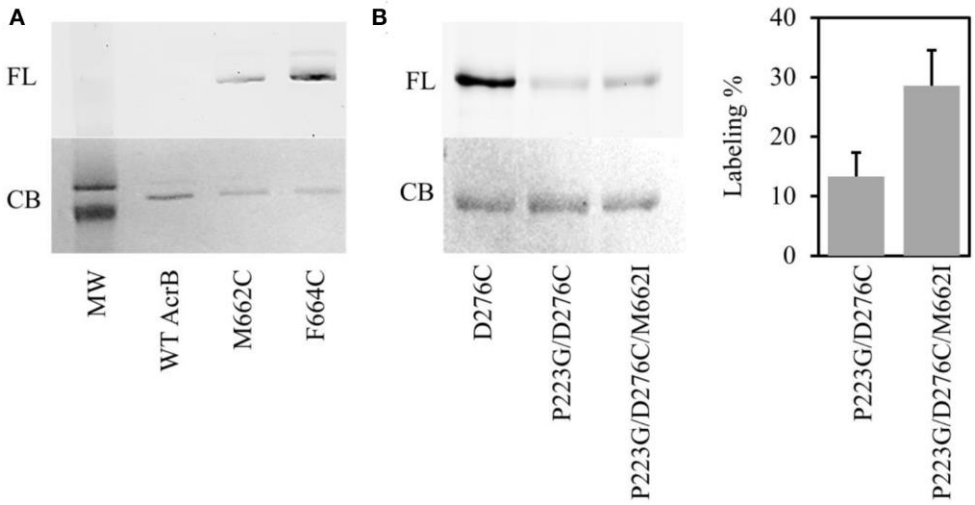

Figure 3.8 Bodipy-FL-maleimide labeling of residues on the substrate translocation pathway. Taken from the reference and done by Meng.[122] ***A.*** Labeling of WT-AcrB, $AcrB_{M662C}$, and $AcrB_{F664C}$. The same gel was stained using Coomassie blue stain. The two bands in the molecular weight marker are 120 kDa (top) and 85 kDa (bottom). ***B.*** Labeling of $AcrB_{D276C}$, $AcrB_{P223G/D276C}$, and $AcrB_{P223G/D276C/M662I}$. The same gel was stained using Coomassie blue stain. The level of labeling in $AcrB_{P223G/D276C}$ and $AcrB_{P223G/D276C/M662I}$ was normalized to the level of labeling in $AcrB_{D276C}$. The average value and standard deviation of three independent experiments were shown.

AcrB binds with substrates from the periplasm and extrudes them through the docking domain.[119] In this process, there are two pockets in the periplasmic domain of AcrB that are involved in drug transport, the proximal binding pocket and distal binding pocket.[52] Considering that M662I did not change the stability of $AcrB_{P223G}$, or increase the trimer association, or increase the interaction with its functional partner, we speculate that there may be two other reasons behind the activity restoration of $AcrB_{P223G}$: 1) it perhaps increased the binding of AcrB binding pockets with substrates; 2) it may increase the

interaction between AcrB and TolC due to the allosteric effect caused by suppressor mutations. Study of the mechanism of functional restoration in suppressor mutation will greatly improve our understanding about the interplay between different aspect of AcrB function, which may eventually lead to new insight into how this delegate molecular machinery function to effectively efflux a large variety of compounds.

Chapter IV. Application of FRET in Study of AcrB Trimer Association

4.1 Introduction

Protein biosynthesis is an essential process to generate new proteins by cells. This process generally includes transcription, translation, protein folding, and post-translational modification.[139-141] In each step, many factors work together to ensure the whole complicated process proceed accurately and efficiently. When protein biosynthesis starts, protein initiation factors including IF1, IF2, and IF3 activate the translocation of mRNA and formylmethionyl-$tRNA_f$ to ribosome. Elongation factor EF-Tu delivers aminoacyl-tRNA to A site of ribosome while EF-G mediates translocation of mRNA and tRNA out of ribosome. Protein synthesis in ribosome is terminated by release factors (RFs) which could recognize stop codons UAA, UAG, and UGA.[142] Post-translational modification is another important step during or after protein biosynthesis. To date, there are more than 300 post-translational modification reactions identified,[143] among which phosphorylation is the most pervasive and best-studied post-translational modification reaction given that it participates in many enzymes' modulating activities.[144]

Through translation in ribosome, a polypeptide chain is synthesized. After that, nascent polypeptide chains need to fold into three-dimensional conformations and sometimes oligomerize into oligomers in order to function normally. However, the folding and oligomerization of polypeptide chains are elusive, especially for membrane proteins. There are two main types of membrane proteins: α-helical membrane proteins and β-barrel membrane proteins. Folding of integral α-helical membrane proteins is considered to follow a two-stage pathway, which begins with the folding and membrane insertion of the

hydrophobic α-helices, followed by the interaction of those α-helices to form tertiary structure.[145] This two-stage pathway is informed by the bacteriorhodopsin, an α-helical membrane protein with seven α-transmembrane helices.[146] Folding of β-barrel membrane proteins happens partially before insertion.[147]

Oligomerization is another important process for proteins to function properly. The oligomeric proteins, accounting for over 35% proteins in cells, are essential in many cellular processes, including mediating gene expression, regulating enzyme activities, and ion channels, *etc*. [149] Although the mechanism of oligomerization is not well understood, results from several studies could shed light on following studies.[148] In one study cadherin monomers was found to dimerize via "swapping" their N-terminal β-strands of the adhesive domains.[149] In another study, Naveed *et al* found that β-barrel membrane protein can oligomerize through the weakly stable interfacial β-strands.[150] Naveed *et al* also found that the structure and amino acid sequence of β-barrel membrane proteins can be used to assess the protein stability and predict whether these proteins are monomers or oligomers with an 91% accuracy rate.

Many different techniques have been developed to determine and characterize protein oligomerization. *In vitro*, biophysical techniques such as size exclusion chromatography, NMR spectroscopy, scattering techniques, isothermal titration calorimeter, mass spectroscopy, and fluorescence anisotropy are commonly used. In cells, cross-linking, fluorescence method, proximity imaging, and complementation approaches are widely applied.[151] Among the techniques developed to investigate protein oligomer association,

FRET is one of the few methods that are compatible with studies of membrane proteins in a lipid bilayer environment. One unique advantage of using fluorescent protein as fusion tags is that it eliminates the laborious labeling process after protein purification. In addition, the ratio of "labeling" is strictly controlled at a one-to-one ratio (i.e. one target protein with one fusion tag), which largely guarantees the sample to be homogenous. GFP and its derivatives are popular tools in studies of protein-protein interaction.[152] GFP is firstly isolated from jellyfish *Aequorea Victoria*.[153] In 1994, Martin Chalfie and his colleagues first expressed the cDNA in *Escherichia. coli* and *Caenorhabditis elegans* and found the main excitation peaked at 395 nm with a minor peak at 470 nm and emitted at 509 nm with a shoulder at 540 nm.[154] GFP has been exploited in many studies because of its bright and stable fluorescence signal. To broaden the application spectra of GFP, derivatives such as CFP and YFP have been created by mutating certain residues in the protein sequence. When the tyrosine at position 66 is substituted by tryptophan, the excitation and emission wavelengths are changed into 436 nm and 476 nm, respectively. The mutations S65G, S72A and so on in the GFP gene sequence create YFP with a wavelength of emission at 529 nm, when excited at 514 nm (Figure 4.1).[153] CFP and YFP have been used as a FRET pair in many studies to probe protein-protein interaction or conformational changes.[155] Using FRET between fluorescent protein pairs CFP and YFP, Miyawaki *et al* [156] investigated the interaction between two proteins (calmodulin and M13) in response to an increasing concentration of Ca^{2+}. When the two fluorescent proteins are fused into the same host protein, intramolecular FRET can be used to study the conformational change of the protein. Kurokawa *et al* [157] used this method to investigate the conformational change of phosphorylated adaptor protein, Crk Ⅱ, *in vivo* and found epidermal growth factor-induced

phosphorylation of Crk II was initiated at the peripheral plasma membrane.

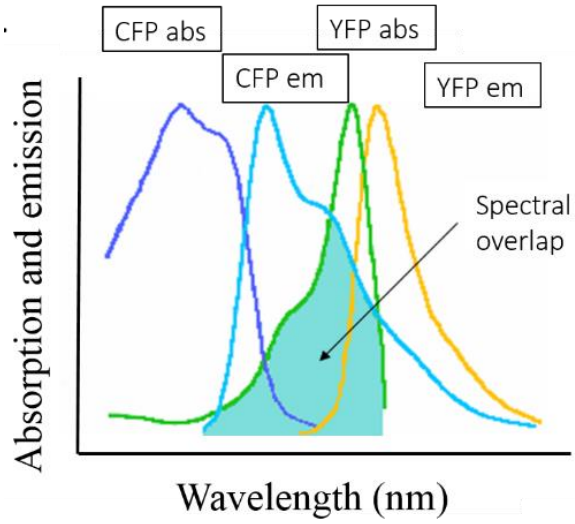

Figure 4.1 Fluorescence excitation and emission of CFP and YFP.[158;159]

Although the crystal structure of AcrB was revealed in 2002 and the whole complex AcrAB-TolC was resolved in 2014, how native synthesized AcrB monomers assemble into AcrB trimers remains elusive. Lu *et al.* in 2011 probed into the question that whether individual subunits of AcrB fold into monomers before all subunits assemble into a trimer (three-stage pathway) or simultaneously (two-stage pathway).[110] The existence of well-folded monomeric AcrB mutant $AcrB_{\Delta loop}$, in which the protruding loop was deleted, suggested that oligomerization occurred through a three-stage pathway. Later, Lu *et al.* found that AcrB trimerization *in vivo* is not completely random.[160] To continue the studies about AcrB oligomerization, I used FRET to investigate the association of AcrB monomers. Two AcrB fusion proteins $AcrB_{P223G}$-5aa-CFP and $AcrB_{P223G}$-5aa-YPet were constructed. Activity assay showed that fusion of CFP or YPet did not change the stability of AcrB. Longer linker between AcrB and fluorescent protein could increase FRET efficiency, but

decrease expression level. Association of AcrB monomers occurred immediately when separately purified monomers were mixed together. Kinetic studies showed that the association of AcrB monomers was strongly cooperative. Reconstitution of AcrB monomers in liposome revealed that association occurred more readily with lipids in the environment.

4.2 Materials and Methods

4.2.1 Construction of *pBAD33-acrB-5aa-CFP, pBAD33-acrB-5aa-YFP*, *pBAD33-acrB-15aa-CFP* and *pBAD33-acrB-15aa-YFP.*

The gene *CFP* or *YFP* was inserted into the plasmid *pBAD33-acrB* using restriction enzyme cutting sites XhoI and HindIII and the DNA sequence was confirmed by DNA sequencing. The primers used for the construction of AcrB-5aa-CFP and AcrB-5aa-YFP are the following:

For AcrB-5aa-CFP:

Forward: GAACCGCTCGAGGGAGGATCAGGAGGAATGGTGAGCAAGGGCGAG (45 bp)

Reverse:

CAACCC AAGCTT ATGATGATGATGATGATG GATCCCGGCGGCGGTCAC (48 bp)

For AcrB-5aa-YFP:

Forward 5'-3':

GAACCGCTCGAGGGAGGATCAGGAGGAATGTCCGCTTTCTGGTATGCC (48 bp)

Reverse:

CAACCC AAGCTT ATGATGATGATGATGATG GATCCCGGCGGCGGTCAC (48 bp)

The primers used to elongate the linker are:

Forward primer: GAT CAT CAT CTC GAG GGT GGT TCT GGT GGT TCT GGT GGT TCT GGA GGA TCA GGA GG

Reverse primer: CC TCC TGA TCC TCC AGA ACC ACC AGA ACC ACC AGA ACC ACC CTC GAG ATG ATG ATC

4.2.2 Protein expression and purification

The plasmids encoding AcrB-5aa-CFP, AcrB-5aa-YFP, AcrB-5aa-YPet or AcrB-15aa-CFP, AcrB-15aa-YFP were transformed into *E. coli* strain BW25113 *ΔacrB* competent cells. Single colony was picked from the LB agar plate and inoculated into tubes, then transferred into larger flask containing fresh LB with relative antibiotics. After incubated at 28 ºC for 24 hours, the bacteria cells were harvested and stored in -80 ºC freezer before purification. The purification protocol was described in 2.2.1 with minor modification. 2 L of fresh LB medium containing relative antibiotic was used to culture the strain. 0.2% arabinose was added in the culture to induce the synthesis when OD_{600} reached 1.0. After sonication, 2% triton was mixed with cell debris and incubated at 4 ºC for 12 hours. 5 mM imidazole was used in binding of Ni-NTA beads to sample and 25 mM imidazole was used in wash buffer.

4.2.3 BN-PAGE

BN-PAGE was conducted as described with minor modifications.[161] Briefly, the purified AcrB samples were mixed with blue native loading buffer with a final concentration of 0.5 M 6-aminohexanoic acid, 5% coomassie blue G-250, 5% glycerol, pH 7.0, and loaded to a 4-20% gradient polyacrylamide gel (BIO-RAD, Hercules, CA). The electrophoresis was

performed using the cathode buffer (50 mM tricine, 7.5 mM imidazoole, 0.02% Coomassie brilliant blue G-250, pH 7.0) and anode buffer (25 mM imidazole, pH 7.0) at 15 mA, in the 4°C refrigerator for 2~4 hours. The protein bands were finally visualized after Coomassie Blue staining and de-staining.

4.2.4 Drug susceptibility assay

AcrB activity was usually determined by a drug susceptibility assay. The MIC of different stains were measured as described.[162] Briefly, an *acrB* deficient E. coli strain (BW25113*ΔacrB*) was used as the host cell. BW25113*ΔacrB* strain transformed with plasmid-encoded WT-AcrB or *pQE70* vector were used as the positive and negative controls, respectively. Plasmids encoding different AcrB mutants were transformed into BW25113*ΔacrB* as well. Freshly transformed cells were plated on LB-agarose plates containing 100 μg/mL ampicillin and 50 μg/mL kanamycin. The same ampicillin and kanamycin concentrations were used throughout the study when noted. A single colony was inoculated into a LB media supplemented with ampicillin and kanamycin. The exponential-phase cultures of different strains were diluted to an OD_{600nm} of 0.1 with LB broth. 10 μL of this diluted culture was used to inoculate into 1 mL LB media containing the indicated concentration of erythromycin or novobiocin. The cultures were incubated under shaking at 37°C for 6 hours. Absorbance at 600 nm of each culture was measured. This activity assay was conducted under the basal AcrB expression condition, which was not supplemented with inducer. Each experiment was repeated at least three times.

4.2.5 Kinetic studies of AcrB association

Protein concentration for $AcrB_{P223G}$-5aa-CFP and $AcrB_{P223G}$-5aa-YPet were estimated using UV/vis and SDS-PAGE. Freshly purified $AcrB_{P223G}$-5aa-CFP and $AcrB_{P223G}$-5aa-YPet of different concentration were mixed according to molar ratio of 1:1 when the concentration of each protein was determined using the standard curves. Fluorescence intensity over time was recorded and initial rate was calculated to determine the association constant.

4.2.6 Reconstitution of $AcrB_{P223G}$-5aa-CFP and $AcrB_{P223G}$-5aa-YPet in liposome.

Reconstitute the fusion proteins into liposomes was conducted following a protocol in literature.[163] Briefly, *E. coli* polar lipid dissolved in chloroform was dried in a glass vial under a gentle stream of N_2 and then incubated in a vacuum oven at 25 ^{o}C overnight. To make liposome, sodium phosphate buffer (pH 7.5) was added into the glass vial to reach a final concentration of 20 mg/mL. The solution was sonicated on ice for 50 minutes until an opaque solution was obtained. Freshly purified AcrB-5aa-CFP or AcrB-5aa-YPet in pH 7.5 phosphate buffer with 0.03% (w/v) DDM was mixed with 4% Triton and lipids on a shaker at room temperature for 0.5 hour. To remove detergent, Bio-beads pretreated with methanol and deionized water was added at a concentration of 40 mg per mL of sample. The sample was incubated for 4 hours, and then Bio-beads was removed after centrifugation. The supernatant contains liposomes was used to investigate the trimerization behavior of AcrB.

4.3 Results

4.3.1 Construction of *pBAD33-acrB-5aa-CFP* and *pBAD33-acrB-5aa-YFP*.

To investigate association of AcrB monomers, fluorescent proteins were fused to AcrB as indicators to yield FRET signals. The strategy is to insert CFP or YFP with His_6 tag between restriction enzyme cutting site XhoI and HindIII (Figure 4.2, *A*). A linker of 5 amino acids "GGSGG" was added between AcrB and CFP or YFP to avoid the influence on AcrB folding. As shown in Figure 4.2 *B*, both AcrB-5aa-CFP and AcrB-5aa-YFP had comparable expression levels as WT-AcrB. Analyzed through fluorescence spectrometer with excitation wavelength of 435 nm and 514 nm, the two proteins showed emission spectra with peaks of 478 nm and 527 nm (Figure 4.2, *C* and *D*) which are signature spectra of CFP and YFP, respectively. The result revealed that the constructs of AcrB-5aa-CFP and AcrB-5aa-YFP expressed well and could be purified.

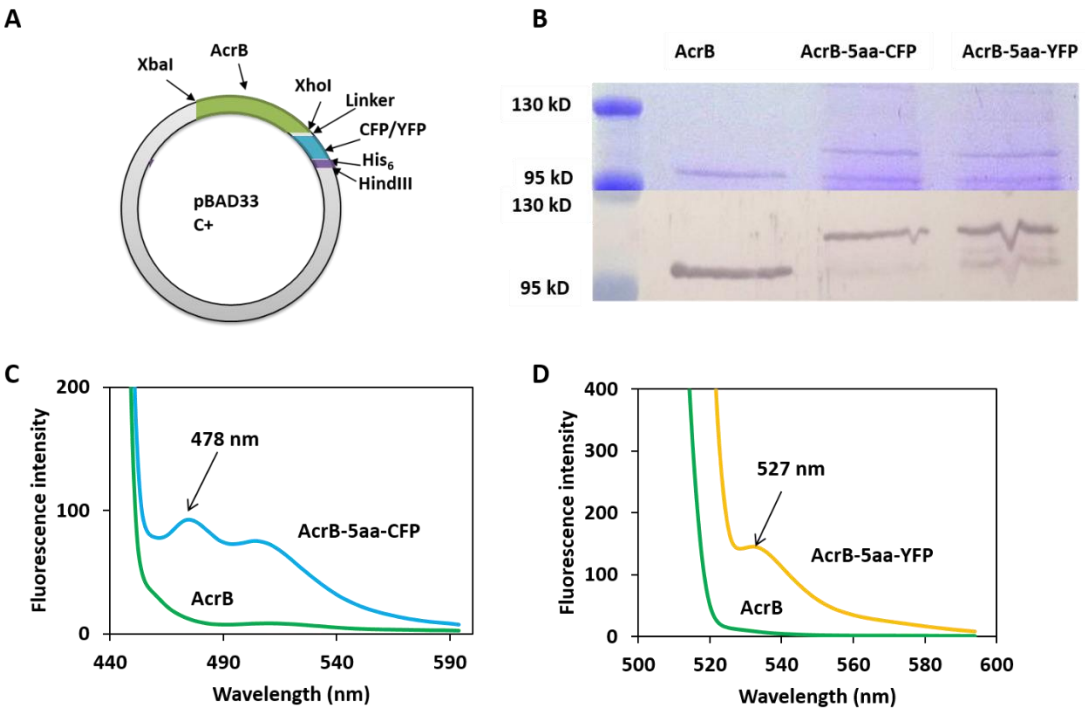

Figure 4.2 Construction of AcrB-5aa-CFP or AcrB-5aa-YFP. *A.* Plasmid map showing how to create the plasmid construct. *B.* SDS-PAGE (on the top) and Western blot (on the bottom) results. *C.* Fluorescence wavelength scan of AcrB-5aa-CFP, excited at 435 nm. ***D.*** Fluorescence wavelength scan of AcrB-5aa-YFP, excited at 514 nm.

4.3.2 Influence of longer linker insertion on expression and fluorescence

To investigate if a longer linker influenced fluorescence of CFP or YFP and FRET between them, a 15-amino acid linker with the sequence of "GGSGGSGGSGGSGGG" was inserted into gene sequence between *acrB* and *CFP* or *YFP* using Quikchange sited directed mutagenesis kit with *pBAD33-acrB-5aa-CFP* and *pBAD33-acrB-5aa-YFP* as templates, respectively. The same number of bacteria cells were harvested followed by purification of AcrB-15aa-CFP or AcrB-15aa-YFP using standard protocol as described in Chapter 2. Both proteins showed comparable expression levels and purities according to the results of

SDS-PAGE and Western blot (Figure 4.3, *A*). Fluorescence wavelength scan results suggested that both proteins had signature spectra of CFP and YFP (Figure 4.3, *B*), respectively. Whether the longer linker had influence on fluorescence and FRET efficiency was determined in the following experiments.

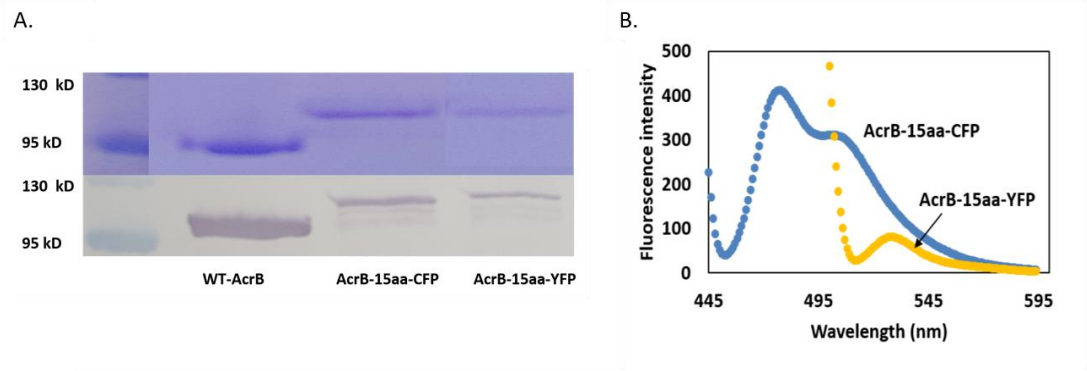

Figure 4.3 Construction of AcrB-15aa-CFP and AcrB-15aa-YFP. *A.* SDS-PAGE (Top picture) and Western blot (bottom piture, anti-whole AcrB antibody was used) analysis of AcrB-15aa-CFP and AcrB-15aa-YFP. *B.* Fluorescence analysis of the two proteins.

4.3.3 Activity of AcrB fusion proteins containing CFP or YFP

Fusion of fluorescent proteins may influence the activity or stability of target proteins. To evaluate the activity of AcrB in all the constructs, MIC test was conducted according to the literature.[164] The resistance to two AcrB substrates novobiocin and erythromycin of the bacteria cells containing plasmid vector encoding different protein constructs were determined, while the bacteria cells with *acrB* gene knocked out was used as negative control. All constructs showed comparable MIC values as WT-AcrB (Table 4.1), suggesting that the fusion of CFP or YFP to AcrB did not influence the efflux activity of AcrB.

Table 4.1 MIC of BW25113*ΔacrB* containing plasmids encoding indicated AcrB constructs.

Strain	MIC (μg/mL)	
	Novobiocin	Erythromycin
WT-AcrB	320	160
AcrB-5aa-CFP	320	160
AcrB-5aa-YFP	320	80
AcrB-15aa-CFP	320	160
AcrB-15aa-YFP	320	80
AcrB-5aa-YPet	320	80
ΔacrB	20	20

4.3.4 Co-expression of AcrB constructs *in vivo*.

AcrB is biosynthesized, folded and oligomerized in bacteria cells, so it is important to observe if there is FRET in AcrB trimers *in vivo*. The strategy was that two compatible plasmids harboring *acrB-CFP* and *acrB-YFP* genes were co-transformed and expressed in the same competent cells. In theory, AcrB monomers with fluorescent proteins associated into AcrB trimers in which only CFP and YFP fused hetero-trimers showed FRET signal. Here the plasmid vector *pBAD18*, compatible with *pBAD33*, was used to harbor gene *acrB-5aa-YFP* or *acrB-15aa-YFP*. And the CFP fusions were inserted in the plasmid pBAD33. Monomers of AcrB-5aa-CFP, AcrB-5aa-YFP, AcrB-15aa-CFP, and AcrB-15aa-YFP were

synthesized in bacteria cells and associated into trimers so that FRET occurred between CFP and YFP. To calculate FRET efficiency, the equation $E = 1 - \frac{F_D}{F_{DA}}$ was used where E indicates FRET efficiency, F_D and F_{DA} indicate fluorescence intensities for donor fluorophore in absence and in presence of acceptor fluorophore, respectively. Since both AcrB-5aa-CFP and AcrB-5aa-YFP were biosynthesized *in vivo*, an external standard curve for concentration versus fluorescence was determined. The result (Figure 4.4, *B*) showed that co-expressed AcrB-15aa-CFP/YFP trimers had higher FRET efficiency than co-expressed AcrB-5aa-CFP/YFP trimers. A possible explanation for higher FRET efficiency was that longer linker made CFP and YFP more flexible to increase the opportunities to interact. Another possible explanation was that longer linker improved the orientation preference for FRET occurrence. However, the expression level of AcrB-15aa-YFP was much lower than that of AcrB-5aa-YFP (Figure 4.7 *A,* Figure 4.2 *A* and Figure 4.3 *A*), which was not suitable for the following experiments, such as kinetic studies in which series dilution would be conducted. Therefore, 5aa linker would be used in the following experiments.

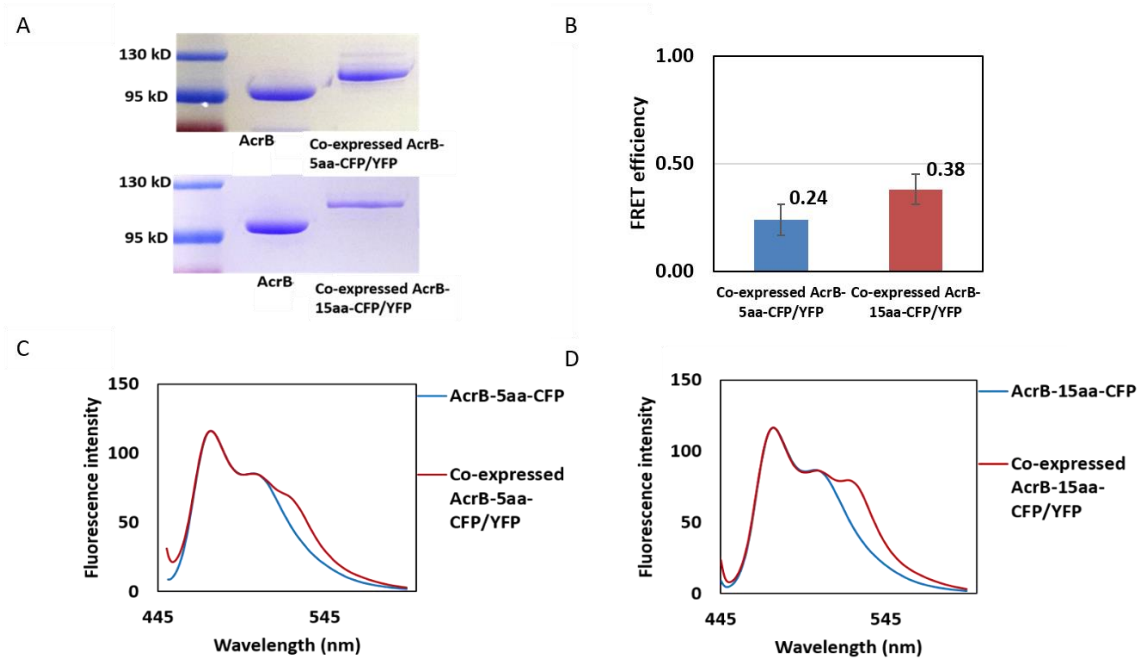

Figure 4.4 Co-expression of AcrB-5aa-CFP/YFP and AcrB-15aa-CFP/YFP. *A.* SDS-PAGE analysis of co-expressed samples. *B.* FRET efficiency calculation. *C.* Fluorescence wavelength scan of co-expressed AcrB-5aa-CFP/YFP. *D.* Fluorescence wavelength scan of AcrB-15aa-CFP/YFP.

4.3.5 Mutation P223G was used to create AcrB monomers

Previous studies showed that Pro223 was critical for the stability of AcrB trimers and mutation Pro223Gly made most of AcrB trimers dissociate into AcrB monomers when they were freshly purified. CD analysis and thermal stability studies revealed that P223G did not change the secondary structure and monomer stability, although it disrupted the trimer and caused the whole AcrB efflux pump non-functional.[165] An interesting finding is that part of AcrB monomers re-associated into AcrB trimers when elution fractions were dialyzed in PBS buffer containing 0.03% DDM, which made the observation of AcrB monomers' association possible. In this study, P223G was introduced to create AcrB

monomers and dialysis was used for the monomers to form trimers. FRET between CFP and YFP was used to monitor the association. (Figure 4.5, *B*). Obviously, the mixed sample showed a FRET bump after dialysis and calculation result showed the FRET efficiency was ~0.13, which is lower than co-expressed AcrB-5aa-CFP/YFP in cells.

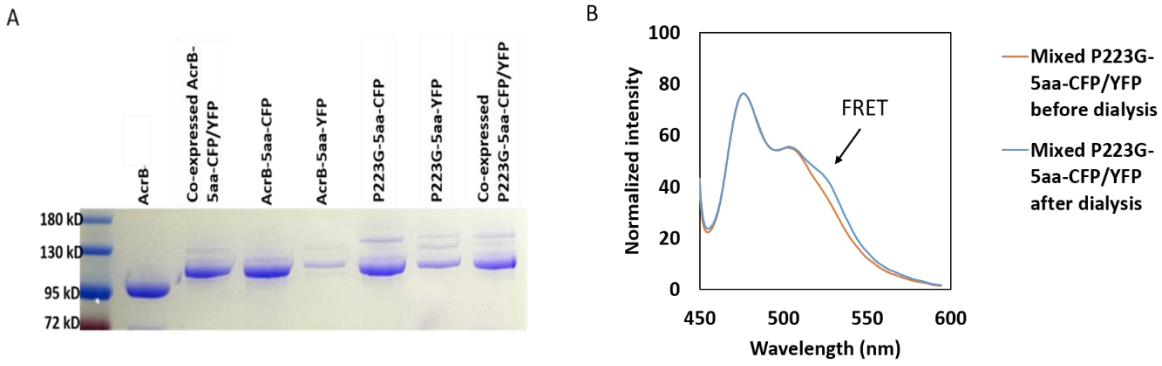

Figure 4.5 Association of AcrB$_{P223G}$ monomers. *A.* SDS-PAGE analysis of freshly purified proteins. *B.* Fluorescence wavelength scan of mixed AcrB$_{P223G}$-5aa-CFP and AcrB$_{P223G}$-5aa-YFP monomers before and after dialysis.

BN-PAGE was firstly developed for purification of mitochondrial membrane protein whose molecular weight was between10 kDa to 10 MDa.[161] Later, BN-PAGE was used to analyze the native masses and oligomeric states of proteins clinically. In this study, BN-PAGE was used to analyze the native states of AcrB fusion proteins before and after dialysis. Before dialysis, most proteins existed as monomers (as shown in Figure 4.6). After dialysis, AcrB monomers formed into trimers and reached equilibrium so that some trimers were observed in the BN-PAGE gel. Band intensities of trimers and monomers were calculated through ImageJ. The result showed that the percentage of trimers was 41% after dialysis, comparing to <5% before dialysis.

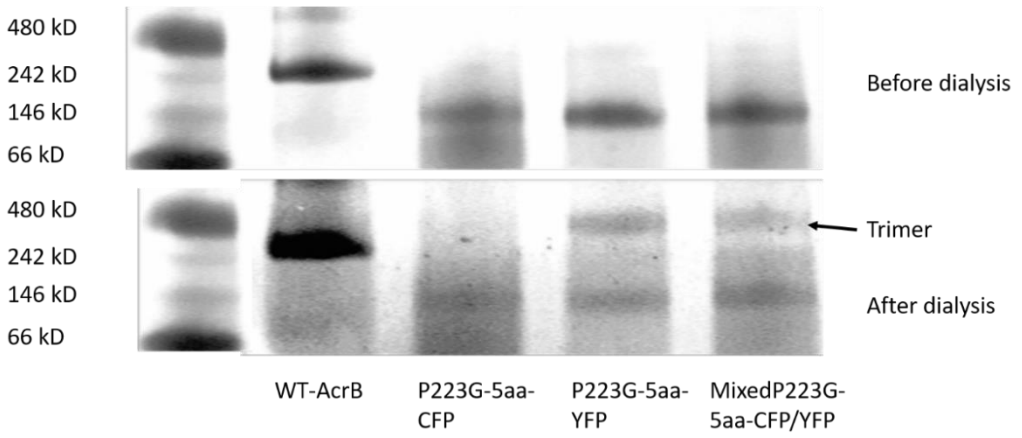

Figure 4.6 BN-PAGE analysis of purified proteins and mixture before and after dialysis.

4.3.7 Co-expression of AcrB$_{P223G}$-5aa-CFP and AcrB$_{P223G}$-5aa-YPet.

Although the FRET efficiency of co-expressed AcrB-15aa-CFP/YFP was higher than co-expressed AcrB-5aa-CFP/YFP, expression level of AcrB-15aa-YFP was not high enough for the following experiments, especially for the kinetic studies. In addition, FRET efficiency for mixed AcrB$_{P223G}$-5aa-CFP/YFP *in vitro* was not high, possibly resulted from the low expression level of AcrB-5aa-YFP and low quantum yield of YFP. To increase the FRET intensity as well as FRET efficiency, YPet was introduced to substitute YFP. YPet, an improved version of YFP, is much brighter than YFP and has excellent photostability.[166] SDS-PAGE result (Figure 4.7, *A*) showed that the expression level of AcrB$_{P223G}$-5aa-YPet was much higher than that of AcrB$_{P223G}$-5aa-YFP. Comparing the FRET efficiency of mixed AcrB$_{P223G}$-5aa-CFP/YFP (~0.13), FRET efficiency of mixed AcrB$_{P223G}$-5aa-CFP/YPet increased to ~0.34 (Figure 4.7, *B*). Fluorescence wavelength scan result also revealed that the FRET bump was much higher for CFP/YPet mixture than CFP/YFP mixture (Figure 4.7 *D* and Figure 4.5 *B*). Another interesting result is that FRET efficiency of mixed purified samples (~0.34) was higher than that (~0.22) of co-expressed sample

(Figure 4.7, *C* and *D*). A possible explanation is the molar ratio of CFP/YPet is not 1 to 1 *in vivo*, while the molar ratio *in vitro* was set as 1 to 1 which could maximize the FRET efficiency between them.

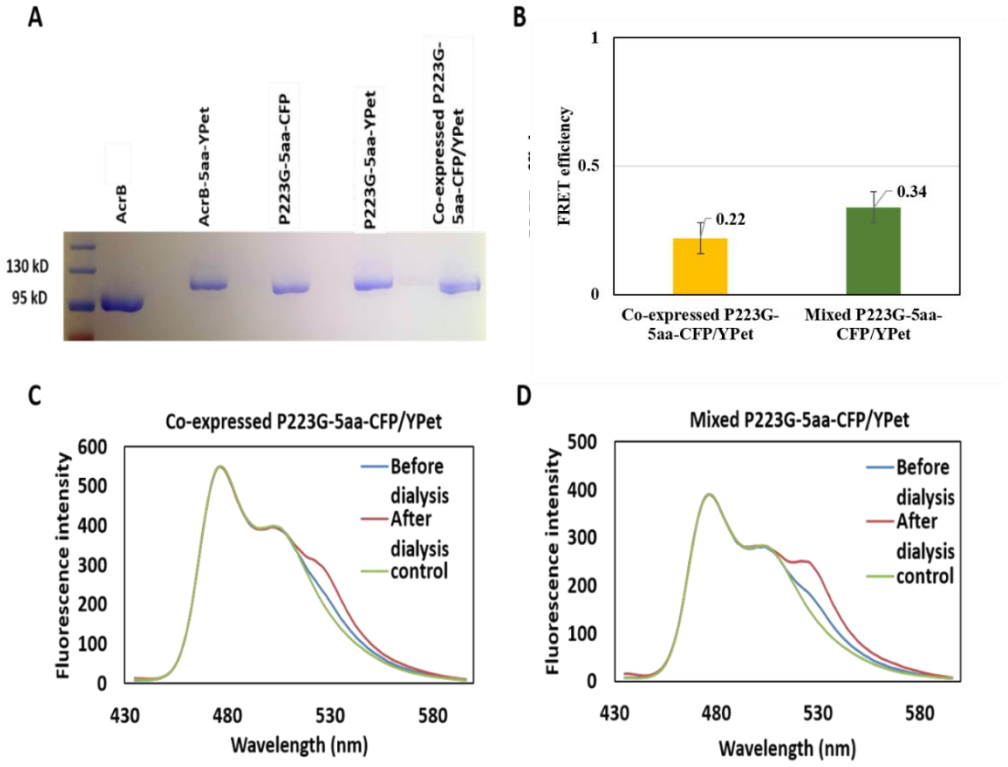

Figure 4.7 Association of AcrB$_{P223G}$-5aa-CFP and AcrB$_{P223G}$-5aa-YPet monomers. *A.* SDS-PAGE analysis of purified proteins. *B.* FRET efficiency calculation. *C.* Fluorescence spectra of co-expressed AcrB$_{P223G}$-5aa-CFP and AcrB$_{P223G}$-5aa-YPet before and after dialysis. *D.* Fluorescence spectra of mixed AcrB$_{P223G}$-5aa-CFP and AcrB$_{P223G}$-5aa-YPet before and after dialysis.

BN-PAGE was conducted to determine the percentage of AcrB monomers and trimers before and after dialysis. The results (Figure 4.8) showed that freshly purified AcrB$_{P223G}$-5aa-CFP and AcrB$_{P223G}$-5aa-YPet monomers oligomerized into trimer in BN-PAGE when

they were mixed and analyzed. The percentage of trimer formed in electrophoresis was about 20%, while it increased to 58% after dialysis which was much higher than mixed AcrB$_{P223G}$-5aa-CFP/YFP (41% after dialysis).

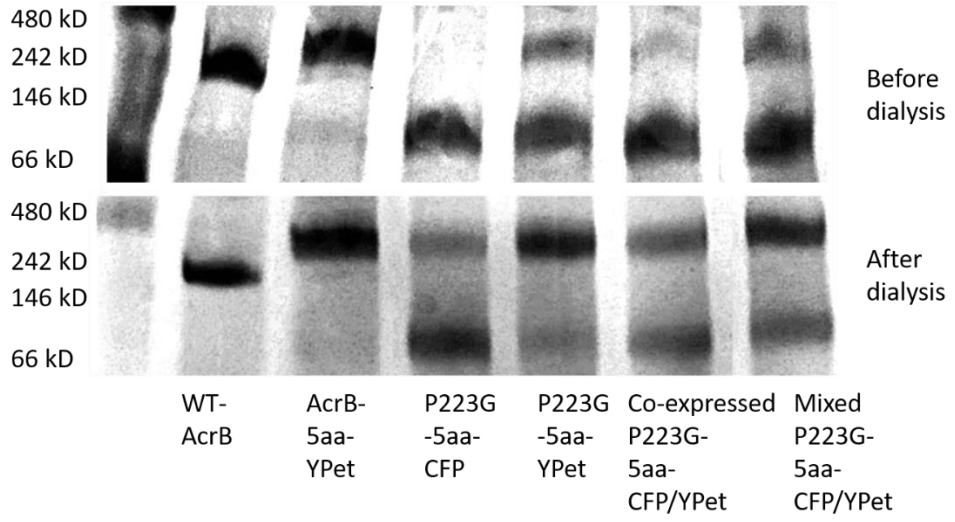

Figure 4.8 BN-PAGE analysis of AcrB$_{P223G}$-5aa-CFP and AcrB$_{P223G}$-5aa-YPet monomers and trimers before and after dialysis.

4.3.8 Association of AcrB monomers occurred immediately when AcrB monomers were mixed

To determine the kinetic properties of AcrB association, 0.1 μM of freshly purified AcrB$_{P223G}$-5aa-CFP and AcrB$_{P223G}$-5aa-YPet were mixed according to molar ratio of 1:1 without dialysis. Before the assay, the samples were pre-warmed in 25 ºC water bath for 5 minutes. The change of FRET intensity over time was used as a reporter of AcrB association. The result (Figure 4.9) showed that FRET signal increased immediately when the two samples were mixed, indicating that AcrB association occurred immediately when the monomers encountered. It went to plateau after about 6-hour incubation at 25 ºC which indicated that an equilibrium reached at that time point.

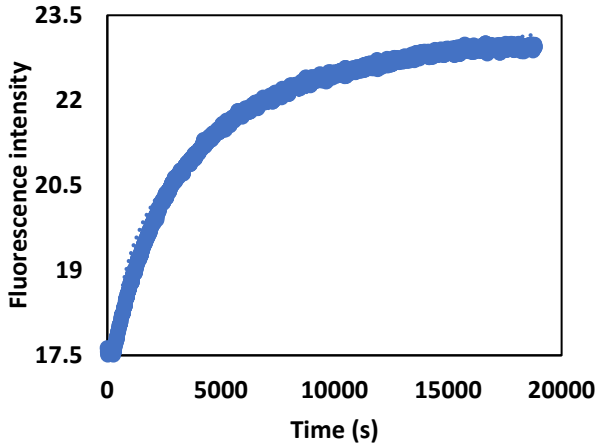

Figure 4.9 Fluorescence analysis of mixed AcrB$_{P223G}$-5aa-CFP and AcrB$_{P223G}$-5aa-YPet freshly purified without dialysis. Excitation wavelength is 400 nm while emission wavelength is 527nm.

4.3.9 Addition of AcrB$_{P223G}$ inhibited the association of AcrB-5aa-CFP/YPet trimer

To determine whether non-fluorescent AcrB monomers inhibit the association of fluorescent tagged AcrB monomers, freshly purified AcrB$_{P223G}$ were added into the mixture when they were mixed at time 0. The result showed FRET signal between AcrB$_{P223G}$-5aa-CFP and AcrB$_{P223G}$-5aa-YPet in the presence of AcrB$_{P223G}$ increased not as fast as the samples in the absence of AcrB$_{P223G}$ (as shown in Figure 4.10, *A*). After incubation at 4 ºC overnight, the FRET bump of AcrB$_{P223G}$-5aa-CFP and AcrB$_{P223G}$-5aa-YPet mixture with AcrB$_{P223G}$ was not as high as the samples without AcrB$_{P223G}$ (as shown in Figure 4.10, *B*). Both results suggested that AcrB$_{P223G}$ participated in association which competed with other monomers with fluorescent protein, so that it inhibited the association of AcrB$_{P223G}$-5aa-CFP and AcrB$_{P223G}$-5aa-YPet monomers.

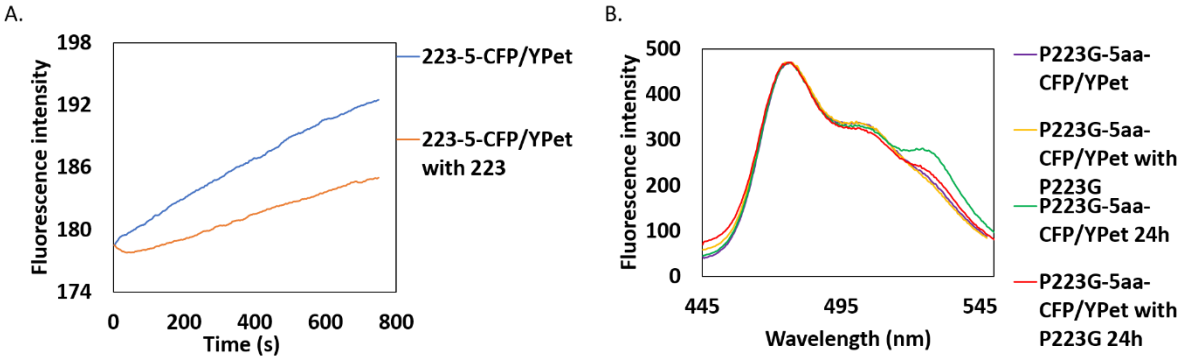

Figure 4.10 Inhibition of AcrB$_{P223G}$-5aa-CFP and AcrB$_{P223G}$-5aa-YPet association by addition of AcrB$_{P223G}$ monomers. *A.* The change of FRET intensity over time. *B.* Fluorescence wavelength scan of mixed AcrB$_{P223G}$-5aa-CFP and AcrB$_{P223G}$-5aa-YPet with or without AcrB$_{P223G}$ after 24-hour incubation.

4.3.10 Kinetic studies of AcrB$_{P223G}$-5aa-CFP and AcrB$_{P223G}$-5aa-YPet monomer association

To characterize the association, kinetic studies were conducted as described in methods. AcrB$_{P223G}$-5aa-CFP and AcrB$_{P223G}$-5aa-YPet monomers with different initial concentration obtained by a series of dilution were mixed according to molar ratio of 1:1. The change of FRET signal intensity over time was monitored using the spectrometer. Plotting FRET intensities on y axis and time on x axis, a linear curve was obtained and the slope (the unit is au/s) indicated the relationship between fluorescence change and time. To calculate the initial rate of the reactions, fluorescence intensities of AcrB-5aa-CFP samples with different concentrations were used to make a linear standard curve and its slope (the unit is au/μM) indicated the relationship between fluorescence intensity and concentration. The first slope (au/s) divided by the second slope (au/μM) was used to obtain the initial rate.

Initial reaction rate with unit of μM/s versus substrate concentration with unit of μM were used to plot the data. The Hill equation as shown in the following which was used to determine cooperativity. The result (Figure 4.11) showed that in association, maximum reaction rate (V_{max}) was 0.24 ± 0.02 μM/s, Hill coefficient "n" was 3.13 ± 0.80, and $K_{0.5}$ was 0.37 ± 0.04 μM. The positive value of n suggested a positive cooperativity among monomers' association into trimers. The value of $K_{0.5}$ reflects AcrB trimer affinity, while V_{max} revealed how fast the trimers formed.

$$v = \frac{V_{max}[s]^n}{{K_{0.5}}^n + [s]^n}$$

where v represents reaction velocity, [S] represents substrate concentration, $K_{0.5}$ represents half maximal concentration constant.[167]

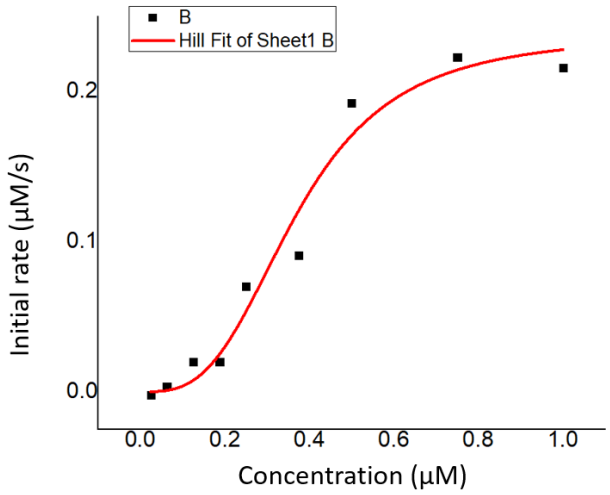

Figure 4.11 Kinetic studies of $AcrB_{P223G}$-5aa-CFP and $AcrB_{P223G}$-5aa-YPet.

4.3.11 Characterization of the interaction of AcrB$_{P223G}$-5aa-CFP and AcrB$_{P223G}$-5aa-YPet in lipid bilayers.

To mimic AcrB association in cell membrane environment, reconstitution of AcrB$_{P223G}$-5aa-CFP and AcrB$_{P223G}$-5aa-YPet in liposome was conducted using *E.coli* polar lipid. The result (Figure 4.12) showed that association in liposome (~1.5 hours) is faster than in detergent (~2 hours). And FRET efficiency for the association in liposome (~0.1) was much higher than in detergent (~0.03). It suggested that liposome is more favorable for AcrB monomers to associate, comparing to the detergent micelles.

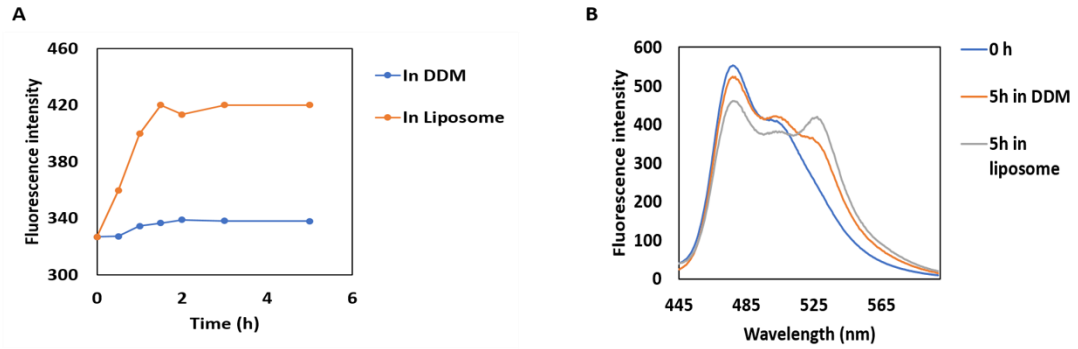

Figure 4.12 Reconstitution of AcrB$_{P223G}$-5aa-CFP and AcrB$_{P223G}$-5aa-YPet in liposome. *A.* Change of FRET intensity over time. *B.* Fluorescence wavelength scan of mixture incubated in liposome and DDM for 5 hours.

4.4 Discussion and Conclusion

It is difficult to determine the kinetic behavior of RND pumps, because the complex spans cytoplasm, periplasm, and two membranes. Another reason is there are three components in the complex, it is uncertain if the kinetic properties are determined from one single component or from the whole complex.[168] To date, there are not many reports about the oligomerization of RND pumps, especially for AcrB, although the crystal structures of

them have been resolved. FRET is a powerful method that can be used to study biological kinetic process. In most cases, fusion of fluorescent proteins does not change the structure and the function of the proteins studied and the sensitivity of fluorescence is relatively higher than many other traditional biochemistry techniques. Conformational change could be reflected by FRET like a switch with on state and off state. Therefore, FRET is appropriate approach to study the association of AcrB monomers.

FRET efficiency which depends on separation distance between donor and acceptor with a reversed 6-th power law provides some insights about the distance among protein subunits in this study. Higher FRET efficiency usually indicates shorter distance between donor and acceptor which is helpful for kinetic studies.[60] To obtain high FRET efficiency, different linker and different fluorescent protein combination were tried. 15aa linker constructs had lower expression level, which is not suitable for further studies. Comparing to YFP, YPet is a better FRET partner for CFP. YPet with brightness value of 238 (product of extinction coefficient and quantum yield, expressed as a percentage of EGFP) is much brighter than YFP which has a brightness value of 151. In addition, the quantum yield of YPet (0.77) is higher than YFP (0.61).[169] Both factors determine that FRET efficiency for CFP-YPet pair is higher than CFP-YFP pair, and expression level of YPet was much higher. Kinetic studies showed a Hill coefficient value greater than 1 which suggested that positive cooperativity in association of AcrB monomers. It indicated that association of AcrB monomers into dimers possibly facilitated the third monomer to bind, which provided some insight about how AcrB trimers formed. Comparing to the association of trimer from three monomers simultaneously, it seemed that forming dimers first was more reasonable. Association of

AcrB$_{P223G}$ monomers *in vitro* occurred immediately when the monomers were mixed, which indicated that the association rate was really fast. Half maximal concentration constant showed AcrB affinity is high. Reconstitution result showed that the presence of lipids and formation of liposome is better for association of AcrB monomers than DDM. The possible explanation is that the presence of fragments of lipid bilayers during and after the formation of liposomes provide a more favorable environment for AcrB monomers to interact and association.

Chapter V. Application of Fluorescence Protein in Kinetic Studies of ssrA-tagged Membrane Protein Degradation

5.1 Introduction

Removing extraneous or damaged protein through protein degradation is critical for cells to function fundamentally. In eukaryotic organisms, there are mainly two important proteolytic machineries: the proteasome and lysosome which are responsible for protein degradation in the ubiquitin-proteasome system and autophagy, respectively.[170] Most studies showed that misfolded membrane protein is dislocated through the endoplasmic reticulum associated degradation (ERAD) pathway, followed by ubiquitination and subsequent degradation by proteasome. An alternative strategy involves proteases cleaving their substrates in the plane of membrane instead of pulling out transmembrane domain of substrates from the membrane.[171] In prokaryotic cells, there are mainly two types of proteases which recognize the substrates and translocate them into core compartment for degradation. One type is degradation complexes such as ClpXP, ClpAP, FtsH, while the other type is proteasome ubiquitin-like proteins like Pup and SAMPs.[75] Similar to ubiquitin in eukaryotes, prokaryotic ubiquitin-like protein does a similar work in Archaea and some bacteria. Prokaryotic ubiquitin-like protein was first discovered in 2008 and named “Pup”. Later, SAMPs indicating ubiquitin-like small archaeal modifier proteins with other related enzymes were identified in *Haloferax volcanii*.[172] For degradation complexes, N-end rule recognition applies in a lot of families, but ClpXP and ClpAP recognize a C-terminal signature peptide called “ssrA” with an amino acid sequence of “AANDENYALAA”. ClpXP system belongs to AAA+ protease, which plays a critical role in degradation of ssrA tagged protein in almost all species. However, it is a challenge to understand how

prokaryotic cells degrade membrane proteins, although degradation of soluble proteins has been well studied. In *E.coli* cells, tm RNA or SsrA ribosome rescue system mediates addition of ssrA tag to nascent peptide in protein biosynthesis when ribosome stalls. Then proteases such as ClpXP, ClpAP or FtsH degrade the ssrA tagged protein.[173]

To expand the use of GFP as reporter, GFP-ssrA and its variants were firstly constructed by Jens Bo Anderson *et al* in 1998.[174] Soon GFP-ssrA, whose conformation change could be monitored in fluorescence and absorption, became a good model substrate of ClpXP or ClpAP to study the mechanism of degradation and even the dynamics in Dr. Sauer's lab and Dr. Baker's lab.[175] Degradation of ssrA-tagged protein is a multistep reaction including five steps: binding of substrates to ClpXP, substrate denaturation, translocation, substrate cleavage and release of peptide fragments. Among them, substrate denaturation limits the overall degradation rate according to the kinetic studies in which ^{35}S labelled GFP peptides were used as indicators. [175] Adaptor protein SspB enhances the degradation of ssrA tagged protein by helping to bring substrates and ClpXP together. In absence of SspB, degradation of GFP-ssrA showed a V_{max} of 0.9 $min^{-1}ClpX^{-1}$ while the value is 1.2 $min^{-1}ClpX^{-1}$ in presence of GFP-ssrA.[176]

Analyzing data collected from the experiments is always an important step in research. Michaelis-Menten kinetics, shown in the following, which was derived in 1913 and named after German biochemist Leonor Michaelis and Canadian physician Maud Menten is one of the best-known approaches to enzyme kinetics.[177] In 1925, Briggs and Haldane interpreted Michaelis-Menten kinetics and assumed the reaction reaches a state called

quasi-steady state in which enzyme-substrate complex remains constant when the concentration of substrates is much higher than that of enzyme.[178]

$$v = \frac{d[P]}{dt} = \frac{V_{max}[S]}{K_M + [S]}$$

where K_M represents Michaelis constant, V_{max} represents the maximum velocity the system achieved, v represents the reaction rate and [S] represents initial substrate concentration. Besides Michaelis-Menten kinetics, the Hill equation is another important approach to enzyme kinetics. The Hill equation as shown in the following, firstly formulated and applied by Archibald Vivian Hill to describe the binding of oxygen to haemoglobin which showed a sigmoidal curve in 1913, has been extensively used in biochemistry, physiology and pharmacology to analyze the interactions between ligands and receptors.[179; 180]

$$\theta = \frac{Bound}{Total} = \frac{[L]^n}{K_d + [L]^n} = \frac{[L]^n}{(K_A)^n + [L]^n} = \frac{1}{\left(\frac{K_A}{[L]}\right)^n + 1}$$

where θ represents fraction of the receptor protein concentration that bound to ligands. [L] represents the concentration of unbound ligands. K_d represents apparent dissociation constant.[180] The derivation of Hill equation used in enzyme kinetics is following:

$$v = \frac{V_{max}[s]^n}{{K_{0.5}}^n + [s]^n}$$

where v represents reaction velocity, [S] represents substrate concentration, $K_{0.5}$ or K_{half} half maximal concentration constant. Hill coefficient "n" is not equal to the number of binding sites, and it tends to the number of binding sites when the cooperativity is strong.[167]

Previous studies in our lab showed that ssrA tag facilitated the degradation of AcrB.[181] Deletion of *clpX* or *clpP* gene increased the expression of AcrB-ssrA, indicating that ClpXP

was involved in the degradation of AcrB-ssrA *in vivo*. Co-transformation experiment and ethidium bromide efflux assay showed that AcrB-ssrA was degraded after membrane insertion. To quantitatively monitor the kinetics of degradation, a real-time assay is essential. In early studies, we created several AcrB-fluorescent protein fusions and confirmed that the fusion proteins are fully active. Here we used AcrB-CFP to investigate its degradation. Monitored using fluorescence spectrometer, the degradation of AcrB-CFP-ssrA showed a lower degradation rate comparing to the degradation of GFP-ssrA. SspB improved the degradation rate drastically.

5.2 Material and methods

5.2.1 Cloning, Expression and Purification of AcrB-15aa-CFP-ssrA.

The plasmid *pFLIPmal-40uDelta1YFP* (plasmid catalog number 18853) harboring CFP gene was purchased from Addgene (Cambridge, MA). Primers encoding 15 amino acid linker GGSGGSGGSGGSGGS and ssrA tag were ordered from Integrated DNA technologies (Coralville, IA). To fuse CFP with AcrB, the restriction enzyme cutting sites XhoI and HindIII in plasmid vector *pBAD33* were applied in digestion and ligation. After DNA sequencing, the plasmid *pBAD33-acrB-15aa-cfp-ssrA* was transformed into *E.coli* DL41Δ*acrB*Δ*clpX* (Kanamycin cassette removed, DE3) competent cells for expression and purification. Purification of AcrB-15aa-CFP-ssrA were conducted as described.[39]

5.2.2 Degradation of AcrB-CFP-ssrA by ClpXP system *In vivo* and *In vitro*.

In vivo, the plasmid *pBAD33-acrB-15aa-CFP-ssrA* or *pBAD33-acrB-15aa-CFP* was transformed into DL41 or DL41Δ*clpX* competent cells separately. Single colonies were

picked from LB agar plates and cultured into tubes containing LB medium and relative antibiotics at 37ºC overnight. Cell pellet after sonication and centrifugation was dissolved in 10% SDS and then incubated at room temperature for 10 min. Supernatant was analyzed through SDS-PAGE and Western blot. To confirm the result of *In vivo* assay, the plasmids *pBAD33-acrB-15aa-cfp-ssrA* and *pET28a-his$_6$-clpX* were co-transformed in DL41*ΔacrB ΔclpX* (Kanamycin cassette removed, DE3) competent cells. The synthesis of ClpX was induced by 0.25 mM IPTG when OD_{600} of the cells reached ~1.0. At time 0, 2.5, 5, 10, 20, 30 min, take out the same amount of the cells and harvest the cells using centrifugation of 7000 rpm, 3min. SDS-PAGE and Western blot were used to analyze left AcrB-CFP-ssrA after degradation.

In vitro, purified protein substrate was mixed with ClpX, ClpP and SspB according to specific molecular ratio according to different protein substrates in PD buffer containing 0.03% DDM which was incubated in ice bath before the assay. 5mM ATP with ATP regeneration system containing 16mM creatine phosphate and 0.32 mg/mL creatine kinase was added into the system to provide energy for proteases. Then the mixture was transferred into 30 ºC water bath for incubation. LS 55 fluorescence spectrometer was used to monitor the change of fluorescence intensity over time. At time 0, 2.5, 5, 10, 20 and 30 min, 30 uL of the mixture was collected and mixed with 4 uL of 6* SDS loading dye containing 100 mM PMSF to stop the reaction. Western blot was conducted to determine the amount of substrate leftover.

5.2.3 Protein stability assay of AcrB-CFP-ssrA and related mutants.

Drug susceptibility of the cells harboring the gene *acrB-cfp-ssrA* and related variants was determined by measuring minimum inhibitory concentration (MIC) of erythromycin and novobiocin. The strains were cultured overnight and then diluted in 10-fold as the starting culture, and then they were added into 1mL LB medium containing two-fold diluted antibiotic. All the cells were incubated at 37ºC for 6 hours, absorbance of the cultured was measured by BioTek Gen5 reader.

The stability of AcrB-CFP-ssrA and relative variants were also determined by the limited trypsin digestion. Trypsin (Sigma-Aldrich, St. Louis, MO) was mixed with WT-AcrB or AcrB-CFP-ssrA with the molecular ratio of 1:30 in buffer (20 mM sodium-phosphate, 200 mM NaCl, 10% glycerol, 0.03% DDM, pH 7.5) at room temperature. At the indicated time point, digestion was quenched by the addition of 6 ×SDS protein loading dye and PMSF. The samples were resolved through Western blot.

5.2.4 Kinetic studies of AcrB-CFP-ssrA degradation by ClpXP SspB system.

All proteins used in the assay were freshly purified using the protocol described in the previous chapter. The degradation assay was conducted according to the reference with minor modification.[175] All the solutions and samples used in the assay were pre-warmed in 30 ºC water bath for 2 minutes. Substrate with different concentration was added after the spectrometer reading reached equilibrium. Data fitting was conducted in OriginLab 9.0.

5.3 Results

5.3.1 Expression level determination of AcrB-CFP-ssrA in different competent cells.

In the previous studies, plasmid encoding *acrB-ssrA* was transformed into different competent cells with *clpX, clpA, clpP* and *sspB* knocked out. AcrB-ssrA expression could be observed in *ΔclpX* and *ΔclpP* cells, indicating ClpX and ClpP played a critical role in degradation of AcrB-ssrA. In this study, CFP was used as an indicator to monitor the degradation of AcrB-ssrA, which is more accurate than Western blot, especially in kinetic studies. To determine whether AcrB-CFP-ssrA was degraded *in vivo*, the plasmid *pBAD33-acrB-CFP-ssrA* was transformed into DL41*ΔacrB* and *DL41ΔacrBΔclpX* competent cells respectively. Clearly, Western blot result (Figure 5.1) showed that AcrB-CFP-ssrA was well expressed in DL41*ΔacrBΔclpX* cells while it was not in DL41*ΔacrB*, indicating that ClpX played a critical role in the degradation and removing *clpX* gene increased the expression of AcrB-CFP-ssrA.

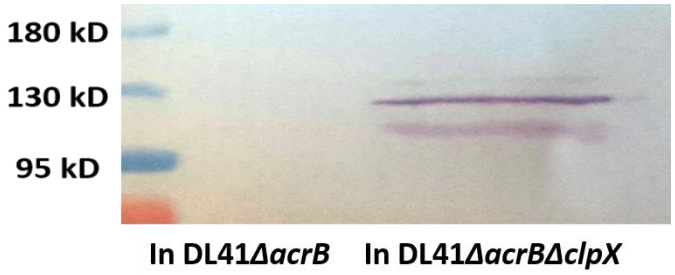

Figure 5.1 Expression level determination of AcrB-CFP-ssrA in DL41*ΔacrB* and DL41*ΔacrBΔclpX* competent cells.

Membrane proteins need to be translocated and inserted into cell membrane by signal recognition particle and chaperone proteins when they are synthesized in ribosome.[182] To determine whether AcrB was degraded after insertion into inner membrane, the plasmid

pBAD33-acrB-CFP-ssrA was co-transformed into DL41*ΔacrBΔclpX* (Kanamycin cassette removed, DE3) competent cells with *pET28a-clpX.* Expression of AcrB-CFP-ssrA did not need induction, while biosynthesis of ClpX was induced with 1 mM IPTG when OD_{600} reached 0.8. The result of Western blot (Figure 5.2) showed that all AcrB-CFP-ssrA expressed was degraded in 10 minutes, which was consistent with the result of expression level determination. The degradation rate was similar as the degradation rates of AcrB-ssrA and GFP-ssrA, which were obtained using radioactive method.[176; 181]

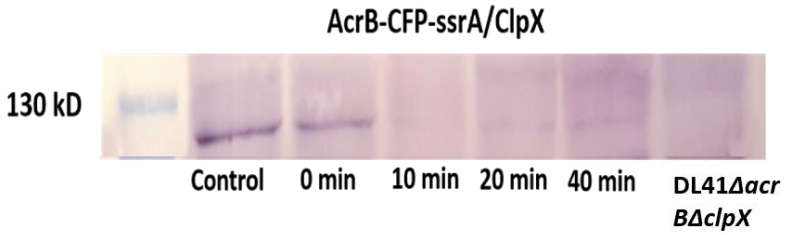

Figure 5.2 Co-expression of AcrB-CFP-ssrA and ClpX.

5.3.2 Activity and stability assay of ssrA tagged AcrB constructs

MIC test result showed that addition of CFP and ssrA tag did not influence the efflux activity of AcrB (Table 5.1). An alternative way to determine protein stability is limited trypsin digestion. Trypsin is a serine protease which catalyze the hydrolysis of protein peptides into small pieces at the carboxyl side of arginine or lysine.[183] To compare the stability of AcrB-CFP with WT-AcrB, limited trypsin digestion was conducted (Figure 5.3). Both protein substrates were resistant to trypsin digestion in 30 minutes and the way the two proteins were digested were similar, indicating that AcrB-CFP had similar conformation as WT-AcrB and fusion of CFP did not change the stability of AcrB.

Table 5.1 MIC test of AcrB-CFP-ssrA.

Strain	MIC (μg/mL)	
	Erythromycin	Novobiocin
WT-AcrB	160	320
AcrB-CFP-ssrA	160	320
ΔacrB	10	20

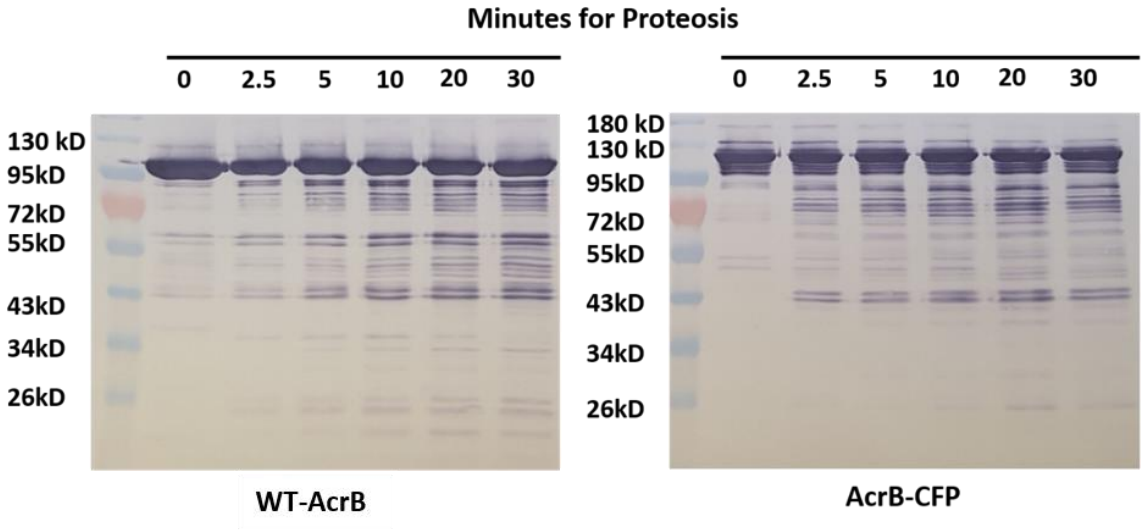

Figure 5.3 Limited trypsin digestion of purified WT-AcrB and AcrB-CFP.

5.3.3 Degradation of AcrB-CFP-ssrA by ClpXP with or without SspB

SspB is a dimeric substrate adaptor aids in delivery of ssrA-tagged substrates to ClpXP degradation system. The effect of the adaptor in the degradation of AcrB-CFP-ssrA was determined by comparing the degradation rate with or without SspB. The molecular ratio of AcrB-CFP-ssrA to SspB was set as 1 to 1. Obviously, the degradation rate was much

faster in the presence of SspB. The role of SspB played in the degradation process was aiding the binding of the substrate with ClpX.

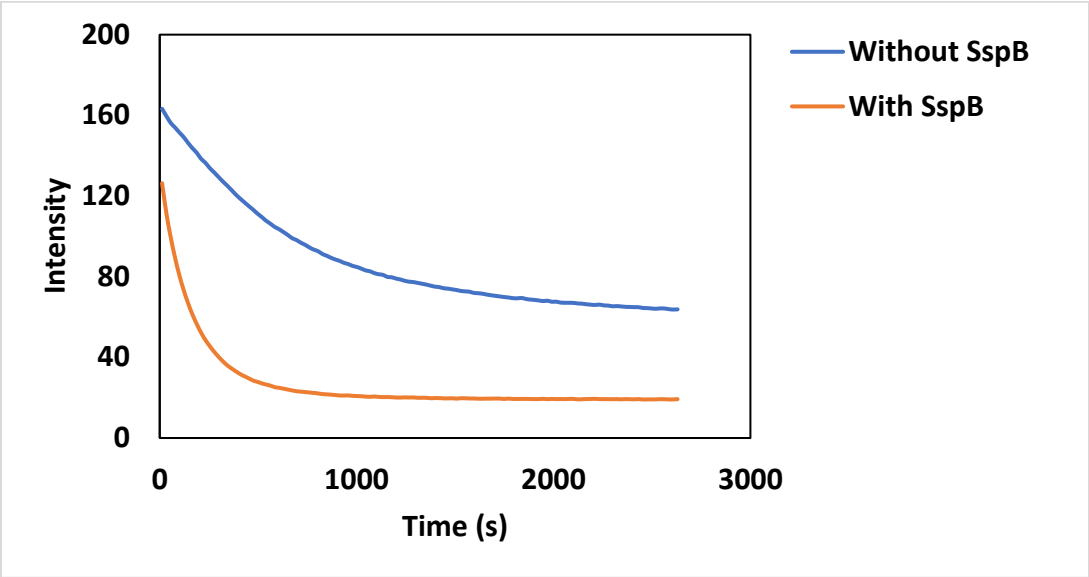

Figure 5.4 Degradation of AcrB-CFP-ssrA in presence or in absence of SspB.

5.3.4 Degradation of freshly purified AcrB-CFP-ssrA by ClpXP SspB *In vitro*.

AcrB-CFP-ssrA was freshly purified with high enough purity for degradation assay. After dialysis, the protein substrate was degraded by ClpXP system with a molar ratio of 1: 3: 6: 1 for AcrB-CFP-ssrA to ClpX, ClpP and SspB. Similar to the degradation of AcrB-CFP-ssrA *in vivo* which was fully degraded in 10 min, the degradation *in vitro* showed that more than 80 percent of the protein substrates were degraded in the first 10 minutes (Figure 5.5, *B* and *C*), although the protein substrate was not fully degraded. To determine if AcrB was degraded by the system, FLAG tag was inserted before CFP and AcrB, respectively. Western blot result showed that both AcrB and CFP were fully degraded by ClpXP (Figure 5.5, *C* and *D*).

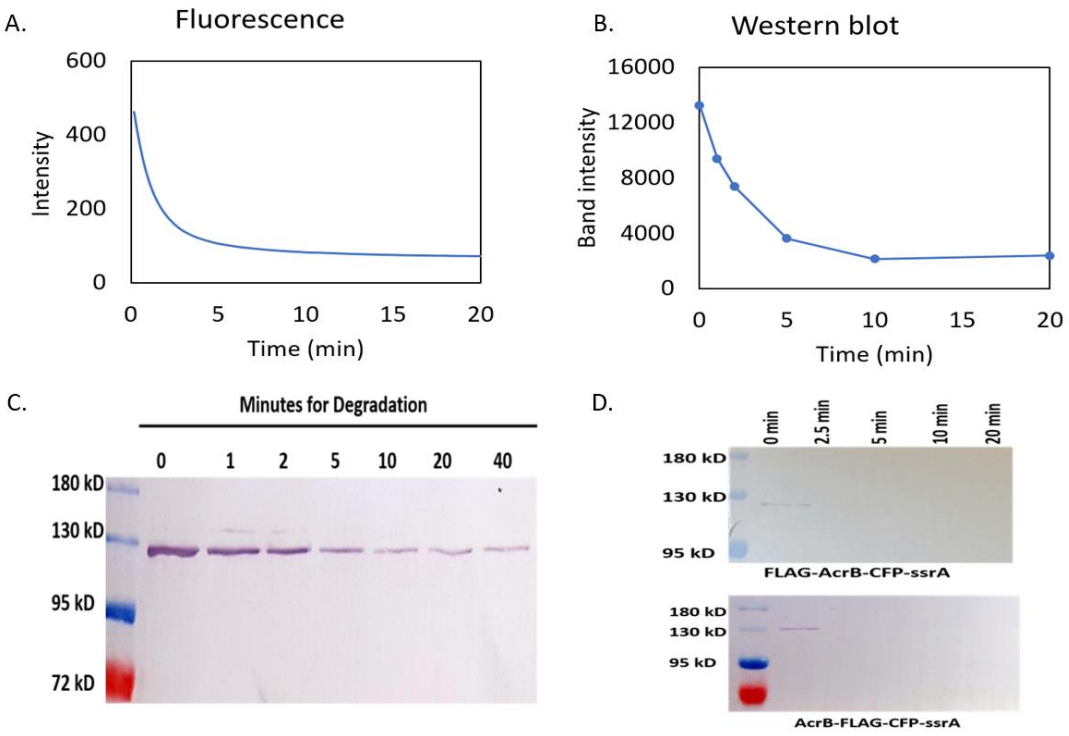

Figure 5.5 Degradation of purified AcrB-FLAG-CFP-ssrA by ClpX, ClpP, SspB *In vitro*. *A.* Determined by fluorescence spectrometer. *B.* Loss percentage calculation of AcrB-CFP-ssrA. *C.* Western blot result showing the degradation of AcrB-CFP-FLAG-ssrA. Anti-FLAG-tag antibody was used. *D.* Western blot result showing the degradation of FLAG-AcrB-CFP-ssrA and AcrB-FLAG-CFP-ssrA. Anti-FLAG tag antibody was used.

5.3.5 Unfolding of AcrB-CFP-ssrA by ClpX

Interestingly, AcrB-CFP-ssrA could be partially unfolded by ClpX alone while GFP-ssrA was unfolded partially in the first several minutes and then refolded back (Figure 5.6). GFP is mainly comprised of 11 beta sheets which make GFP a relatively tight structure.[64] The degradation level was higher and the rate was faster when SspB was added to help unfolding in the system.

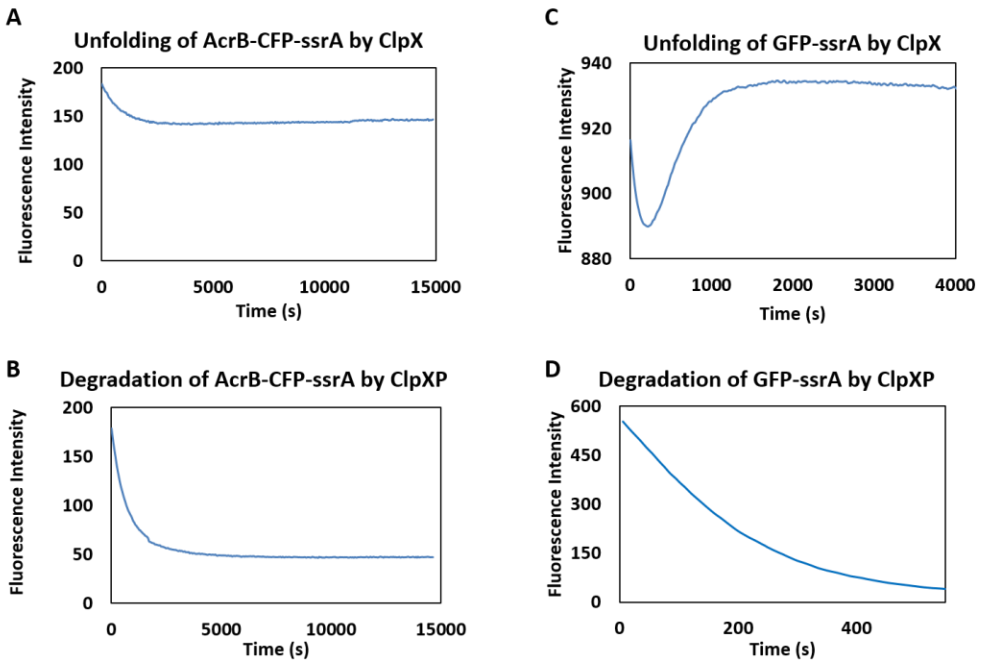

Figure 5.6 Degradation of AcrB-CFP-ssrA and GFP-ssrA. *A.* Degradation of AcrB-CFP-ssrA by ClpX alone. *B.* Degradation of AcrB-CFP-ssrA by ClpXP. *C.* Degradation of GFP-ssrA by ClpX alone. *D.* Degradation of GFP-ssrA by ClpXP.

5.3.6 Kinetic studies of degradation of AcrB-CFP-ssrA.

Comparing to the degradation of GFP-ssrA, Michaelis-Menten kinetics showed worse fitting result than The Hill equation fitting (Figure 5.7). And the maximum velocity of the degradation of AcrB-CFP-ssrA is much slower than GFP-ssrA (Table 5.2). However, the binding of substrates to enzyme seemed higher for AcrB-CFP-ssrA than GFP-ssrA. The Hill equation fit the data of AcrB-CFP-ssrA degradation better than Michaelis-Menten kinetics, suggesting the degradation behavior of AcrB-CFP-ssrA might be different from GFP-ssrA degradation.

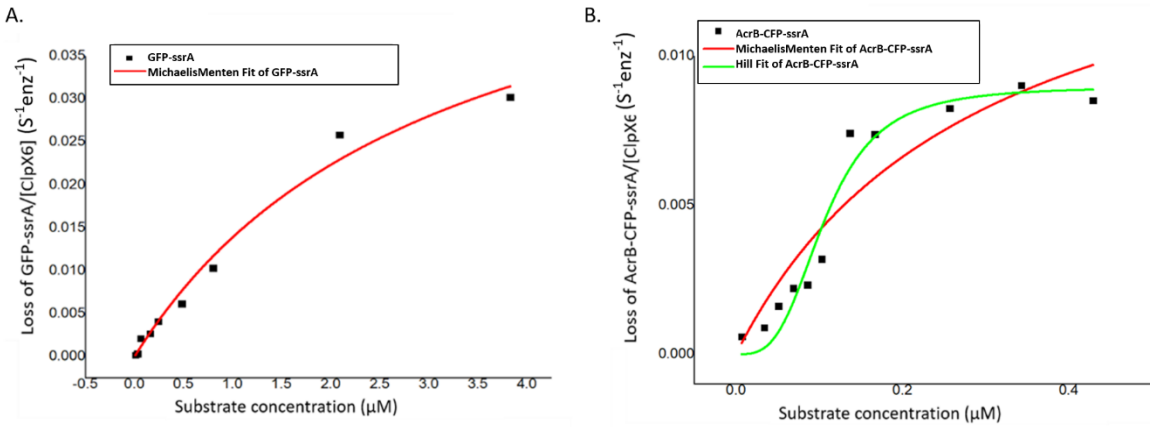

Figure 5.7 Kinetic studies of ssrA tagged protein degradation. *A.* Degradation of GFP-ssrA. Michaelis-Menten kinetics was used to fit the data. *B.* Degradation of AcrB-CFP-ssrA. Michaelis-Menten kinetics and the Hill equation were used to fit the data.

Table 5.2 Michaelis-Menten kinetics and the Hill equation fitting results.

Parameter	GFP-ssrA	AcrB-CFP-ssA	
	Michaelis-Menten kinetics fitting	Michaelis-Menten kinetics fitting	The Hill equation fittting
K (μM)	3.10 ± 0.84	0.296 ± 0.148	0.106 ± 0.009
V_{max} ($s^{-1}enz^{-1}$)	0.050 ± 0.008	0.016 ± 0.005	0.009 ± 0.001
R^2	0.98	0.86	0.95
n	N/A	N/A	3.26 ± 0.75

5.4 Discussion and Conclusion

How misfolded or nonfunctional membrane proteins are removed from *E.coli* is poorly

understood, although the degradation of soluble protein has been well studied. In the previous study, degradation of ssrA-tagged AcrB, an inner membrane protein in *E.coli*, was investigated. The result showed that ssrA tagged AcrB was degraded in 15 minutes consistent with what was shown through pulse chase experiment. Here we inserted CFP as an indicator between AcrB and ssrA tag to create a better method to monitor the degradation and determine the kinetic properties of the degradation. The results showed that insertion of CFP did not change the activity and stability of AcrB shown through MIC test and limited trypsin digestion. The 5-amino acid linker between AcrB and CFP ensured that folding of AcrB was not influenced by insertion of CFP. CFP folds tightly when it is synthesized, and also the size, only 230 amino acid, is much smaller than AcrB which has 1049 amino acid with a 15-amino-acid tail at C terminus. Insertion of CFP did not influence the degradation of AcrB-ssrA, which could be concluded from the degradation rate observed *in vivo*. *In vitro*, it seemed that insertion of CFP increased the efficiency of degradation, possibly due to improved binding between CFP and ClpX or SspB.

To determine whether the degradation occurred after the insertion of AcrB in the membrane, co-expression of AcrB-CFP-ssrA and ClpX was conducted. AcrB was synthesized before synthesis of ClpX which need induction of IPTG. Degradation of freshly purified AcrB-CFP-ssrA provided insights about the roles of ClpX, ClpP and SspB play in the degradation. SspB is an adaptor which aids the substrate to bind with ClpX. With the help of SspB, the degradation of GFP-ssrA is much faster than the degradation without SspB.[176] But it is still not clear that whether all the three protein interactions (ClpX •SspB, SspB•ssrA, and ssrA•ClpX) occurs simultaneously or only two of them contacts (ClpX•SspB and

SspB•ssrA). ClpX unfolds the protein substrates and translocates them to the chamber of ClpP, however itself does not have the ability to degrade the unfolded polypeptides into small pieces. In both degradation experiments, SspB also contributed to the decrease. As a control, the unfolding of GFP-ssrA showed an even more interesting fluorescence change in which the fluorescence decreased firstly and then recovered to the original level indicating that GFP-ssrA was unfolded and refolded back to original structure. It has been reported that GFP has a very tight structure with 11 β-sheets and 1 α-helix which formed a structure called β-can. Without the continuous degradation of ClpP, partially unfolded GFP-ssrA polypeptides are easily refolded due to the special structure. However, the existence of AcrB prevent the refolding in the construct of AcrB-CFP-ssrA so that the fluorescence intensity did not recover. ClpP has a chamber by which the unfolded polypeptides can be digested into small pieces of several amino acids. In the presence of ClpP, both degradation of GFP-ssrA and AcrB-CFP-ssrA reached a final degradation state in which over 80 percentage of fluorescence signal was lost due to the expose of chromophore in the degradation process.

Another question need to be answered is that did the result of fluorescence decrease reflect the degradation of AcrB. The answer is yes. Since there are two components in the construct, AcrB and CFP. The fluorescence decrease only reflects the degradation of CFP, so FLAG tag was inserted at different positions of the plasmid: before AcrB, between AcrB and CFP, and after CFP. Anti-FLAG Western blot was used to monitor the degradation of AcrB-CFP-ssrA. The results (Figure5.5, *A, C* and *D*) showed that the degradation of AcrB over time was consistent with the decrease of fluorescence intensity for all the three

constructs with FLAG tag. Therefore, in the following experiments which mainly focus on the kinetic studies only used fluorescence as the indicator to show the level of degradation.

The measurement of the initial digestion rate versus substrate concentration yielded a sigmoidal plot with a positive Hill coefficient around 3, indicating the substrate binding and degradation to one AcrB subunit positively affected the binding and degradation of the neighboring subunits. Degradation of AcrB-CFP-ssrA seemed more difficult than the degradation of GFP-ssrA as reflected in V_{max}, because AcrB has 12 transmembrane α-helices which make AcrB more stable. Binding of AcrB-CFP-ssrA displayed a tighter affinity than GFP-ssrA. This is an interesting observation since the AcrB moiety is far away from the initial binding site, the ssrA tag. Several factors may affect the K value, including the accurate estimation of the substrate concentration and measurement of the degradation rate. Additional experiments will be necessary to validate this initial finding.

Appendix --- Miscellaneous Studies

6.1 Application of FRET to study AcrB trimer affinity

6.1.1 Materials and Method

AlexaFluor350-Maleimide labelling

To investigate the application of FRET on AcrB affinity, two mutants $AcrB_{W13C}$ and $AcrB_{W13C/P223G}$ were created by sited mutagenesis. Expression and purification was conducted as described above. For labeling, freshly purified CL-$AcrB_{W13C}$ or CL-$AcrB_{W13C/P223G}$ samples were incubated in the dialysis buffer in the presence of a 20-fold molar excess of AF350-MLM. The reaction mixture was incubated on ice for 1 h, and then Tris-Cl (pH 8.0) was added to a final concentration of 10 mM. Free dye was removed through dialysis of twice overnight. The molar ratio of labeling was estimated from the UV absorbance of the protein (extinction coefficient of 90 000 cm^{-1} M^{-1} at 280 nm) and AF350 (extinction coefficient of 19 000 cm^{-1} M^{-1} at 346 nm). For FRET measurement, the excitation wavelength was 280 nm. To determine the contribution of leaky emission of AF350 excited at 280 nm, emission spectra of a solution containing 1 μM of AF350-MLM and 1 mM DDT were measured with an excitation wavelength of 280 nm and 346 nm, respectively. When excited at 346 nm, the emission peak intensity at 440 nm was measured to be 6.6-fold of the peak intensity when excited at 280 nm. For AF350-MLM-labeled AcrB samples, emission spectra were collected at excitation wavelengths of 280 and 346 nm. The peak intensity observed at 440 nm, when excited at 346 nm, was used to back calculate the contribution from the direct excitation at 280 nm. This reference trace was subtracted from the FRET spectra.[116]

6.1.2 Results and discussion

Measurement of FRET between tryptophan and AF350

To design a FRET pair with minimum disruption to the structure of AcrB, I decided to take advantage of an intrinsic Trp to serve as the donor to form a FRET pair with Alexa Fluor 350 (AF350) (Figure 6.1). Two Trp residues from neighboring subunits are close to each other at the inter-subunit interface, W13 and W895. To facilitate site-specific labeling, I first replaced the two intrinsic Cys from the sequence of AcrB with Ala and then introduced a W13C mutation. The triple mutant, CL-AcrB$_{W13C}$, was fully active (data not shown). To create a negative control, I introduced an additional mutation, P223G, into the triple mutant to create CL-AcrB$_{W13C/P223G}$. We have known from previous studies that the P223G mutation leads to trimer dissociation. We used CL-AcrB$_{W13C/P223G}$ as a "low affinity control" to compare with CL-AcrB$_{W13C}$, which is our high affinity sample. Both CL-AcrB$_{W13C}$ and CL-AcrB$_{W13C/P223G}$ were purified and characterized using CD (Figure 6.1, *A*). The traces overlap with the spectrum of WT-AcrB, indicating the mutations did not cause protein unfolding.

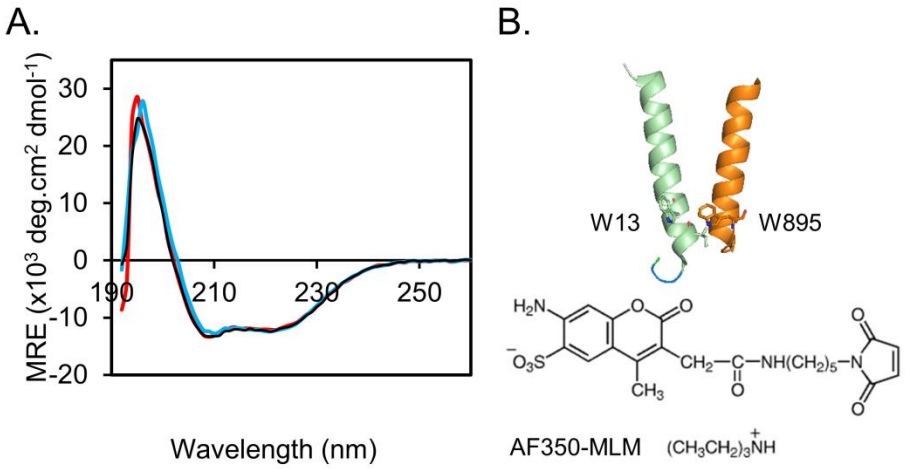

Figure 6.1 *A*. CD spectra of WT (black), CL-AcrB$_{W13C}$ (red), and CL-AcrB$_{W13C/P223G}$ (blue) are very similar. *B*. Location of W13 and W895 from neighboring subunits. Trp can serve as a FRET donor to AF350.

Purified CL-AcrB$_{W13C}$ and CL-AcrB$_{W13C/P223G}$ were labeled as described in materials and methods. After removing free dye using dialysis, UV/Vis spectra were used to determine the labelling efficiency of CL-AcrB$_{W13C}$ and CL-AcrB$_{W13C/P223G}$ using the molar ratio of AF350-MLM (346 nm) to AcrB (280 nm) (Figure 6.2). The labelling efficiency of CL-AcrB$_{W13C/P223G}$ was close to 1.0, which was approximately twice of that of CL-AcrB$_{W13C}$ labeling. This difference is likely a result of the difference in intrinsic accessibility of C13, as C13 in CL-AcrB$_{W13C}$ is less accessible to AF350-MLM during labeling because of the higher trimer affinity. Then FRET between tryptophan and AF350 was measured using fluorescence spectrometer. The result shown in panel B confirmed the calculation of labelling efficiency. The ratio of FL430 (intensity at 430 nm) to FL340 (intensity at 340 nm) reflected the degree of FRET. The value of ratio was 0.61 for CL-AcrB$_{W13C}$ and was

2.11 for CL-AcrB$_{W13C/P223G}$.

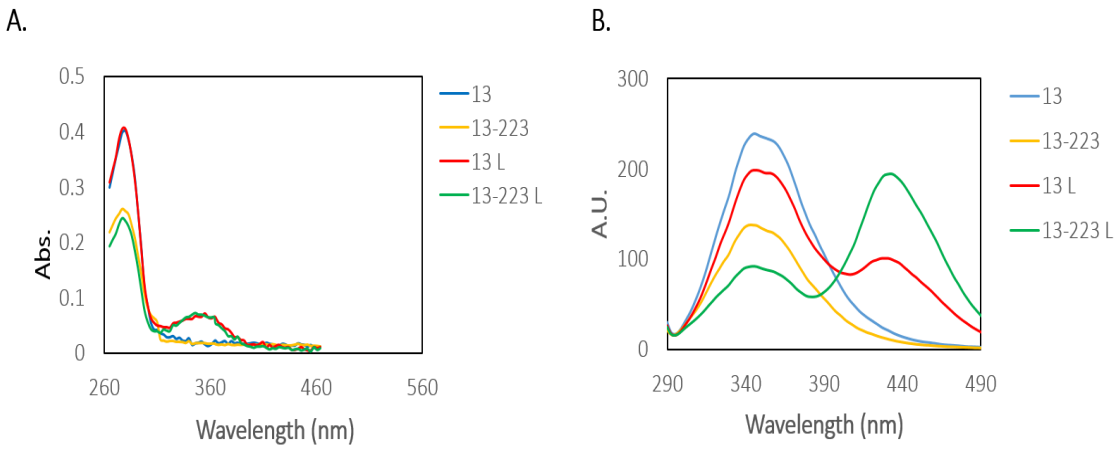

Figure 6.2 Spectroscopic analyses of AcrB$_{W13C}$, AcrB$_{W13C/P223G}$ and their labelled products. *A*. UV/vis spectra of control and labeled samples. The peak intensity at 280 nm and 350 nm was used to calculate the ratio of labeling. *B*. Fluorescence emission spectra of control and labeled samples. Excitation wavelength is 280 nm.

To promote AcrB dissociation/unfolding, we titrated small aliquots of concentrated SDS into the samples (Figure 6.3 *A*). The traces are color coded to shift from red to blue with the increase in the SDS concentration. The intrinsic fluorescence of AcrB decreased drastically with the increase in the SDS concentration, presumably due to protein denaturation. The observed change of fluorescence was mainly contributed by Trp residues in the soluble domain.[116] Monitoring the change of intrinsic fluorescence could reflect the process of AcrB gradually losing the folded periplasmic domain, which could be coupled with, or occur after, trimer dissociation. The peak at 340 nm was plotted against the concentration of SDS to reveal the protein unfolding profile (Figure 6.3, *B*). The unfolding profile of the labeled mutant proteins were very similar as the one we collected for wild-

type AcrB, further confirming that the W13C mutation and the labeling did not have a large impact on the overall structure.

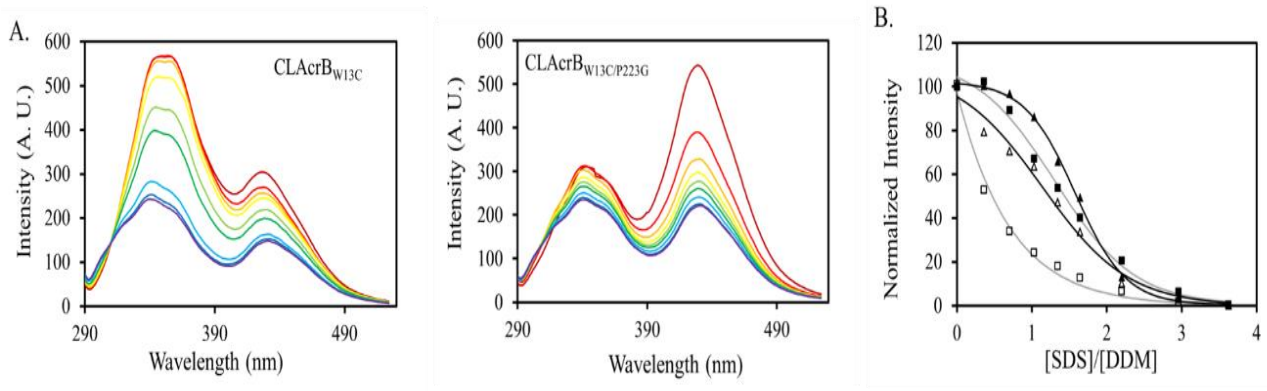

Figure 6.3 *A*. Fluorescence emission of AF350 labeled CL-AcrB$_{W13C}$ (top) and CL-AcrB$_{W13C/P223G}$ (bottom) when excited at 280 nm. The traces are color coded to shift from red to blue with the increase of SDS concentration. The two peaks at 345 and 430 nm corresponded to the intrinsic fluorescence emission of AcrB and emission from AF350, respectively. Both decreased with the increase of SDS concentration. *B*. Normalized fluorescence intensity of CL-AcrB$_{W13C}$ at 345 nm (filled triangles) and 430 nm (open triangles), and CL-AcrB$_{W13C/P223G}$ at 345 nm (filled squares) and 430 nm (open squares). While the structure of CL-AcrB$_{W13C/P223G}$ began to unfold at a slightly lower SDS concentration than the structure of CL-AcrB$_{W13C}$, the decrease of the FRET efficiency occurred as a much lower SDS concentration for CL-AcrB$_{W13C/P223G}$. The lines are used to illustrate the trend of the data.

Using the change of the intrinsic fluorescence as a beacon of AcrB dissociation/unfolding, researchers could evaluate the change of FRET efficiency during the process (Figure 6.3, *B*). Since CL-AcrB$_{W13C}$ and CL-AcrB$_{W13C/P223G}$ were intrinsically labeled to different

levels, I normalized the AF350 signal changes using equation: $(Y-Y_{min})/(Y_{max}-Y_{min})$, with the peak intensity in the absence of SDS designated as Y_{max} and the peak intensity at the highest SDS concentration designated as Y_{min}. While the complexity of the system ruled out a numerical interpretation of the trimer affinity, it was clear that the FRET efficiency decreased more dramatically with the increase of SDS concentration for CL-AcrB$_{W13C/P223G}$.

While working on the FRET experiment, I also had an unexpected discovery. Our lab has established through previous studies that freshly purified WT-AcrB exists predominantly as trimers. After prolonged incubation at 4^{o}C in the time scale of days, trimer dissociation occurs and a monomer band can be observed in BN-PAGE analysis. The change is unidirectional. The intensity of the trimer band decreases over time, and the intensity of the monomer band grows. We have never observed a dimer band. For AcrB$_{P223G}$, freshly purified sample is predominantly monomer. However, I found that after dialysis overnight, a large portion of AcrB$_{P223G}$ reassociated into trimers. The same is true for CL-AcrB$_{W13C/P223G}$ (Figure 6.4).

Next, I designed an experiment using FRET to monitor the trimer reassociation of CL-AcrB$_{W13C/P223G}$. The result showed that when low concentration of SDS was used to trigger trimer association (0.006% w/v), re-association of monomer could be observed when DDM was added (0.6% w/v) (Figure 6.4, *C*). This result was consistent with Cui's study on unfolding and refolding of AcrB.[124] At this low concentration, AcrB unfolding has not occurred, as revealed by the lack of change of intrinsic fluorescence emission (Figure 6.4, *B*). AcrB trimer dissocaited when 0.006% (w/v) SDS was added and re-associated partly

when DDM was added to dilute the effect of SDS. It is critical to use this low SDS concentration, as AcrB unfolded at higher SDS concentration and could not reversibly refold under the current condition.

In summary, FRET is a useful technique in studies of AcrB oligomer association. When SDS is titrated into a sample of AF350-labelled $AcrB_{W13C}$ or $AcrB_{W13C/P223G}$, a change of FRET could be monitored at a SDS concentration lower than the concentration that triggers monomer unfolding. This dissociation of trimer is partly reversibly, and monomers re-association could be observed when DDM is added to dilute SDS.

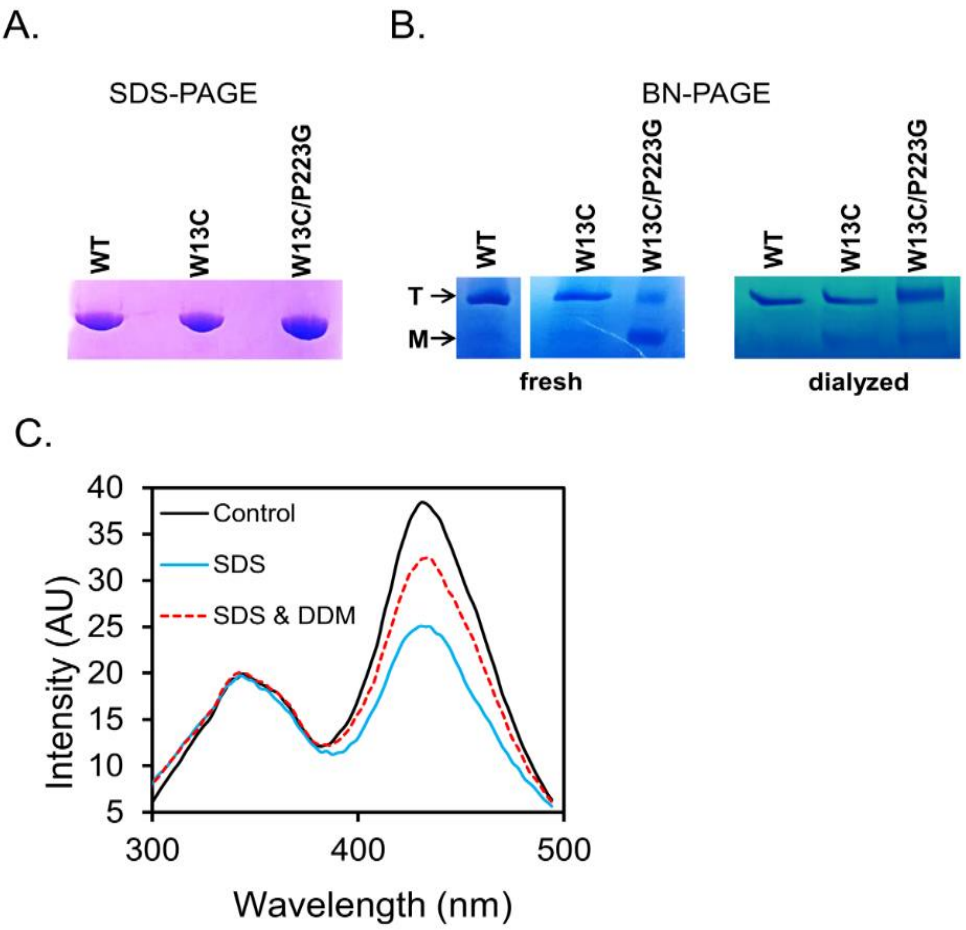

Figure 6.4 *A*. SDS-PAGE of purified AcrB samples. *B*. BN-PAGE analysis of the indicated AcrB samples. *C*. Fluorescence emission of AF350 labeled CL-AcrB$_{W13C/P223G}$ (black), in the presence of 0.006% (w/v) SDS (Blue) or 0.006% (w/v) SDS followed by 0.6% (w/v) DDM (red).

6.2 How many copies of AcrB in one *E.coli* cell are enough to make the cell survive?

To answer this question, the strategy is that the number of AcrB expressed from plasmid was controlled by dilution fold and the activity of relative diluted sample was determined through ethidium bromide accumulation assay. The protocol is following: the strain with

plasmid *pBAD33-wt-acrB* was cultured to OD_{600} of 1.0, and then diluted into fresh LB medium with different dilution folds. In the meantime, 0.2% glucose was added into the culture to inhibit AcrB synthesis. The diluted cells were re-cultured to OD_{600} of 0.6 to 0.8. Ethidium bromide accumulation assay was conducted to determine the activity of each sample. To get an accurate result, some related questions need to be answered: 1) what is the Western blot detection limit for AcrB; 2) how many copies of AcrB could be expressed from plasmid; 3) is there leaky expression for AcrB even glucose was used to inhibit its synthesis.

Western blot detection limit is determined as following:

Freshly purified AcrB was diluted in different folds, then the diluted samples were analyzed by Western blot (Figure 6.5). When OD_{280} is 0.0002, molar concentration is 0.7 nM which was calculated by the equation following, the Western blot band is almost not visible, suggesting the detection limit.

$c=A/(\varepsilon l) = 0.0002 \div (89700\ cm^{-1}M^{-1}\times 3\times 1\ cm) = 0.7\ nM$

And the mass is calculated by the quation:

$m=c*v*M_w = 0.7\ nM \times 16\ \mu L \times 113665\times 3\ g/mol = 3.8\ ng.$

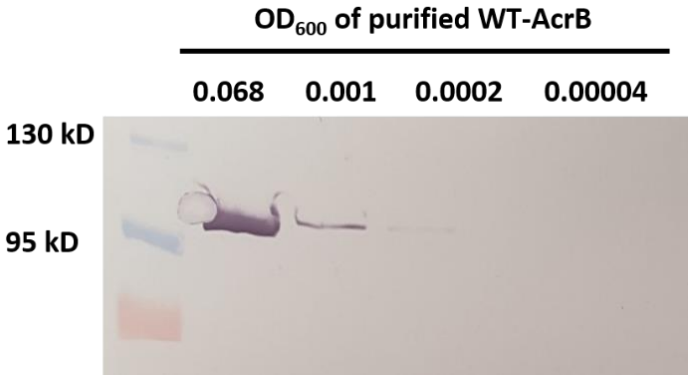

Figure 6.5 Western blot analysis of purified WT-AcrB.

Using purified WT-AcrB as control, the amount of AcrB expressed from the plasmid *pBAD33-wt-acrB* was analyzed through Western blot (Figure 6.6). 2 mL of culture contains $2*10^9$ cells when OD_{600} is 1.0. For *pBAD33-wt-acrB*, 25-fold dilution is similar to WT-AcrB with OD_{280} of 0.0002 in the standard. Therefore, there are $40 \times 10^{-6} \times 25 \times 0.7 \times 10^{-9} \times 6.02 \times 10^{23} = 13244 \times 10^8$ copies of AcrB exist in the 2 mL cells. In each cell, there are $13244 \times 10^8 \div 2 \div 10^9 \approx 220$ copies of AcrB expressed from the plasmid.

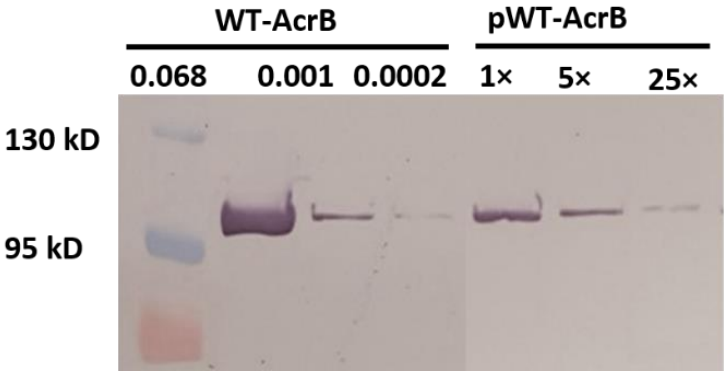

Figure 6.6 Determination of AcrB copy numbers expressed from the plasmid *pBAD33-wt-acrB* which was named as "pWT-AcrB".

Glucose is always used to repress the expression mediated by the P_{BAD} promoter of *araBAD* (arabinose) operon.[184] In the study, 0.2% glucose was added into the culture to repress AcrB expression. Comparing Western blot result to ethidium bromide accumulation result, the cells could still survive after 100,000 dilutions (Figure 6.7) which was not expected. One possible explanation is that the inhibition effect of glucose is incomplete, and thus some AcrB are still expressed, although it cannot be detected by Western blot.

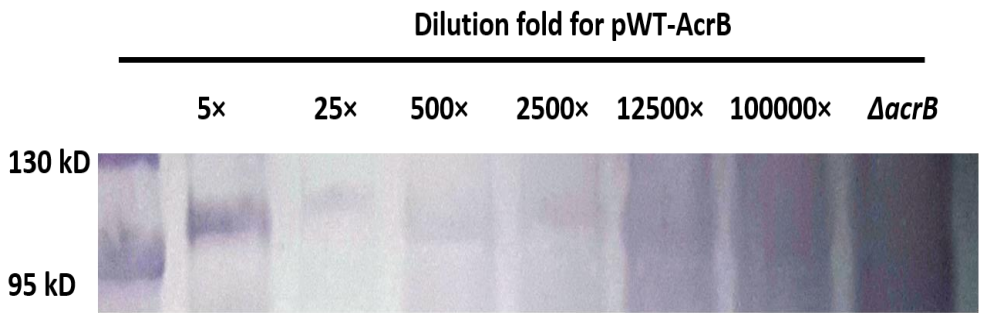

Figure 6.7 Western blot analysis of diluted pWT-AcrB.

Ethidium bromide accumulation assay was conducted as the protocol described in the previous chapter. The result showed that even for the sample diluted in 100,000 folds, the cells are still active, suggesting that the number of AcrB in the cells is enough for pumping out ethidium bromide dye.

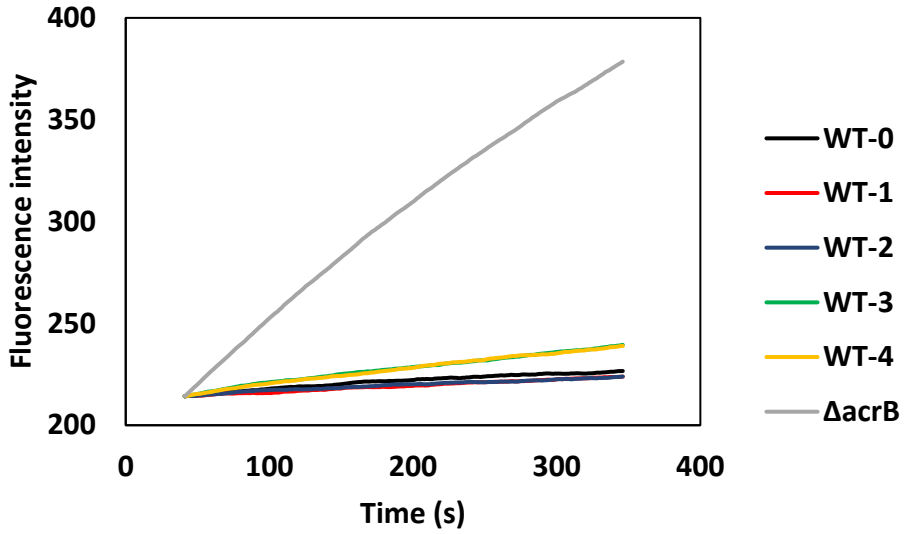

Figure 6.8 Ethidium bromide accumulation assay of diluted samples. WT-0, 1, 2, 3, and 4 represents the dilution folds of 5, 25, 500, 12500, 100000, respectively. The strain *ΔacrB* was used as negative control.

Leaky expression of glucose inhibited pWT-AcrB was determined through Western blot and purified WT-AcrB was used as a control. As shown in Figure 6.9, band intensity analyzed through Image J for the sample "Gi-WT 0×" is 717, while it is 1442 for "WT-AcrB 25×". The ratio is 717 ÷ 1442 = 0.4972. So, the leaky expression is about: 0.00111 $\times 10^{-6}$ mol/L × 40 $\times 10^{-6}$ L × 6.022×10^{23} ÷ (2 mL $\times 1 \times 10^{9}$/mL) ≈ 13 copies for each cell, indicating that the cells with about 13 copies of AcrB could survive. The exact copy number is possibly smaller than 13, but it could not be determined through traditional biochemistry techniques such as Western blot. More advanced method need to be applied to determine the exact number.

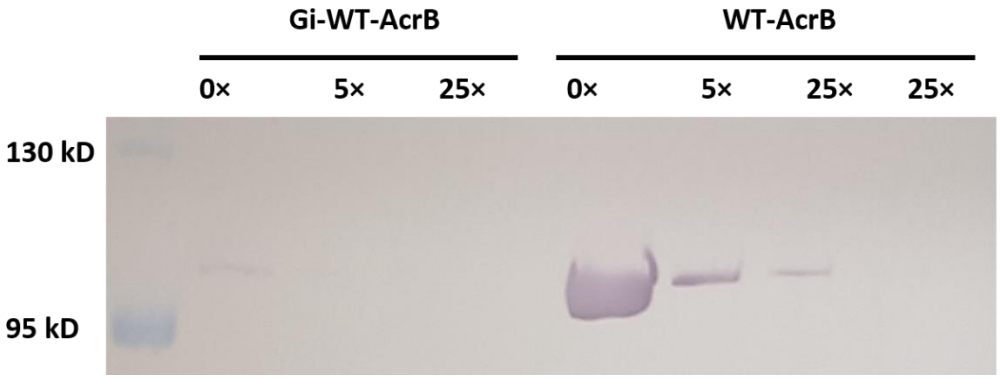

Figure 6.9 Leaky expression level determination of glucose inhibited WT-AcrB (Gi-WT-AcrB).

6.3 Expression and purification of Hepatitis B virus core protein CP149.

6.3.1 Materials and Methods

The gene encoding *CP149* was cloned into vector *pET24a* for expression without any tag and the sequence was confirmed via DNA sequencing. The plasmid *pET24a-CP149* was then transformed into BL21(DE3) strain for protein expression. A single colony was used

to inoculate 10 mL of LB media supplemented with 50 ug/mL kanamycin (kan). The culture was incubated with shaking at 250 rpm overnight at 37 ºC. The next morning, the overnight culture was diluted into 1 L fresh LB/kan media. The culture was incubated at 37 ºC with shaking at 250 rpm until the OD_{600} reached 0.8, and then Isopropyl β-D-1-thiogalactopyranoside (IPTG) was added to a final concentration of 2 mM to induce the expression of CP149. After an additional incubation of 5 hours, cells were collected by centrifugation at 7000×g for 10 minutes. The cell pellet was stored at -80 ºC until purification. Purification was conducted following published procedure.[185] Briefly, cells were resuspended in a buffer containing 50 mM Tris-HCl (pH 7.4), 1 mM EDTA, 5 mM DTT, 0.01 mg/mL RNase, and 2U/mL DNase. The cells were lysed by sonication in ice/water bath and centrifuged to collect the supernatant. Solid sucrose was added to the supernatant to a concentration of 0.15 M followed by centrifugation. Solid $(NH_4)_2SO_4$ was added to the supernatant to a final concentration of 40% saturation. The solution was incubated with gentle stirring at room temperature for 1 hour and then centrifuged again to collect the pellet. The pellet was resuspended in a buffer containing 100 mM Tris-HCl (pH 7.5), 100 mM NaCl, 50 mM sucrose, and 2 mM DTT (buffer A) and loaded on a Sephadex G-100 column equilibrated with the same buffer. Fractions were analyzed using SDS-PAGE. The fractions with high concentration of CP149 were combined and concentrated into 25 mL through Amicon® Ultra-15 (EMD Millipore Corporation, Darmstadt, Germany). Solid urea was added into concentrated sample to a final concentration of 3 M. EDTA was added into the solution to a final concentrationo of 1 mM. After incubated for 3 hours on ice, the sample solution was loaded onto a Sephadex G-100 column. The fractions were collected after elution with Buffer A and analyzed using SDS-PAGE. The

fractions containing dimers with high purity were collected and concentrated using Amicon® Ultra-15.

6.3.2 Results

The following pictures showed the analysis result of each step in purification.

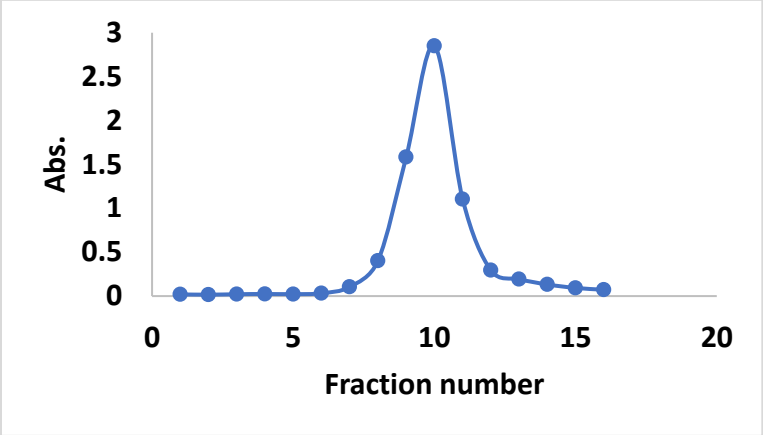

Figure 6.10 Chromatography profile as monitored using absorbance at 280 nm.

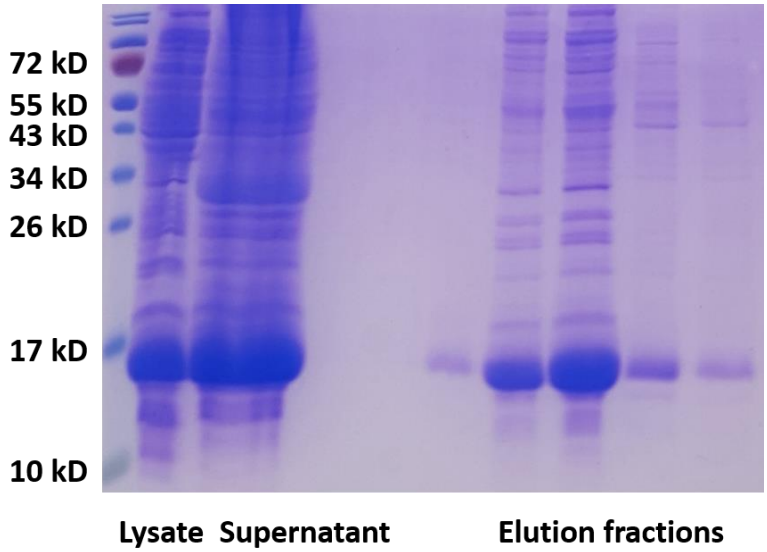

Figure 6.11 SDS-PAGE analysis of fractions. The major band close to 17 kD is CP149 monomer.

Then frations 7 to 12 were combined and concentrated using ultrafiltration with a Centricon-10 (Amicon). Urea and EDTA were added to final concentrations of 3 M and 1 mM, respectively, and the sample was incubated on ice for 3 hours. The treated sample was loaded and analyzed using the Sephadex G-100 column again. Fractions were analyzed by UV-VIS and SDS-PAGE.

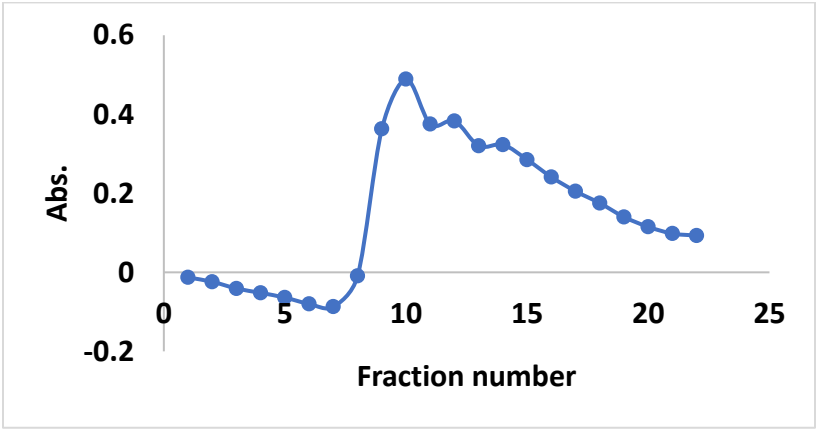

Figure 6.12 Chromatography profile as monitored using absorbance at 280 nm after treated with urea and EDTA.

Fractions with high purity was combined and concentrated through Amicon. SDS-PAGE was used to analyze the purity. The gel showed that the purity of CP149 is more than 90% and most of them are dimers, even the samples were treated with 2 mM DTT.

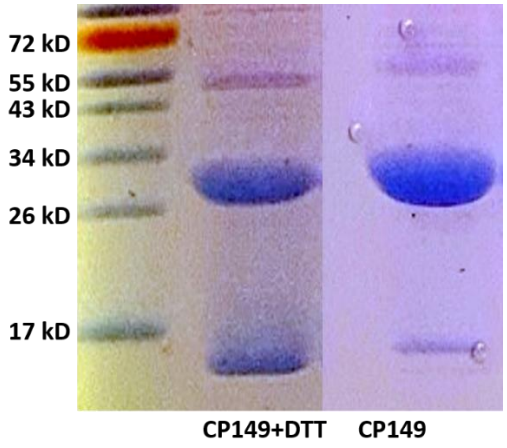

Figure 6.13 Purified CP149 treated DTT and CP149 control.

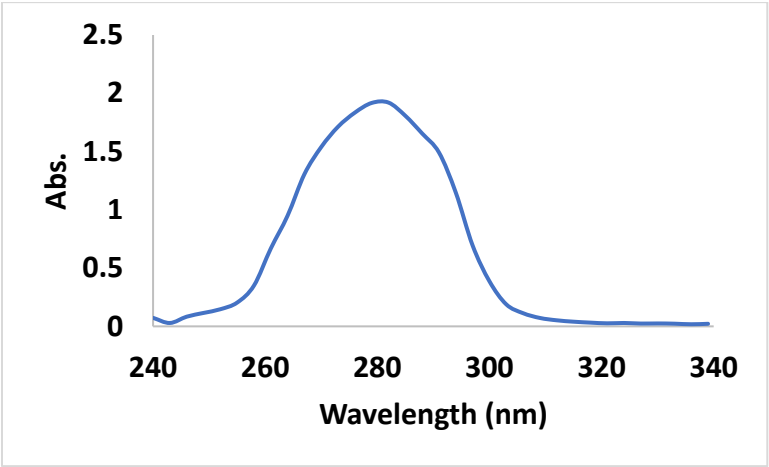

Figure 6.14 UV wavelength scan of purified CP149.

Analysis of purified samples.

CD and fluorescence analyses of purified Cp149. Fraction 14 was used for these analyses. CD spectrum revealed two negative peaks at 208/222 nm, consistent with the overall helical structure of CP149.

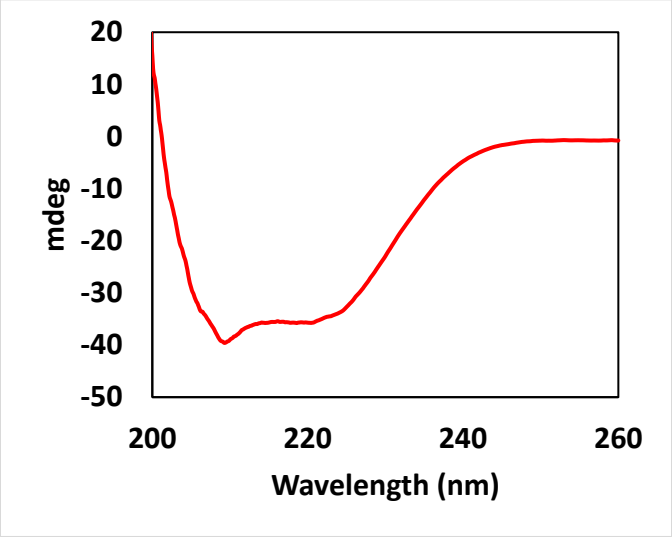

Figure 6.15 CD analysis of purified CP149 sample.

Fluroescence spectra

Wavelength scan was conducted at following condition: exicted at 280nm, ex slit 10nm, em slit 4nm, scan from 290nm to 400nm. The emission peak is at 342nm. Clearly, emission at 342nm for CP149 treated with 0.8M KCl is stronger than that for Cp149 alone, which could be due to assembly of CP149.

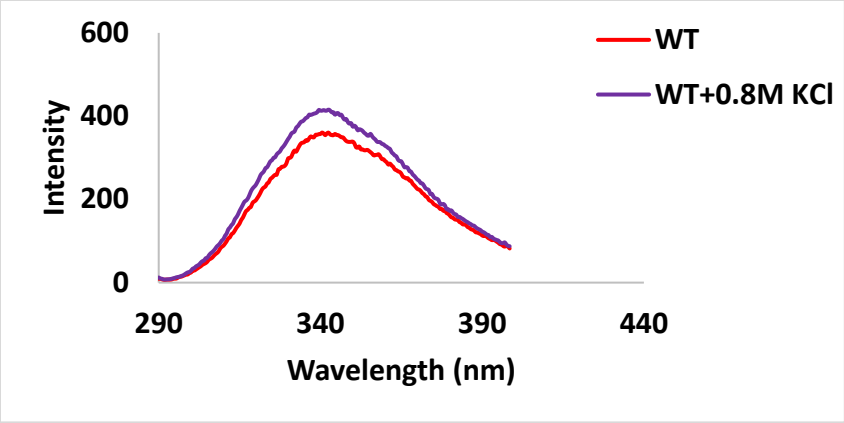

Figure 6.16 Fluorescence analysis of purified CP149 and purified CP149 treated with 0.8 M KCl.

6.4 Degradation of ssrA-tagged membrane protein by ClpXP

6.4.1 Degradation of AcrB-cI-ssrA by ClpXP

Lambda repressor protein cI is a transcriptional repressor that allows virus to establish and maintain latency which prevents both the viral DNA replication and the exit programs. Inserted as a linker between AcrB and ssrA tag, cI was used to determine whether it facilitated the degradation. AcrB-cI-ssrA was expressed well in *clpX* knock-out strain while it was not in the strain containing *clpX*. To clarify the degradation occurred after the protein was inserted in the membrane, the plasmid *pBAD33-acrB-cI-ssrA* was co-transformed into *pET28a-clpX.* Biosynthesis of ClpX was induced with 1.0 mM IPTG when OD_{600} reached 1.0, and then degradation of AcrB-cI-ssrA started. All the substrates were degraded in 80 minutes, indicating that the degradation occurred after the insertion of AcrB-cI-ssrA to membrane.

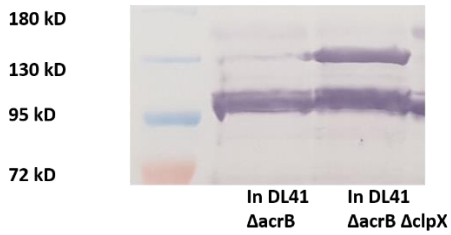

Figure 6.17 Expression level determination of AcrB-cI-ssrA in competent cells with or without *clpX* gene.

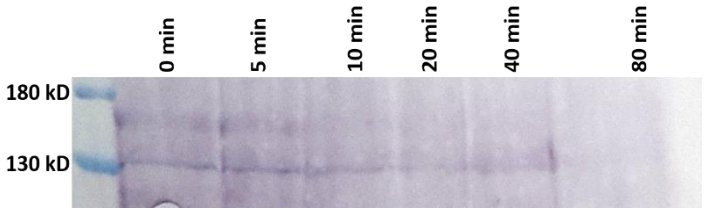

Figure 6.18 Co-expression of AcrB-cI-ssrA and ClpX.

To confirm AcrB-cI-ssrA was degraded by ClpXP system, freshly purified AcrB-cI-ssrA was mixed with purified ClpX, ClpP and SspB in PD buffer containing 5mM ATP and ATP regeneration system. Over 60% of the substrate degraded in 10 minutes which had similar degradation rate with AcrB-CFP-ssrA and GFP-ssrA.

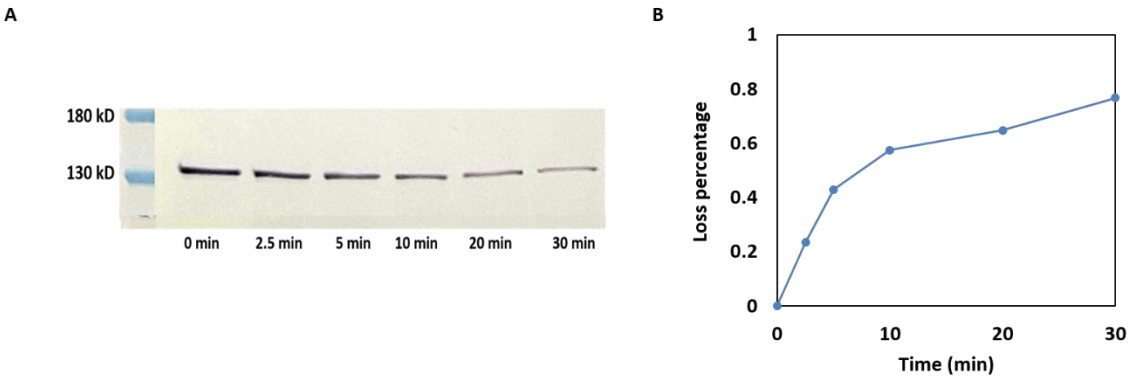

Figure 6.19 Degradation of AcrB-cI-ssrA *in vitro*. *A.* The degradation was shown through

Western blot. *B.* The degradation was shown in loss percentage which was obtained through calculation of band intensities.

6.4.2 Degradation of other ssrA tagged membrane protein.

To investigate whether other ssrA tagged membrane proteins were degraded by ClpXP, YajC-ssrA was expressed and purified. Freshly purified YajC-ssrA was mixed with ClpXP system, and it was completely degraded in 6 minutes which was much faster than that of AcrB-CFP-ssrA and AcrB-cI-ssrA (Figure 6.20).

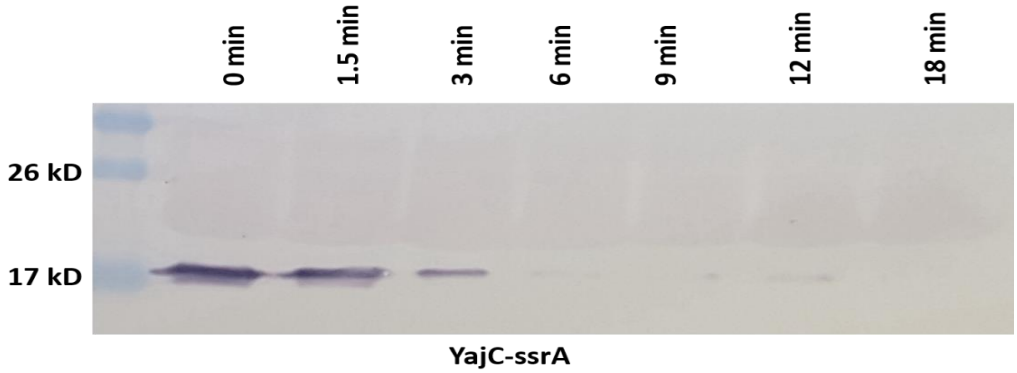

Figure 6.20 Degradation of YajC-ssrA *in vitro*.

References

1. Davies J, Davies D. (2010) Origins and evolution of antibiotic resistance. *Microbiol Mol Biol Rev* 74:417-433.
2. Nikaido H, Pages JM. (2012) Broad-specificity efflux pumps and their role in multidrug resistance of Gram-negative bacteria. *FEMS Microbiol Rev* 36:340-363.
3. Aminov RI. (2010) A brief history of the antibiotic era: lessons learned and challenges for the future. *Front Microbiol* 1:134.
4. Davies J. (1994) Inactivation of Antibiotics and the Dissemination of Resistance Genes. *Science* 264:375-382.
5. Nathan Citri ASaNZ. (1976) Acquisition of Substrate-Specific Parameters during the Catalytic Reaction of Penicillinase. *Proceedings of the National Academy of Sciences* 73:1048-1052.
6. Kumar A, Schweizer HP. (2005) Bacterial resistance to antibiotics: active efflux and reduced uptake. *Adv Drug Deliv Rev* 57:1486-1513.
7. Spratt BG. (1994) Resistance to Antibiotics Mediated by Target Alterations. *Science* 264:388-393.
8. Nobili S, Landini I, Mazzei T, Mini E. (2012) Overcoming tumor multidrug resistance using drugs able to evade P-glycoprotein or to exploit its expression. *Med Res Rev* 32:1220-1262.
9. Wright GD. (2007) The antibiotic resistome: the nexus of chemical and genetic diversity. *Nat Rev Microbiol* 5:175-186.
10. Sun J, Deng Z, Yan A. (2014) Bacterial multidrug efflux pumps: mechanisms, physiology and pharmacological exploitations. *Biochem Biophys Res Commun*

453:254-267.

11. Madej MG. (2014) Function, Structure, and Evolution of the Major Facilitator Superfamily: The LacY Manifesto. *Advances in Biology* 2014:1-20.
12. Wisedchaisri G, Park MS, Iadanza MG, Zheng H, Gonen T. (2014) Proton-coupled sugar transport in the prototypical major facilitator superfamily protein XylE. *Nat Commun* 5:4521.
13. Yan N. (2015) Structural Biology of the Major Facilitator Superfamily Transporters. *Annu Rev Biophys* 44:257-283.
14. Nikaido H, Takatsuka Y. (2009) Mechanisms of RND multidrug efflux pumps. *Biochim Biophys Acta* 1794:769-781.
15. Vasilis Vasiliou KVaDWN. (2009) Human ATP-binding cassette (ABC) transporter family. *Human Genomics* 3:281-290.
16. Bay DC, Rommens KL, Turner RJ. (2008) Small multidrug resistance proteins: a multidrug transporter family that continues to grow. *Biochim Biophys Acta* 1778:1814-1838.
17. Bellmann-Sickert K, Stone TA, Poulsen BE, Deber CM. (2015) Efflux by small multidrug resistance proteins is inhibited by membrane-interactive helix-stapled peptides. *J Biol Chem* 290:1752-1759.
18. Moriyama Y, Hiasa M, Matsumoto T, Omote H. (2008) Multidrug and toxic compound extrusion (MATE)-type proteins as anchor transporters for the excretion of metabolic waste products and xenobiotics. *Xenobiotica* 38:1107-1118.
19. Lu M. (2016) Structures of multidrug and toxic compound extrusion transporters and their mechanistic implications. *Channels (Austin)* 10:88-100.

20. José A Caminero GS, Alimuddin Zumla, Giovanni Battista Migliori. (2010) Best drug treatment for multidrug-resistant and extensively drug-resistant tuberculosis. *Lancet Infect Dis* 10:621–629.
21. Sharma A, Hill A, Kurbatova E*, et al.* (2017) Estimating the future burden of multidrug-resistant and extensively drug-resistant tuberculosis in India, the Philippines, Russia, and South Africa: a mathematical modelling study. *The Lancet Infectious Diseases* 17:707-715.
22. Aharon Abbo SN-V, Orly Hammer-Muntz, Tami Krichali,, Yardena Siegman-Igra aYC. (2005) Multidrug-resistant Acinetobacter baumannii. *Emerging Infectious Diseases* 11:22-29.
23. Matteo Bassetti ER, Silvano Esposito, Nicola Petrosillo, Laura Nicolini. (2008) Drug treatment for multidrugresistant *Acinetobacter baumannii* infections. *Future Microbiol* 3:649–660.
24. Manchanda V, Sanchaita S, Singh N. (2010) Multidrug resistant acinetobacter. *J Glob Infect Dis* 2:291-304.
25. Tuon FF, Rocha JL, Merlini AB. (2015) Combined therapy for multi-drug-resistant Acinetobacter baumannii infection--is there evidence outside the laboratory? *J Med Microbiol* 64:951-959.
26. Li XZ, Plesiat P, Nikaido H. (2015) The challenge of efflux-mediated antibiotic resistance in Gram-negative bacteria. *Clin Microbiol Rev* 28:337-418.
27. Fernando DM, Kumar A. (2013) Resistance-Nodulation-Division Multidrug Efflux Pumps in Gram-Negative Bacteria: Role in Virulence. *Antibiotics (Basel)* 2:163-181.
28. Chen J, Kuroda T, Huda MN, Mizushima T, Tsuchiya T. (2003) An RND-type

multidrug efflux pump SdeXY from Serratia marcescens. *J Antimicrob Chemother* 52:176-179.

29. Kumar A, Worobec EA. (2005) Cloning, sequencing, and characterization of the SdeAB multidrug efflux pump of Serratia marcescens. *Antimicrob Agents Chemother* 49:1495-1501.
30. Blanco P, Hernando-Amado S, Reales-Calderon JA*, et al.* (2016) Bacterial Multidrug Efflux Pumps: Much More Than Antibiotic Resistance Determinants. *Microorganisms* 4.
31. Daury L, Orange F, Taveau JC*, et al.* (2016) Tripartite assembly of RND multidrug efflux pumps. *Nat Commun* 7:10731.
32. Papadopoulos CJ, Carson CF, Chang BJ, Riley TV. (2008) Role of the MexAB-OprM efflux pump of Pseudomonas aeruginosa in tolerance to tea tree (Melaleuca alternifolia) oil and its monoterpene components terpinen-4-ol, 1,8-cineole, and alpha-terpineol. *Appl Environ Microbiol* 74:1932-1935.
33. Trepout S, Taveau JC, Benabdelhak H*, et al.* (2010) Structure of reconstituted bacterial membrane efflux pump by cryo-electron tomography. *Biochim Biophys Acta* 1798:1953-1960.
34. Du D, Wang Z, James NR*, et al.* (2014) Structure of the AcrAB-TolC multidrug efflux pump. *Nature* 509:512-515.
35. Wang Z, Fan G, Hryc CF*, et al.* (2017) An allosteric transport mechanism for the AcrAB-TolC multidrug efflux pump. *Elife* 6.
36. Misra R, Bavro VN. (2009) Assembly and transport mechanism of tripartite drug efflux systems. *Biochim Biophys Acta* 1794:817-825.

37. Weeks JW, Bavro VN, Misra R. (2014) Genetic assessment of the role of AcrB beta-hairpins in the assembly of the TolC-AcrAB multidrug efflux pump of Escherichia coli. *Mol Microbiol* 91:965-975.

38. Mikolosko J, Bobyk K, Zgurskaya HI, Ghosh P. (2006) Conformational flexibility in the multidrug efflux system protein AcrA. *Structure* 14:577-587.

39. Tikhonova EB, Yamada Y, Zgurskaya HI. (2011) Sequential mechanism of assembly of multidrug efflux pump AcrAB-TolC. *Chem Biol* 18:454-463.

40. Lobedanz S, Bokma E, Symmons MF*, et al.* (2007) A periplasmic coiled-coil interface underlying ToIC recruitment and the assembly of bacterial drug eff lux pumps. *Proc Natl Acad Sci U S A* 104:4612-4617.

41. Krishnamoorthy G, Tikhonova EB, Zgurskaya HI. (2008) Fitting periplasmic membrane fusion proteins to inner membrane transporters: mutations that enable Escherichia coli AcrA to function with Pseudomonas aeruginosa MexB. *J Bacteriol* 190:691-698.

42. Tikhonova EB, Dastidar V, Rybenkov VV, Zgurskaya HI. (2009) Kinetic control of TolC recruitment by multidrug efflux complexes. *Proc Natl Acad Sci U S A* 106:16416-16421.

43. Xu Y, Lee M, Moeller A*, et al.* (2011) Funnel-like hexameric assembly of the periplasmic adapter protein in the tripartite multidrug efflux pump in gram-negative bacteria. *J Biol Chem* 286:17910-17920.

44. Koronakis V, Sharff A, Koronakis E, Luisi B, Hughes C. (2000) Crystal structure of the bacterial membrane protein TolC central to multidrug efflux and protein export. *Nature* 405:914-919.

45. Koronakis V, Eswaran J, Hughes C. (2004) Structure and function of TolC: the bacterial exit duct for proteins and drugs. *Annu Rev Biochem* 73:467-489.

46. Murakami S, Nakashima R, Yamashita E, Yamaguchi A. (2002) Crystal structure of bacterial multidrug efflux transporter AcrB. *Nature* 419:587-593.

47. Pos KM. (2009) Drug transport mechanism of the AcrB efflux pump. *Biochim Biophys Acta* 1794:782-793.

48. Seeger MA, Schiefner A, Eicher T*, et al.* (2006) Structural asymmetry of AcrB trimer suggests a peristaltic pump mechanism. *Science* 313:1295-1298.

49. Murakami SN, Ryosuke; Yamashita, Eiki; Matsumoto, Takashi; Yamaguchi, Akihito. (2006) Crystal structures of a multidrug transporter reveal a functionally rotating mechanism. *Nature* 443:173-179.

50. Husain F, Nikaido H. (2010) Substrate path in the AcrB multidrug efflux pump of Escherichia coli. *Mol Microbiol* 78:320-330.

51. Takatsuka Y, Chen C, Nikaido H. (2010) Mechanism of recognition of compounds of diverse structures by the multidrug efflux pump AcrB of Escherichia coli. *Proc Natl Acad Sci U S A* 107:6559-6565.

52. Nakashima R, Sakurai K, Yamasaki S, Nishino K, Yamaguchi A. (2011) Structures of the multidrug exporter AcrB reveal a proximal multisite drug-binding pocket. *Nature* 480:565-569.

53. Martyn F. Symmons EB, Eva Koronakis, Colin Hughes, and Vassilis Koronakis. (2009) The assembled structure of a complete tripartite bacterial multidrug efflux pump. *Proceedings of the National Academy of Sciences* 106:7173-7178.

54. Markus A. Seeger AS, Thomas Eicher, François Verrey, KayDiederichs and Klaas

M. Pos. (2006) Structural Asymmetry of AcrB Trimer Suggests a Peristaltic Pump Mechanism. *Science* 313:1295-1298.

55. Abdali N, Parks JM, Haynes KM*, et al.* (2017) Reviving Antibiotics: Efflux Pump Inhibitors That Interact with AcrA, a Membrane Fusion Protein of the AcrAB-TolC Multidrug Efflux Pump. *ACS Infect Dis* 3:89-98.
56. Attilio V. Vargiu PR, Timothy J. Opperman, Son T. Nguyen, Hiroshi Nikaido. (2014) Molecular Mechanism of MBX2319 Inhibition of Escherichia coli AcrB Multidrug Efflux Pump and Comparison with Other Inhibitors. *Antimicrobial Agents and Chemotherapy* 58:6224-6234.
57. Valeur B, Berberan-Santos MrN. (2011) A Brief History of Fluorescence and Phosphorescence before the Emergence of Quantum Theory. *Journal of Chemical Education* 88:731-738.
58. Safford WE. 1916. Lignum nephriticum : its history and an account of the remarkable fluorescence of its infusion, Smithsonian, Washington.
59. Clegg RM. 2006. Reviews in Fluorescence, Springer, New York.
60. Pietraszewska-Bogiel A, Gadella TW. (2011) FRET microscopy: from principle to routine technology in cell biology. *J Microsc* 241:111-118.
61. Helms V. 2008. Principles of Computational Cell Biology, Wiley, Weinheim.
62. Clegg RM. (1995) Fluorescence resonance energy transfer. *Current Opinion in Biotechnology* 6:103-110.
63. Taraska JW. (2012) Mapping membrane protein structure with fluorescence. *Curr Opin Struct Biol* 22:507-513.
64. Tsien RY. (1998) The Green Fluorescent Protein. *Annu Rev Biochem* 67:509-544.

65. Johnson F. H. OS, Y. Saiga, L. C. Gershman, G. T. Reynolds and J. R. Water. (1962) Quantum efficiency of Cypridina luminescence, with a note on that of Aequorea. *J Cell Comp Physiol* 60:85-104.

66. Prasher DC1 EV, Ward WW, Prendergast FG, Cormier MJ. (1992) Primary structure of the Aequorea victoria green-fluorescent protein. *Gene* 111:229-233.

67. Ormö M1 CA, Kallio K, Gross LA, Tsien RY, Remington SJ. (1996) Crystal structure of the Aequorea victoria green fluorescent protein. *Science* 273:1392-1395.

68. Yang F ML, Phillips GN Jr. (1996) The molecular structure of green fluorescent protein. *Nat Biotechnol* 14:1246-1251.

69. Zhang GG, Vanessa ; Kain, Steven R. (1996) An Enhanced Green Fluorescent Protein Allows Sensitive Detection of Gene Transfer in Mammalian Cells. *Biochem Biophys Res Commun* 227:707-711.

70. Arpino JA, Rizkallah PJ, Jones DD. (2012) Crystal structure of enhanced green fluorescent protein to 1.35 A resolution reveals alternative conformations for Glu222. *PLoS One* 7:e47132.

71. Shaner NC, Steinbach PA, Tsien RY. (2005) A guide to choosing fluorescent proteins. *Nat Methods* 2:905-909.

72. Lam AJ, St-Pierre F, Gong Y*, et al.* (2012) Improving FRET dynamic range with bright green and red fluorescent proteins. *Nat Methods* 9:1005-1012.

73. Piston DW, Kremers GJ. (2007) Fluorescent protein FRET: the good, the bad and the ugly. *Trends Biochem Sci* 32:407-414.

74. Lee SJ, Escobedo-Lozoya Y, Szatmari EM, Yasuda R. (2009) Activation of CaMKII in single dendritic spines during long-term potentiation. *Nature* 458:299-304.

75. Sauer RT, Baker TA. (2011) AAA+ proteases: ATP-fueled machines of protein destruction. *Annu Rev Biochem* 80:587-612.

76. Sousa MCT, Christine B. Tsuruta, Hiro Wilbanks, Sigurd M. Reddy, Vijay S. Mckay, David B. (2000) Crystal and Solution Structures of an HslUV Protease–Chaperone Complex. *Cell* 103:633-643.

77. Glynn SE, Martin A, Nager AR, Baker TA, Sauer RT. (2009) Structures of asymmetric ClpX hexamers reveal nucleotide-dependent motions in a AAA+ protein-unfolding machine. *Cell* 139:744-756.

78. Rabl J, Smith DM, Yu Y*, et al.* (2008) Mechanism of gate opening in the 20S proteasome by the proteasomal ATPases. *Mol Cell* 30:360-368.

79. Bedford L, Paine S, Sheppard PW, Mayer RJ, Roelofs J. (2010) Assembly, structure, and function of the 26S proteasome. *Trends Cell Biol* 20:391-401.

80. Robert T SA, Wali Karzai, Eric D Roche. (2000) The SsrA–SmpB system for protein tagging, directed degradation and ribosome rescue. *Nat Struct Mol Biol* 7:449-455.

81. McGinness KE, Baker TA, Sauer RT. (2006) Engineering controllable protein degradation. *Mol Cell* 22:701-707.

82. Hersch GL, Burton RE, Bolon DN, Baker TA, Sauer RT. (2005) Asymmetric interactions of ATP with the AAA+ ClpX6 unfoldase: allosteric control of a protein machine. *Cell* 121:1017-1027.

83. Wang JH, James A ; Flanagan, John M. (1997) The Structure of ClpP at 2.3 Å Resolution Suggests a Model for ATP-Dependent Proteolysis. *Cell* 91:447-456.

84. Maurizi MC, W ; Kim, Seung-Ho ; Gottesman, S Maurizi, M. (1990) Clp P represents a unique family of serine proteases. *J Biol Chem* 265:12546-12552.

85. Maurizi MT, M ; Singh, S ; Kim, Sh Maurizi, M. (1994) Endopeptidase Clp: ATP-dependent Clp protease from *Escherichia coli*. *Methods Enzymol* 244:314-331.

86. Thompson MWM, M R. (1994) Activity and specificity of Escherichia coli ClpAP protease in cleaving model peptide substrates. *J Biol Chem* 269:18201-18208.

87. Baker TA, Sauer RT. (2012) ClpXP, an ATP-powered unfolding and protein-degradation machine. *Biochim Biophys Acta* 1823:15-28.

88. Geiger SR, Bottcher T, Sieber SA, Cramer P. (2011) A conformational switch underlies ClpP protease function. *Angew Chem Int Ed Engl* 50:5749-5752.

89. Julia M. Flynn IL, Meredith Seidel, Sue H. Wickner, Robert T. Sauer, and Tania A. Baker. (2001) Overlapping recognition determinants within the ssrA degradation tag allow modulation of proteolysis. *Proceedings of the National Academy of Sciences* 98:10584 –10589.

90. Levchenko I, Grant RA, Wah DA, Sauer RT, Baker TA. (2003) Structure of a Delivery Protein for an AAA+ Protease in Complex with a Peptide Degradation Tag. *Molecular Cell* 12:365-372.

91. Yeh AP, McMillan A, Stowell MH. (2006) Rapid and simple protein-stability screens: application to membrane proteins. *Acta Crystallogr D Biol Crystallogr* 62:451-457.

92. Hong H, Joh NH, Bowie JU, Tamm LK. (2009) Methods for Measuring the Thermodynamic Stability of Membrane Proteins. *Methods Enzymol* 455:213-236.

93. Kashino Y. (2003) Separation methods in the analysis of protein membrane complexes. *J Chromatogr B* 797:191-216.

94. Kelly SM, Jess TJ, Price NC. (2005) How to study proteins by circular dichroism. *Biochim Biophys Acta* 1751:119-139.

95. Popot JLE, D. M. (2000) Helical Membrane Protein Folding, Stability and Evolution. *Annu Rev Biochem* 69:881-922.

96. Alexandrov AI, Mileni M, Chien EY, Hanson MA, Stevens RC. (2008) Microscale fluorescent thermal stability assay for membrane proteins. *Structure* 16:351-359.

97. O'Malley MA, Naranjo AN, Lazarova T, Robinson AS. (2010) Analysis of adenosine A(2)a receptor stability: effects of ligands and disulfide bonds. *Biochemistry* 49:9181-9189.

98. Senisterra G, Chau I, Vedadi M. (2012) Thermal denaturation assays in chemical biology. *Assay Drug Dev Technol* 10:128-136.

99. Manolaridis I, Kulkarni K, Dodd RB*, et al.* (2013) Mechanism of farnesylated CAAX protein processing by the intramembrane protease Rce1. *Nature* 504:301-305.

100. Lee SC, Bennett BC, Hong WX*, et al.* (2013) Steroid-based facial amphiphiles for stabilization and crystallization of membrane proteins. *Proc Natl Acad Sci U S A* 110:E1203-1211.

101. Tol MB, Deluz C, Hassaine G*, et al.* (2013) Thermal unfolding of a mammalian pentameric ligand-gated ion channel proceeds at consecutive, distinct steps. *J Biol Chem* 288:5756-5769.

102. Tao H, Fu Y, Thompson A*, et al.* (2012) Synthesis and properties of dodecyl trehaloside detergents for membrane protein studies. *Langmuir* 28:11173-11181.

103. Haberstock S, Roos C, Hoevels Y*, et al.* (2012) A systematic approach to increase the efficiency of membrane protein production in cell-free expression systems. *Protein Expr Purif* 82:308-316.

104. Thompson AA, Liu JJ, Chun E*, et al.* (2011) GPCR stabilization using the bicelle-like architecture of mixed sterol-detergent micelles. *Methods* 55:310-317.

105. Tarttelin EE, Fransen MP, Edwards PC*, et al.* (2011) Adaptation of pineal expressed teleost exo-rod opsin to non-image forming photoreception through enhanced Meta II decay. *Cell Mol Life Sci* 68:3713-3723.

106. Borgnia MJ, Kozono D, Calamita G, Maloney PC, Agre P. (1999) Functional reconstitution and characterization of AqpZ, the E. coli water channel protein. *Journal of molecular biology* 291:1169-1179.

107. Symmons MF, Bokma E, Koronakis E, Hughes C, Koronakis V. (2009) The assembled structure of a complete tripartite bacterial multidrug efflux pump. *Proceedings of the National Academy of Sciences* 106:7173-7178.

108. Fothergill L, Fothergill J. (1970) Thiol and disulphide contents of hen ovalbumin. C-terminal sequence and location of disulphide bond. *Biochemical Journal* 116:555-561.

109. Canfield RE, Liu AK. (1965) The disulfide bonds of egg white lysozyme (muramidase). *Journal of biological chemistry* 240:1997-2002.

110. Lu W, Zhong M, Wei Y. (2011) Folding of AcrB Subunit Precedes Trimerization. *J Mol Biol* 411:264-274.

111. Finkelstein AV, Badretdinov AY, Gutin AM. (1995) Why do protein architectures have boltzmann-like statistics? *Proteins: Structure, Function, and Bioinformatics* 23:142-150.

112. Goddard ED, Harva O, Jones TG. (1953) THE EFFECT OF UNIVALENT CATIONS ON THE CRITICAL MICELLE CONCENTRATION OF SODIUM

DODECYL SULPHATE. *Transactions of the Faraday Society* 49:980-984.

113. Banerjee P, Joo JB, Buse JT, Dawson G. (1995) DIFFERENTIAL SOLUBILIZATION OF LIPIDS ALONG WITH MEMBRANE-PROTEINS BY DIFFERENT CLASSES OF DETERGENTS. *Chem Phys Lipids* 77:65-78.

114. Xie M, Schowen RL. (1998) Secondary Structure and Protein Deamidation. *J Pharm Sci* 88:8-13.

115. Calamita G. (2000) The Escherichia coli aquaporin-Z water channel. *Mol Microbiol* 37:254-262.

116. Ye C, Wang Z, Lu W*, et al.* (2014) Correlation between AcrB Trimer Association Affinity and Efflux Activity. *Biochemistry* 53:3738-3746.

117. Bennion BJ, Daggett V. (2003) The molecular basis for the chemical denaturation of proteins by urea. *Proc Natl Acad Sci U S A* 100:5142-5147.

118. Blair JM, Piddock LJ. (2009) Structure, function and inhibition of RND efflux pumps in Gram-negative bacteria: an update. *Curr Opin Microbiol* 12:512-519.

119. Murakami S, Nakashima R, Yamashita E, Matsumoto T, Yamaguchi A. (2006) Crystal structures of a multidrug transporter reveal a functionally rotating mechanism. *Nature* 443:173-179.

120. Su CC, Li M, Gu R*, et al.* (2006) Conformation of the AcrB multidrug efflux pump in mutants of the putative proton relay pathway. *J Bacteriol* 188:7290-7296.

121. Elkins CAN, Hiroshi. (2002) Substrate Specificity of the RND-Type Multidrug Efflux Pumps AcrB and AcrD of Escherichia coli Is Determined Predominately by Two Large Periplasmic Loops. *The Journal of Bacteriology* 184:6490-6498.

122. Wang Z, Zhong M, Lu W, Chai Q, Wei Y. (2015) Repressive mutations restore

function-loss caused by the disruption of trimerization in Escherichia coli multidrug transporter AcrB. *Front Microbiol* 6:4.

123. Yu L, Lu, W. & Wei, Y. (2011) AcrB Trimer Stability and Efflux Activity, Instight from Mutagenesis Studies. *PLoS One* 6:1-8.

124. Ye C, Wang Z, Lu W, Wei Y. (2014) Unfolding study of a trimeric membrane protein AcrB. *Protein Sci* 23:897-905.

125. Woody RW. (1995) Circular dichroism. *Methods in Enzymology* 246:34-71.

126. A.J. Alder NJGaGDF. (1973) Circular Dichroism and Optical Rotatory Dispersion of Proteins and Polypeptides. *Methods Enzymology* 27:675-735.

127. Greenfield NJ. (2006) Using circular dichroism spectra to estimate protein secondary structure. *Nat Protoc* 1:2876-2890.

128. Kodadek DAFaT. (1999) Chemistry for the analysis of protein–protein interactions: Rapid and efficient cross-linking triggered by long wavelength light. *Proc Natl Acad Sci USA* 96:6020-6024.

129. Sinz A. (2006) Chemical cross-linking and mass spectrometry to map three-dimensional protein structures and protein-protein interactions. *Mass Spectrom Rev* 25:663-682.

130. Mitsuru Akita EN, and Kenneth Keegstra. (1997) Identification of Protein Transport Complexes in the Chloroplastic Envelope Membranes via Chemical Cross-Linking. *The Journal of Cell Biology* 136:983-994.

131. Charalambous K, O'Reilly AO, Bullough PA, Wallace BA. (2009) Thermal and chemical unfolding and refolding of a eukaryotic sodium channel. *Biochim Biophys Acta* 1788:1279-1286.

132. Alexandrov AI MM, Chien EY, Hanson MA, Stevens RC. (2008) Microscale fluorescent thermal stability assay for membrane
proteins. *Structure* 16:351–359.

133. Fonseca LC, Arvelos LR, Netto RC*, et al.* (2010) Influence of the albumin concentration and temperature on the lysis of human erythrocytes by sodium dodecyl sulfate. *J Bioenerg Biomembr* 42:413-418.

134. Wang Z, Ye C, Zhang X, Wei Y. (2015) Cysteine residue is not essential for CPM protein thermal-stability assay. *Anal Bioanal Chem* 407:3683-3691.

135. Rose GD, Geselowitz, A.R.,Lesser, G.J.,Lee,R.H. ,and Zehfus,M.H. . (1985) Hydrophobicity of amino acid residues in globular proteins. *Science* 229:834-838.

136. Sigalov AB. (2010) Protein intrinsic disorder and oligomericity in cell signaling. *Mol Biosyst* 6:451-461.

137. Eicher T, Seeger MA, Anselmi C*, et al.* (2014) Coupling of remote alternating-access transport mechanisms for protons and substrates in the multidrug efflux pump AcrB. *Elife* 3.

138. Kinana AD, Vargiu AV, Nikaido H. (2013) Some ligands enhance the efflux of other ligands by the Escherichia coli multidrug pump AcrB. *Biochemistry* 52:8342-8351.

139. Soll PLaD. (1969) Mechanism of Protein Biosynthesis. *Bacteriological Reviews* 33:264-301.

140. Hiroaki Suga NL, Yoshitaka Bessho,Kenneth Wei,Jack W Szostak. (2000) Ribozyme-catalyzed tRNA aminoacylation. *Nature structural biology* 7:28-33.

141. Pejaver V, Hsu WL, Xin F*, et al.* (2014) The structural and functional signatures of proteins that undergo multiple events of post-translational modification. *Protein Sci*

23:1077-1093.

142. Berg JM TJ, Stryer L. 2002. Biochemistry. 5th edition., W H Freeman, New York.

143. Kumar GK, Prabhakar NR. (2008) Post-translational modification of proteins during intermittent hypoxia. *Respir Physiol Neurobiol* 164:272-276.

144. Humphrey SJ, James DE, Mann M. (2015) Protein Phosphorylation: A Major Switch Mechanism for Metabolic Regulation. *Trends Endocrinol Metab* 26:676-687.

145. Engelman J-LPaDM. (1990) Membrane Protein Folding and Oligomerization: The Two-Stage Model. *Biochemistry* 29:4031-4037.

146. Paula JBooth AR. (1999) Membrane protein folding. *Current Opinion in Structural Biology* 9:115-121.

147. EF Eppens NN, J Tommassen. (1997) Folding of a bacterial outer membrane protein during passage through the periplasm. *EMBO J* 16:4295-4301.

148. Panchenko KHaAR. (2010) Mechanisms of protein oligomerization, the critical role of insertions and deletions in maintaining different oligomeric states. *Proceedings of the National Academy of Sciences of the United States of America* 107:20352–20357.

149. Chien Peter Chen SP, Avinoam Ben-Shaul, Lawrence Shapiro, and Barry H. Honig. (2005) Specificity of cell–cell adhesion by classical cadherins: Critical role for low-affinity dimerization through β-strand swapping. *Proceedings of the National Academy of Sciences of the United States of America* 102:8531–8536.

150. Hammad Naveed RJJ, and Jie Liang. (2009) Predicting weakly stable regions, oligomerization state, and protein–protein interfaces in transmembrane domains of outer membrane proteins. *Proceedings of the National Academy of Sciences of the*

United States of America 106:12735–12740.

151. Gell DA, Grant RP, Mackay JP. The Detection and Quantitation of Protein Oligomerization. In: Matthews JM, Ed. (2012) Protein Dimerization and Oligomerization in Biology. Springer New York, New York, NY, pp. 19-41.

152. Zimmermann T, Rietdorf J, Girod A, Georget V, Pepperkok R. (2002) Spectral imaging and linear un-mixing enables improved FRET efficiency with a novel GFP2-YFP FRET pair. *FEBS Lett* 531:245-249.

153. Tsien RY. (1998) The green fluorescent protein. *Annu Rev Biochem* 67:509-544.

154. Chalfie M, Tu Y, Euskirchen G, Ward WW, Prasher DC. (1994) GREEN FLUORESCENT PROTEIN AS A MARKER FOR GENE-EXPRESSION. *Science* 263:802-805.

155. Giepmans BN, Adams SR, Ellisman MH, Tsien RY. (2006) The fluorescent toolbox for assessing protein location and function. *Science* 312:217-224.

156. Miyawaki A, Llopis J, Heim R*, et al.* (1997) Fluorescent indicators for Ca2+ based on green fluorescent proteins and calmodulin. *Nature* 388:882-887.

157. Kurokawa K, Mochizuki N, Ohba Y*, et al.* (2001) A pair of fluorescent resonance energy transfer-based probes for tyrosine phosphorylation of the CrkII adaptor protein in vivo. *J Biol Chem* 276:31305-31310.

158. Bregestovski P, Waseem T, Mukhtarov M. (2009) Genetically encoded optical sensors for monitoring of intracellular chloride and chloride-selective channel activity. *Front Mol Neurosci* 2:15.

159. Bhat RA, Lahaye T, Panstruga R. (2006) The visible touch: in planta visualization of protein-protein interactions by fluorophore-based methods. *Plant methods* 2:12.

160. Lu W, Chai Q, Zhong M*, et al.* (2012) Assembling of AcrB trimer in cell membrane. *J Mol Biol* 423:123-134.

161. Wittig I, Braun HP, Schagger H. (2006) Blue native PAGE. *Nat Protoc* 1:418-428.

162. Takatsuka Y, Nikaido H. (2006) Threonine-978 in the transmembrane segment of the multidrug efflux pump AcrB of Escherichia coli is crucial for drug transport as a probable component of the proton relay network. *J Bacteriol* 188:7284-7289.

163. Cladera J, Rigaud JL, Villaverde J, Dunach M. (1997) Liposome solubilization and membrane protein reconstitution using Chaps and Chapso. *Eur J Biochem* 243:798-804.

164. Yu L, Lu W, Ye C*, et al.* (2013) Role of a conserved residue R780 in Escherichia coli multidrug transporter AcrB. *Biochemistry* 52:6790-6796.

165. Linliang Yu WL, Yinan Wei. (2011) AcrB Trimer Stability and Efflux Activity, Insight from Mutagenesis Studies. *PLoS ONE* 6:e28390.

166. Day RN, Davidson MW. (2009) The fluorescent protein palette: tools for cellular imaging. *Chem Soc Rev* 38:2887-2921.

167. Gonze D, and M. Kaufman. (2016) Chemical and enzyme kinetics.

168. Nikaido KNaH. (2009) Kinetic behavior of the major multidrug efflux pump AcrB of *Escherichia coli*. *Proceedings of the National Academy of Sciences of the United States of America* 106:5854-5858.

169. Shaner NC, Lambert GG, Chammas A*, et al.* (2013) A bright monomeric green fluorescent protein derived from Branchiostoma lanceolatum. *Nat Methods* 10:407-409.

170. Wang X, Robbins J. (2014) Proteasomal and lysosomal protein degradation and

heart disease. *J Mol Cell Cardiol* 71:16-24.

171. Avci D, Lemberg MK. (2015) Clipping or Extracting: Two Ways to Membrane Protein Degradation. *Trends Cell Biol* 25:611-622.

172. Humbard MA, Maupin-Furlow JA. (2013) Prokaryotic proteasomes: nanocompartments of degradation. *J Mol Microbiol Biotechnol* 23:321-334.

173. Christopher M. Farrell ADG, Robert T. Sauer. (2005) Cytoplasmic degradation of ssrA-tagged proteins. *Molecular Microbiology* 57:1750-1761.

174. Andersen JB, Sternberg, C., Poulsen, L.K., Bjorn, S.P., Givskov, M., and Molin, S. (1998) New unstable variants of green fluorescent protein for studies of transient gene expression in bacteria. *Applied And Enviromental MIcrobiology* 64:2240-2246.

175. Yong-In Kim REB, Briana M, Burton, Robert T. Sauer, Tania A. Baker. (2000) Dynamics of Substrate Denaturation and Translocation by the ClpXP Degradation Machine. *Molecular Cell* 5:639-648.

176. Greg L Hersch TAB, Robert T Sauer. (2004) SspB delivery of substrates for ClpXP proteolysis probed by the design of improved degradation tags. *Proceedings of the National Academy of Sciences of the United States of America* 101:12136-12141.

177. Michaelis L, Menten ML, Johnson KA, Goody RS. (2011) The original Michaelis constant: translation of the 1913 Michaelis-Menten paper. *Biochemistry* 50:8264-8269.

178. Haldane. GEBaJBS. (1925) A Note on the Kinetics of Enzyme Action. *Biochemical Journal* 19:338-339.

179. Hill AV. (1913) The combination of haemoglobin with oxygen and with carbon monoxide. *Biochemistry Journal* 7:471-480.

180. Weiss JN. (1997) The Hill equation revisited: uses and misuses. *The FASEB Journal* 11:835-841.

181. Chai Q, Wang Z, Webb SR, Dutch RE, Wei Y. (2016) The ssrA-Tag Facilitated Degradation of an Integral Membrane Protein. *Biochemistry* 55:2301-2304.

182. Lorna Brundage JPH, Elmar Schiebel, Arnold JM Driessen, and William Wickner. (1990) The purified E. coli integral membrane protein SecYE is sufficient for reconstitution of SecA-dependent precursor protein translocation. *Cell* 62:649-657.

183. Neil D.Rawlings AJB. (1994) Families of serine peptidases. *Methods in Enzymology* 244:19-61.

184. Guzman L-M, Belin D, Carson MJ, Beckwith J. (1995) Tight regulation, modulation, and high-level expression by vectors containing the arabinose PBAD promoter. *Journal of bacteriology* 177:4121-4130.

185. A. Zlotnick NC, J. F. Conway , F. P. Booy , A. C. Steven , S. J. Stahl and P. T. Wingfield. (1996) Dimorphism of Hepatitis B Virus Capsids Is Strongly Influenced by the C-Terminus of the Capsid Protein. *Biochemistry* 35:7412-7421.

Vita

Personal information

Name	Zhaoshuai Wang
Place of Birth	China
Nationality	China

Education Background:

- 2009-2012 **M.S.** in Pharmacognosy Tianjin University, Tianjin, China
- 2005-2009 **B.S.** in Pharmaceutical Sciences Tianjin University, Tianjin, China

Publication:

1. Q Chai, SR Webb, **Z Wang**, RE Dutch, Y Wei. (2016) Study of the degradation of a multidrug transporter using a non-radioactive pulse chase method. *Analytical and bioanalytical chemistry*. 408 (27), 7745-7751.
2. Q Chai, **Z Wang,** SR Webb, RE Dutch, Y Wei. (2016) The ssrA-tag facilitated degradation of an integral membrane protein. *Biochemistry.* 55 (16), 2301-2304.
3. **Z Wang*,** (co-first author) M Zhong*, W Lu, Q Chai, Y Wei. (2015) Repressive mutations restore function-loss caused by the disruption of trimerization in *Escherichia coli* multidrug transporter AcrB. *Frontiers in microbiology*. 6: 4.
4. **Z Wang,** C Ye, X Zhang, Y Wei. (2015**)** Cysteine residue is not essential for CPM protein thermal-stability assay. *Analytical and bioanalytical chemistry***.** 407 (13), 3683-3691.

5. C Ye, **Z Wang,** W Lu, Y Wei. (2014) Unfolding study of a trimeric membrane protein AcrB. *Protein Scienc**e***. 23(7):897-905

6. C Ye, **Z Wang,** W Lu, M Zhong, Q Chai, Y Wei. (2014) Correlation between AcrB Trimer Association Affinity and Efflux Activity. *Biochemistry.* 53(23):3738-46.

7. W Lu, M Zhong, Q Chai, **Z Wang**, L Yu, Y Wei. (2014) Functional Relevance of AcrB Trimerization in Pump Assembly and Substrate Binding. *PloS one* 9 (2), e89143

8. L Yu, W Lu, C Ye, **Z Wang,** M Zhong, Q Chai, M Sheetz, Y Wei. (2013) Role of a conserved residue R780 in Escherichia coli multidrug transporter AcrB. *Biochemistry.* 52 (39), 6790-6796

9. Chen, **Z Wang,** L Yang. (2012) Analysis of euphornin in *Euphorbia helioscopia L*. and its cytotoxicity to mice lung adenocarcinoma cells (LA795). *Natural product research* 26 (22), 2112-2116

10. G Lan, H Chen, **Z Wang**, W Zhang, L Zhang. (2011) Extraction of *Polygonatum odoratum* polysaccharides using response surface methodology and preparation of a compound beverage. *Carbohydrate Polymers,* 86, 1175– 1180.

11. **Z Wang,** H Chen, W Zhang, G Lan, L Zhang. (2011) Comparative studies on the chemical composition and antioxidant activities of *Schisandra chinensis* and *Schisandra sphenanthera* fruits. *Journal of Medicinal Plants Research.* Vol. 5(7), pp. 1207-1216.

12. H Chen, **Z Wang,** Z Qu, L Fu, P Dong, X Zhang, (2009) Physicochemical characterization and antioxidant activity of a polysaccharide isolated from oolong tea. *Eur Food Res Technol*, 229:629–635.

13. H Chen, **Z Wang,** X Lu, B Xie. (2008) Isolation and chemical characterization of a polysaccharide from green tea (*Camellia Sinensis* L.) *J Sci Food Agric*, 88:2523–2528.

Honors and Awards:

2014-2017	Research Challenge Trust Fund (I) Fellowship, University of Kentucky
Aug 2016	Max Steckler Fellowship, University of Kentucky
Nov 2014	The third place of oral competition in 100th KAS meeting
2009-2011	Scholarship of SPST, Tianjin University (consecutive for 3 years)
Oct 2011	Scholarship of "Wang Kechang", Tianjin University
Oct 2010	"Three As" Student, Tianjin University
Apr 2009	The first prize of "Challenge Cup" National Undergraduate of Tianjin City